The Auxin Biosynthesis Metabolic Network

A DISSERTATION
SUBMITTED TO THE FACULTY OF
THE UNIVERSITY OF MINNESOTA
BY

Molly A. Tillmann

IN PARTIAL FULFILLMENT OF THE REQUIREMENTS
FOR THE DEGREE OF
DOCTOR OF PHILOSOPHY

Advisor: Jerry D. Cohen

January 2021

© Copyright Molly Tillmann 2021

Acknowledgements

First and foremost, I want to express my deepest thanks to my advisor, Dr. Jerry Cohen, for his exceptional mentorship. He guided my research with expertise and enthusiasm in a way that made every day in the lab an exciting chance to explore and learn. I am grateful for the countless ways he went above and beyond to provide scientific and professional development opportunities that enriched the training I received in his lab.

I am incredibly grateful for all the encouragement, thoughtful feedback, and helpful suggestions I received from my advisory committee. Thank you to Dr. Gary Gardner for mentoring me in the area of photobiology and spending many hours helping me design and interpret experiments, to Dr. Adrian Hegeman for sharing his deep expertise in plant biochemistry, to Dr. Sue Gibson for raising thoughtful questions and comments to strengthen my research, and to Dr. Don Wyse for supporting me as a member of the Forever Green team.

I thank all the members of the Cohen/Gardner/Hegeman lab group who have shared ideas and instruction over the years, especially Dr. Dana Freund, Dr. Renata Pincelli-Souza, Qian Tang, and Kate Sammons for their training and assistance, and Doug Brinkman for growth chamber support. I also thank the Plant and Microbial Biology graduate program and the Department of Horticultural Science for hosting and supporting my graduate studies, and I am deeply grateful for the friendship and advice I received from my fellow graduate students.

My research was funded by the Forever Green Initiative, the US Department of Agriculture National Institute of Food and Agriculture (USDA-NIFA), the National Science Foundation (NSF), and the Gordon and Margaret Bailey Endowment for Environmental Horticulture. I am also very grateful for the travel grants and awards I received from the Microbial and Plant Genomics Institute (MPGI), USDA North Central Extension & Research Activity-101 (NCERA-101), and the Plant and Microbial Biology

Graduate Program, which allowed me to present my research at national and international meetings and connect with plant biologists around the world.

I thank all my friends and family, whose encouragement means so much to me. Thank you to my parents and parents-in-law for their consistent, loving support over the years and for helping me find balance in being a grad student and a mother. And finally, an enormous thank you to my husband, Anton, and daughter, Marina, who fill my life with love and joy every day.

Dedication

This dissertation is dedicated to my grandparents, Joseph and Regina Leisen, who inspired my interest in plant science.

Abstract

The plant hormone auxin plays a central role in regulation of plant growth and response to environmental stimuli. Multiple pathways have been proposed for biosynthesis of indole-3-acetic acid (IAA), the primary auxin in a number of plant species. However, utilization of these different pathways under various environmental conditions and developmental time points remains largely unknown. To trace the involvement of various biosynthetic routes to indole-3-acetic acid (IAA), I monitored label incorporation from three different stable isotope-labeled precursors ([$^{13}C_6$]anthranilate, [$^{15}N_1$]indole, and [$^{13}C_3$]serine) into a number of proposed biosynthesis intermediates as well as IAA under conditions that induce adventitious root formation in *Arabidopsis* hypocotyls. [$^{13}C_3$]Serine-derived ^{13}C incorporation into IAA was nearly eliminated in seedlings treated with inhibitors targeting tryptophan aminotransferases and flavin monooxygenases of the YUCCA pathway (tryptophan→indole-3-pyruvate→IAA), suggesting this pathway is a significant contributor to the auxin pool in de-etiolating hypocotyls that can be effectively blocked using chemical inhibitors. Labeling treatment with both [$^{13}C_6$]anthranilate and [$^{15}N_1$]indole simultaneously resulted in higher label incorporation into IAA from [$^{15}N_1$]indole than from [$^{13}C_6$]anthranilate; however, this result was reversed in the proposed precursors that were monitored, with the majority of isotope label originating from [$^{13}C_6$]anthranilate. An even greater proportion of IAA became [$^{15}N_1$]-labeled compared to [$^{13}C_6$]-labeled in seedlings treated with YUCCA pathway inhibitors, suggesting a portion of IAA biosynthesis comes from an origin independent of the measured pool of Trp in these tissues. I also describe in detail the techniques I used for pathway analysis in *Arabidopsis thaliana* seedlings employing multiple stable isotope-labeled precursors and chemical inhibitors coupled with highly sensitive liquid chromatography-mass spectrometry (LC-MS) methods. These methods should prove to be useful in future studies exploring routes of IAA biosynthesis *in vivo* in a variety of plant tissues.

Table of Contents

List of Tables

List of Figures

Chapter 1: Introduction

Auxin regulation of light-induced adventitious root formation

Adventitious roots (AR), defined as roots originating from non-root tissues such as shoots, are vital structures for water and nutrient acquisition as well as response to environmental changes in many horticultural crops that are vegetatively propagated from stem or leaf cuttings (Bellini et al., 2014). A vigorous root system is necessary for survival and health of these asexually propagated plants; however, some species and genotypes can be especially difficult to root, making AR formation a limiting factor to their productivity (Steffens and Rasmussen, 2016). The plant hormone auxin plays a central role in AR initiation, and methods for inducing AR in horticultural plants often include treatment with indole-3-butyric acid (IBA), a naturally occurring auxin which is converted *in vivo* to indole-3-acetic acid (IAA), the primary auxin in the reference species *Arabidopsis thaliana* (Epstein et al., 1989; Strader et al., 2011; Liu et al., 2012; Kreiser et al., 2016). Limited understanding of the mechanisms controlling AR formation is a major hindrance to advancements in vegetative propagation efficiency (Sang et al., 2016).

AR primordia typically originate from cambium or procambium tissue in *Arabidopsis* (da Rocha Correa et al., 2012; Liu et al., 2014) and their development follows seven defined stages of cell divisions: (I) anticlinal division of founder cells, (II) periclinal division to form outer and inner layers, (III) periclinal division of the outer layer, (IV) periclinal division of inner layer, (V) anticlinal division of central cells of the two outer cell layers, (VI) periclinal divisions of the two outer cell layers, (VII) enlargement of a dome-shaped primordium. This progression is analogous to the more well-defined process of lateral root development (Malamy and Benfey, 1997; Della Rovere et al., 2013; Bellini et al., 2014). Auxin accumulates in founder cells, and as AR initiation progresses an auxin gradient with a maximum at the primordium tip is formed (Della Rovere et al., 2013). IAA synthesized *de novo* in surrounding tissues is transported to the site of the AR initial to form this gradient (Chen et al., 2016).

Many biotic and abiotic factors influence adventitious root formation, one of which is light (Bellini et al., 2014; da Costa et al., 2018). Etiolated *Arabidopsis* seedlings

grown in the dark for several days can form adventitious roots upon transfer to light (Sorin et al., 2005; da Costa et al., 2018), a phenomenon that is dependent on IAA homeostasis by conjugation and *de novo* biosynthesis (Sorin et al., 2005; Sorin et al., 2006; Cano et al., 2018). Dark pretreatment has been used to promote rooting in other agriculturally important and woody species as well, including lilac (Howard and Ridout, 1992), petunia (Klopotek et al., 2010; Yang et al., 2019), and avocado (Gleeson et al., 2014). In *Arabidopsis*, light-induced AR primordia become visible under a microscope approximately 2-4 days after transition to light (da Costa et al., 2018), providing a convenient and interesting assay for studying genetic and biochemical factors involved in adventitious root initiation absent exogenous auxin or wounding. My research described in Chapter 2 examines changes in auxin levels and utilization of different IAA biosynthetic pathways in hypocotyls during this process.

Mass spectrometry in the study of auxin biosynthesis

The plant hormone auxin regulates many aspects of plant growth and response to environmental changes and plays a crucial role in root development (Overvoorde et al., 2010). A combination of genetic and biochemical tools has been used to build current understanding of auxin biosynthesis, though many uncertainties have yet to be resolved regarding the roles of various proposed intermediates and the utilization of different pathways (Chandler, 2009; Kasahara, 2016). One major route to IAA in *Arabidopsis* is through the YUCCA pathway, in which the amino acid tryptophan (Trp) is converted to indole-3-pyruvic acid (IPyA) via an aromatic amino transferase (Won et al., 2011), and IPyA is then converted to IAA by YUCCA flavin monooxygenases (Mashiguchi et al., 2011). *Arabidopsis* has also been shown to synthesize IAA from Trp through indole-3-acetaldoxime (IAOx), which is converted to indole-3-acetamide (IAM) and possibly an indole-3-acetonitrile (IAN) intermediate (Sugawara et al., 2009). Other potential intermediates of IAA synthesis downstream of Trp have been proposed, such as indole-3-acetaldehyde (IAAld) (Rajagopal, 1971; Koshiba and Matsuyama, 1993; Tsurusaki et al., 1997) and tryptamine (TAM) (Quittenden et al., 2009), though their places within the web of auxin biosynthesis have not been determined. A Trp-independent route has also

been proposed, in which indole or another upstream compound serves as the IAA precursor (Wright et al., 1991; Normanly et al., 1993; Tivendale et al., 2014); however, possible intermediates, if involved in this pathway, have not been identified (Nonhebel, 2015). Mass spectrometry (MS) has been and continues to be an important technique in deciphering these routes of auxin biosynthesis, enabling accurate quantitation of IAA and its precursors, identification of intermediates, and tracking of isotopic labels through distinct pathways.

Quantitative methods for IAA and precursor analysis by MS have been invaluable tools in elucidating auxin biosynthesis pathways and have continuously evolved over time with advances in analytical sensitivity and resolution (Ljung et al., 2005; Barkawi et al., 2008; Barkawi et al., 2010; Liu et al., 2012; Novák et al., 2012; Tivendale and Cohen, 2015). Absolute quantitation can be achieved with isotope dilution, where concentration is calculated from the relative signal intensities of the endogenous compound and an isotopically labeled standard that has been added to the sample in a known amount (Rittenberg and Foster, 1940; Cohen et al., 1986; Barkawi et al., 2010; Novák et al., 2017). Isotope dilution corrects for any loss of compound occurring during the extraction process after addition of the internal standard, making it a reliable method for quantitation of low-abundance compounds. Quantification of IAA and its intermediates by MS is often used as a means of comparing auxin-related mutants or overexpressor lines to wild type plants. Several studies have reported decreased IAA levels in mutants defective in the synthesis of IPyA from Trp (Stepanova et al., 2008; Tao et al., 2008; Phillips et al., 2011; Stepanova et al., 2011) and monitored accumulation of the proposed intermediates IPyA, IAAld, and TAM in higher order *yucca* mutants and overexpressor lines (Mashiguchi et al., 2011), providing key evidence toward establishing the current understanding of the YUCCA pathway. MS quantitation of the intermediates IAM and IAN in IAOx-related mutants also supplied critical evidence for characterization of the IAOx pathway in *Arabidopsis* (Sugawara et al., 2009). In Chapter 2 (Figures 2-1, 2-7, and 2-8) we use isotope dilution employing a [$^{13}C_6$]IAA internal standard to quantify changes in IAA levels over time in deetiolating hypocotyls and to quantify the effects of chemical inhibitor treatments targeting the YUCCA pathway.

Insight into various auxin biosynthesis pathways comes also from tracing stable isotope labels through intermediates and into IAA itself using MS. Plant tissue may be supplied with one or more labeled precursors, such as indole and/or anthranilate (Rapparini et al., 1999; Epstein et al., 2002; Rapparini et al., 2002), and label incorporation into suspected downstream intermediates is monitored to determine whether synthesis from the labeled precursor has occurred. This approach can also provide information regarding direction of flow and flux through different steps (Sugawara et al., 2009). Furthermore, labeled precursors that are unique to one pathway in particular can be applied to measure contributions of a specific pathway to the IAA pool. Such an approach was taken by Mashiguchi et al.(2011) to demonstrate the YUCCA pathway in *Arabidopsis* was the primary route from supplied Trp: when they fed [$^{13}C_{11}$ $^{15}N_1$]Trp to tryptophan auxotroph mutants to determine which Trp-dependent pathways were being utilized, they observed 95% label incorporation into IPyA and 91% into IAA. Determining utilization of the YUCCA pathway specifically can also be approached by measuring label incorporation from $^{18}O_2$ given that the reaction catalyzed by YUCCA monooxygenases is the only point of oxygen incorporation in IAA biosynthesis (Chen, 2017). A number of labeling studies have also used a combination of Trp and anthranilate to track label incorporation into IAA, and lower levels of label incorporation from Trp relative to upstream precursors provide evidence for a Trp-independent route to IAA biosynthesis (Baldi et al., 1991; Wright et al., 1991; Normanly et al., 1993; Rapparini et al., 1999; Rapparini et al., 2002; Wang et al., 2015).

Tracing stable isotope labels using high resolution accurate mass (HRAM)-MS provides advantages over tracking radioactivity in that isotopes of different elements can be differentiated due to unique mass defects (for example, incorporation of ^{13}C can be differentiated from incorporation of ^{15}N). In Chapter 3, I describe HRAM MS-based methods for stable isotope labeling and analysis of IAA and biosynthetic precursors from multiple labels, including [$^{13}C_3$]Ser, which can be used to trace biosynthesis through Trp specifically (Erdmann and Schiewer, 1971). These methods were used in Chapter 2 to investigate auxin biosynthesis under conditions that promote AR formation and to study the effects of chemical inhibitors as well as light.

Another useful labeling approach in the study of auxin biosynthesis is treatment with deuterium oxide (^2H_2O) (Pengelly and Bandurski, 1983). Although exposure to high concentrations of ^2H_2O has toxic effects on plant growth, treatment with up to 30% ^2H_2O is a uniquely advantageous labeling method because it rapidly diffuses into different subcellular compartments and does not require prior knowledge of precursor compounds. Quantifying deuterium incorporation into IAA over time by MS enables determination of *de novo* biosynthesis rates, as was described by Ljung et al. (2005) for use in a highly sensitive assay for monitoring auxin biosynthesis in roots. Moreover, ^2H_2O can be used as a tracer to determine which pathways are active (Cooney and Nonhebel, 1991) and can also be used in combination with other labeling strategies, as was done by Michalczuk et al. (1992) to monitor isotopic enrichment of IAA from ^2H_2O, [$^2H_5$]Trp, and [$^{15}N_1$]indole in carrot cultures.

Tandem mass spectrometry (MS/MS) provides structural information and can be used to identify potential pathway intermediates (Cooney and Nonhebel, 1989), which should be confirmed using authentic standards to avoid misidentification (Tivendale et al., 2010). Modern approaches utilizing HRAM-MS can screen complex matrices for potential auxin precursors, as in the methods developed by Yu et al. (2014) for identifying a wide range of novel indolic compounds from plant extracts. In Chapter 3 we describe a MS/MS method to identify potential metabolites derived from stable isotope labeled indole using the signature quinolinium ion.

Future work toward understanding routes of auxin biosynthesis will likely utilize increasingly sensitive MS coupled with increasingly sophisticated dissection methods to obtain higher spatial resolution of biosynthesis in different plant tissues to better understand hormonal regulation of developmental events (Ljung et al., 2005; Muñoz-Sanhueza et al., 2018; Shrestha, 2020). One such example of highly tissue-specific auxin analysis is described in Appendix B of this thesis, where we quantified free IAA in laser microdissected samples from poinsettia tissues undergoing abcission (Muñoz-Sanhueza et al., 2018). Advancements in this area would enable a more thorough understanding of the mechanisms controlling root formation, given that localized auxin biosynthesis is the

driving force behind the creation and maintenance of root meristems (Brumos et al., 2018).

Chapter 2: Complexity of indole-3-acetic acid biosynthesis in *Arabidopsis* hypocotyls revealed by multiple precursor labeling

Introduction

Biosynthesis of the plant hormone auxin is a key driver of numerous aspects of plant growth and development (Zhao, 2018), and multiple biosynthetic routes to the auxin indole-3-acetic acid (IAA) have been proposed (Korasick et al., 2013; Tivendale et al., 2014). The most thoroughly characterized of these pathways in *Arabidopsis* involves formation of indole-3-pyruvate (IPyA) from tryptophan (Trp) catalyzed by the TRYPTOPHAN AMINOTRANSFERASE OF ARABIDOPSIS (TAA) aminotransferase family, followed by conversion of IPyA to IAA by YUCCA (EC 1.14.13.168) flavin monooxygenases (Stepanova et al., 2011; Won et al., 2011); it was shown that supplied Trp predominantly labeled IAA through this pathway (Mashiguchi et al., 2011). In another pathway believed to function specifically in *Arabidopsis* and other cruciferous plants, IAA is synthesized through an indole-3-acetaldoxime (IAOx) intermediate (Sugawara et al., 2009). Additional pathways that have yet to be fully characterized are also likely to be active. Genetic and biochemical evidence suggest a Trp-independent pathway proceeding through indole-3-glycerol phosphate (IGP) and indole is an important contributor to embryogenesis in *Arabidopsis* (Wang et al., 2015) and could be a general mechanism of IAA biosynthesis in a number of different species (Baldi et al., 1991; Wright et al., 1991; Michalczuk et al., 1992; Normanly et al., 1993). Other compounds such as tryptamine (TAM) (Winter, 1966; Zhao et al., 2001) and indole-3-acetaldehyde (IAAld) (Seo et al., 1998) have been proposed to function as intermediates in IAA biosynthesis; however, their specific roles remain unclear (Tivendale et al., 2014) (Figure 2-1).

Using a mass spectrometric method that allowed us to simultaneously trace an array of precursors, we monitored the utilization of proposed IAA biosynthesis

intermediates in *Arabidopsis* hypocotyls from three different stable isotope-labeled pathway tracers: [$^{13}C_6$]anthranilate, [$^{15}N_1$]indole, and [$^{13}C_3$]serine. Previous studies have used labeled Trp to track Trp-dependent IAA biosynthesis (Baldi et al., 1991; Wright et al., 1991; Östin et al., 1999; Rapparini et al., 1999); however, treatment with higher concentrations of Trp feedback inhibits anthranilate synthase (EC 4.1.3.27) and anthranilate phosphoribosyltransferase (EC 2.4.2.18) and therefore would be expected to alter the measurement of IAA biosynthesis (Sugimoto and Shiio, 1983; Niyogi and Fink, 1992; Poulsen et al., 1993). To avoid this unintended feedback inhibition and not significantly alter the rate for tryptophan synthase (EC 4.2.1.20) (Anderson et al., 1991), we selected [$^{13}C_3$]serine as a Trp-dependent pathway tracer because the [$^{13}C_3$] label is incorporated into the Trp sidechain by Trp synthase β (Berlyn et al., 1989; Watkins-Dulaney et al., 2020). We used these labeling strategies in combination with IAA biosynthesis inhibitors to gain insight into auxin biosynthesis in deetiolating *Arabidopsis* hypocotyls, in which auxin and light signaling trigger initiation of adventitious root development (Sorin et al., 2005).

A number of chemical inhibitors targeting the YUCCA pathway have been identified, providing tools to decipher the role of this pathway and re-direct auxin biosynthesis toward other possible routes. Yucasin (5–(4–chlorophenyl)-4H-1,2,4–triazole-3–thiol) inhibits YUCCA in a competitive manner, and was shown to reduce IAA content in *Arabidopsis* roots, particularly in *taa1* mutants (Nishimura et al., 2014). AVG (aminoethoxyvinylglycine) and AOPP (amino-oxyphenylpropionic acid), which target pyridoxal phosphate (PLP)-dependent enzymes, including TAA1-mediated conversion of Trp to IPyA, have been shown to decrease endogenous IAA levels in *Arabidopsis* seedlings (Soeno et al., 2010). We used two recently developed YUCCA and AOPP derivatives with increased potency and specificity to target the YUCCA pathway: yucasin DF (YDF), a difluorinated analog of yucasin with increased persistence *in vivo* (Tsugafune et al., 2017) and PVM2153, a pyruvamine found to have an exceptionally strong inhibitory effect on IAA levels *in vivo* without significant inhibition of off-target PLP enzymes such as phenylalanine ammonia-lyase (EC 4.3.1.5) (Narukawa-Nara et al., 2016) (Figure 2-2).

Results

YDF and PVM2153 treatments alter IAA content in hypocotyls

Upon transferring dark-grown seedlings onto media containing 100 μM YDF, free IAA levels in hypocotyls initially decreased and then recovered to control levels over the course of several days in a light-dependent manner. Free IAA levels decreased to 54% and 57% of control after one day in the light and dark, respectively (Figure 2-3a). IAA levels on YDF recovered to control levels by three days in the light; however, this recovery was not observed in the dark. To test whether the observed recovery of IAA levels could have been caused by YDF degradation in the light over the course of several days, a follow-up experiment was conducted in which seedlings were transferred onto freshly prepared media containing YDF after two days. IAA levels again recovered in the presence of freshly prepared YDF (Figure 2-7). Treatment with PVM2153 also altered auxin levels, with free IAA decreasing to 24% of control after one day of treatment in the light (Figure 2-8). IAA levels then increased over the course of four days in the presence of PVM2153 but were slower to recover and did not return to control levels over this time period, as they did on YDF. Interestingly, when both inhibitors were applied together a less pronounced partial recovery in IAA levels, starting after the second day, was noted in the light (Figure 2-3b).

[$^{13}C_6$]Anthranilate and [$^{15}N_1$]Indole labeling

Treating seedlings with a labeling solution containing both [$^{13}C_6$]anthranilate and [$^{15}N_1$]indole for 16 h resulted in significant label incorporation from both stable-labeled precursors into a number of proposed IAA biosynthesis intermediates as well as IAA (Figure 2-4a). After the labeling period, Trp was almost completely (96%) labeled through the two supplied precursors, primarily by [$^{13}C_6$]anthranilate which accounted for 68% of total Trp. The label incorporation pattern into IAA differed from that of Trp, with a much greater proportion of labeled IAA originating from [$^{15}N_1$]indole (52% of labeled IAA versus 29% of labeled Trp). The ratio of [$^{13}C_6$] and [$^{15}N_1$]IAA was also inconsistent

with the labeling pattern of IPyA, which, like Trp, had greater label incorporation from [$^{13}C_6$]anthranilate than [$^{15}N_1$]indole (Figures 2-4 and 2-5).

Several compounds monitored in this study did not incorporate significant [$^{13}C_6$]- or [$^{15}N_1$]-label, suggesting that, in contrast to their proposed roles in IAA biosynthesis, they were either not actively biosynthesized in hypocotyls under our experimental conditions, or their biosynthesis did not proceed at significant rates from indole or anthranilate precursors. For example, unlabeled TAM was consistently present in hypocotyl samples. However, no labeled TAM was detected. IAM was only detected in some samples, and only the unlabeled form. Interestingly, IAOx and IAN, which have been suggested to function in the same biosynthetic pathway as IAM (Sugawara et al., 2009), each incorporated significant label from both tracers.

Treatment with YUCCA pathway inhibitors altered label incorporation into IAA and some biosynthetic intermediates. In the presence of YDF, a greater proportion of IAA was labeled through [$^{15}N_1$]indole compared to [$^{13}C_6$]anthranilate (Figure 2-4a), suggesting that blocking YUCCA activity could shift IAA biosynthesis toward a different route utilizing indole as a precursor. [$^{15}N_1$]Indole and [$^{13}C_6$]anthranilate labeling treatments were also performed in both light and dark conditions after 1 and 3 days of YDF treatment (Figure 2-5) to provide insight into IAA synthesis at the time points at which we observed reduction and recovery of free IAA levels. In these experiments, we also observed a higher ratio of [$^{15}N_1$] to [$^{13}C_6$]-enrichment into IAA in the presence of YDF (Figure 2-5a). The labeling pattern of Trp changed very little with the addition of any of the three inhibitor treatments, with [$^{13}C_6$] and [$^{15}N_1$] accounting for 66-68% and 28-30% respectively of all Trp in all treatments (Figure 2-4a). The differences between labeling patterns of Trp and IAA present in the control treatment were more pronounced under the inhibitor treatments: 69%, 57%, and 83% of labeled IAA was labeled through [$^{15}N_1$]indole in the YDF, PVM2153, and YDF + PVM2153 treatments, respectively, while consistently less than one-third of the total labeled Trp contained the [$^{15}N_1$]-label.

YUCCA pathway inhibitors more severely impacted the labeling patterns of IAA and IPyA than other compounds that were monitored. Label incorporation from both [$^{15}N_1$]indole and [$^{13}C_6$]anthranilate tracers into IPyA was significantly reduced in the

YDF+PVM2153 combination treatments ($p < 0.05$, n=3, Student's *t* test). In the presence of both inhibitors, label incorporation into IAA dropped to 2.1% from [$^{13}C_6$]anthranilate and 10% from [$^{15}N_1$]indole (Figure 2-4a), with 88% of IAA remaining unlabeled under these conditions in contrast to only 26% unlabeled in the mock treatment (Figure 2-4b).

[$^{13}C_3$]Serine labeling

[$^{13}C_3$]Serine was supplied at a higher concentration (3 mM) than [$^{13}C_6$]anthranilate and [$^{15}N_1$]indole treatments in order to obtain a detectable level of label incorporation into IAA after 16 h; however, at this level it provided an effective method to trace Trp-dependent biosynthesis. In the absence of YUCCA pathway inhibitors, similar levels of [^{13}C]-incorporation were observed into Trp (25-35%) and IPyA (24-30%). Label incorporation into IAA was lower, ranging from 9.4 to 14% (Figure 2-6a-c).

YDF treatment decreased [$^{13}C_3$]-label incorporation into IAA from 13% in the control treatment to 4.8% but did not substantially change label incorporation into IPyA or Trp, indicating that YDF effectively targets YUCCA activity catalyzing the formation of IAA from IPyA. Similarly, PVM2153 treatment reduced label incorporation into IPyA (24% in control to 11%) and IAA (9.4% to 2.1%) but did not significantly change Trp labeling. Incorporation of [^{13}C] from serine into IAA and IPyA was further reduced in the YDF+PVM2153 inhibitor treatment, with no detectable level of [^{13}C]-labeled IPyA present and only 1.1% [^{13}C]-enrichment in IAA.

Discussion

The aim of this study was to trace active routes of auxin biosynthesis in *Arabidopsis* hypocotyls during light-induced adventitious rooting using multiple stable isotope labeled precursors, and to characterize changes in utilization of different intermediates when key steps in the YUCCA pathway are inhibited. We employed three stable isotope tracers: [$^{13}C_6$]anthranilate, [$^{15}N_1$]indole, and [$^{13}C_3$]L-serine, which enter the auxin biosynthetic pathway at different points upstream of IAA. A possible expected

result, should the simple case that a single tryptophan pathway predominates, would be equivalent results with each utilized precursor. However, these three compounds, which are not known to significantly feedback inhibit the major enzymes of the tryptophan pathway, produced unique labeling patterns into several proposed intermediates, and labeling patterns were differentially affected by light treatments and also by IAA biosynthesis inhibitors. Labeled Trp has previously been used in a number of studies, either on its own (Mashiguchi et al., 2011) or in combination with indole (Michalczuk et al., 1992; Östin et al., 1999; Rapparini et al., 2002) or anthranilate (Wright et al., 1991; Normanly et al., 1993; Rapparini et al., 1999), to trace biosynthesis of IAA and pathway intermediates. However, exogenous Trp would be expected to increase free Trp levels *in vivo* and thus feedback inhibit both anthranilate synthase and anthranilate phosphoribosyltransferase (Matsui et al., 1987; Li and Last, 1996), causing an overestimate of Trp utilization in auxin biosynthesis. We employed [$^{13}C_3$]Ser, with which Trp synthase β catalyzes a condensation with indole to produce [$^{13}C_3$]Trp (Berlyn et al., 1989), to avoid feedback inhibition while monitoring Trp-dependent IAA biosynthesis. A similar approach was taken decades ago by Erdmann and Schiewer (Erdmann and Schiewer, 1971) in a double labeling study using [^{3}H]Ser and [$^{14}C_1$]indole to quantify contributions of Trp to IAA biosynthesis. Serine has not been commonly used in studies of IAA biosynthesis, however, and this may be due to the observation that the rate of metabolic flux through the serine pool is high relative to that for Trp (Yang et al., 2010) that necessitated using higher levels of the supplied amino acid. Under our conditions, incubation with [$^{13}C_3$]Ser resulted in significant label incorporation into Trp, IPyA, and IAA. However, in the presence of both YDF and PVM2153, [^{13}C]-enrichment into IAA was nearly eliminated (Figure 2-6c), suggesting near complete inhibition of IAA biosynthesis through [$^{13}C_3$]Ser-derived labeled Trp. IAA labeling through [$^{13}C_6$]anthranilate was similarly reduced by 94% in the YDF + PVM2153 treatment (Figure 2-4a), although 66% of Trp was [$^{13}C_6$]-labeled under these conditions, and free IAA levels were only reduced by 37% (Figure 2-3b).

The *Arabidopsis* genome contains multiple *YUCCA* genes and higher order *yucca* mutants can have severe developmental defects (Cheng et al., 2006, 2007; Müller-Moulé et al., 2016), making it difficult to study the effects of fully blocking this pathway using

targeted knockout mutations. Chemical inhibitors allow pathway steps to be blocked at a particular developmental time point or for an experimental interval, as was done in this study to inhibit the YUCCA pathway when etiolated seedlings were transferred into light. Several chemical inhibitors have been shown to significantly decrease IAA levels *in vivo*. For example, treatment with the YUCCA inhibitor yucasin decreased IAA levels in maize coleoptile tips after a 1.5 h treatment to only 15-25% of control levels (Nishimura et al., 2014). The physiological effects of yucasin were additive with kynurenine (Kyn), a competitive inhibitor of AtTAA1, contributing to an apparent IAA-deficient "auxin-null" phenotype in *Arabidopsis* (He et al., 2011). YDF was discovered as a more potent inhibitor of IAA biosynthesis *in planta* than yucasin due to its higher persistence *in vivo* (Tsugafune et al., 2017). An inhibitor cocktail consisting of YDF combined with TAA1 inhibitors Kyn and AOPP was used in the *Arabidopsis cyp79b2 79b3* mutant to achieve near-complete petiole growth inhibition, presumably via suppression of the known pathways through IPyA and IAOx (Tsugafune et al., 2017). Although plant development was severely impaired, a small amount of growth still occurred under these conditions and could be further reduced by chemical inhibition of auxin perception, which was attributed to perhaps the presence of other uninhibited routes to IAA or potentially to the action of other auxin forms such as phenylacetic acid (PAA). Extreme reduction in IAA levels was also reported after treatment with PVM2153, one of a number of compounds identified in a screen for more potent derivatives of AOPP. PVM2153 showed much greater efficacy than AOPP *in vivo*, reducing IAA levels immediately following a 3 h treatment by approximately 90% in *Arabidopsis* seedlings (Narukawa-Nara et al., 2016).

In the present study, treatment with either YDF or PVM2153, or both, substantially reduced free IAA levels in *Arabidopsis* hypocotyls within one day (Figures 2-3, 2-7, and 2-8), indicating the YUCCA pathway is likely a significant regulator of IAA levels in this tissue. IAA and IPyA showed less label incorporation from indole and anthranilate in the presence of YUCCA pathway inhibitors (especially when the treatment was with both YDF and PVM2153), demonstrating that IAA biosynthesis from these precursors was largely blocked by the YDF and PVM2153 treatments (Figure 2-4). However, IAA levels recovered partially or fully to control levels over a period of 3-4 days in a light-dependent manner (Figures 2-3, 2-7, and 2-8), suggesting mechanisms

other than YUCCA-mediated IAA biosynthesis are activated in the light. The proportion of unlabeled IAA exceeded the proportion of unlabeled Trp (Figure 2-4b), and one possible source of the observed unlabeled IAA is the release of IAA from "storage" compounds such as indole-3-butyric acid (IBA), which serves as an important precursor for IAA during a number of developmental processes (Strader et al., 2011), or conjugates with amino acids, sugars, or proteins that are hydrolyzed to make free IAA available (Bialek et al., 1983; Seidel et al., 2006; Korasick et al., 2013). Although the entire plant was labeled under our experimental conditions we also cannot exclude transport of unlabeled IAA from other tissues, with lower rates of IAA turnover, into the hypocotyl that may also play a role in the recovery of auxin levels, as transport has been shown to be a major contributor to auxin homeostasis (Ding et al., 2012; Liu et al., 2012).

Labeling experiments with [$^{15}N_1$]indole and [$^{13}C_6$]anthranilate resulted in Trp becoming primarily labeled through [$^{13}C_6$]anthranilate while a greater proportion of IAA was labeled through [$^{15}N_1$]indole in the light (Figures 2-4 and 2-5). This became more pronounced in the presence of YUCCA pathway inhibitors: when YDF was supplied in the media, label incorporation from [$^{15}N_1$]indole into IAA was more than twice that of [$^{13}C_6$]anthranilate, while Trp labeling remained relatively consistent with a majority of Trp incorporating the [$^{13}C_6$] label from [$^{13}C_6$]anthranilate (Figures 2-4 and 2-5). Both 1 and 3 d periods of YDF treatment increased the proportion of IAA labeling occurring via [$^{15}N_1$]indole relative to [$^{13}C_6$]anthranilate (Figure 2-5a), even though IAA levels were much higher at the 3 d time point (Figure 2-3a). These results indicate one or more of three hypotheticals may occur: **1)** IAA possibly is not synthesized from a single Trp pool, suggesting the possibilities that multiple pools of Trp exist; **2)** IAA is potentially preferentially synthesized from one or more specific pools of Trp (Cooney and Nonhebel, 1991; Rapparini et al., 1999; Nonhebel, 2015), and/or **3)** that a portion of IAA is possibly synthesized via a Trp-independent route through indole (Wright et al., 1991; Normanly, 2010).

The possibility that IAA biosynthesis draws from a Trp pool with higher [^{15}N]-enrichment from [$^{15}N_1$]indole than the total Trp pool draws from evidence from earlier studies supporting utilization of a specialized Trp pool in IAA biosynthesis. For example,

Cooney and Nonhebel (Cooney and Nonhebel, 1991) observed greater label incorporation into IPyA than Trp or IAA during a 10 h labeling period in 30% $^{2}H_2O$, and proposed that IPyA biosynthesis occurs from a Trp pool with faster synthesis than the overall rate for Trp. Our data, however, do not support this conclusion given that after a 16 h labeling treatment the majority of Trp was labeled through [$^{15}N_1$]anthranilate (and was therefore newly synthesized), which was not reflected in the labeling pattern of IAA. Additional prior evidence for utilization of restricted Trp pools in IAA biosynthesis comes from labeling experiments employing both [$^{2}H_5$]Trp and [$^{15}N_1$]anthranilate by Rapparini et al. (1999), showing that IAA became relatively more enriched in [$^{2}H_5$]-label while the total Trp pool had greater enrichment of [^{15}N]. These data suggest IAA is synthesized preferentially from supplied [$^{2}H_5$]Trp over [$^{15}N_1$]Trp newly synthesized from [$^{15}N_1$]anthranilate. The observed discrepancies in labeling patterns between Trp and IAA in the present study could also be explained by uneven distribution of labeled precursors into different tissue types within the hypocotyl having different rates of Trp-dependent IAA biosynthesis. With indole and anthranilate differing in polarity, it is possible that [$^{15}N_1$] indole preferentially labels IAA by diffusing more readily into tissues with higher expression of Trp aminotransferases or YUCCA enzymes, which are known to have highly variable expression in different tissues (Cheng et al., 2006; Yang et al., 2014; Nonhebel, 2015). Separation of subcellular metabolite pools may also contribute to labeling inconsistencies between Trp and IAA. Tryptophan aminotransferases and YUCCA monooxygenases have been shown to localize both to the endoplasmic reticulum and cytosol (Kriechbaumer et al., 2012; Kriechbaumer et al., 2017), while Trp synthesis occurs in chloroplasts (Zhao and Last, 1995), thus the rate at which different labeled precursors are imported into various subcellular compartments could affect the observed labeling patterns. However, uneven distribution of labeled precursors into tissues or subcellular regions with different rates of IAA biosynthesis fails to explain our observation that an even greater proportion of IAA synthesis occurs through [$^{15}N_1$]indole relative to [$^{13}C_6$]anthranilate in the presence of YDF. Treatment with YDF alone slightly increased label incorporation from [$^{15}N_1$]indole into IAA (Figures 2-4 and 2-5), but reduced label incorporation from [$^{13}C_3$] serine by 62% (Figure 2-6a). Taken together with the observation that IAA levels increased over time in the light during inhibitor

treatments (Figures 2-3, 2-7, and 2-8), these results suggest a Trp-independent route of IAA biosynthesis using indole as a precursor is active in de-etiolating hypocoytls and may be utilized more heavily when the YUCCA pathway is inhibited.

Two of the proposed IAA biosynthesis intermediates we monitored in this study – TAM and IAM – did not incorporate detectable label from either [$^{13}C_6$]anthranilate or [$^{15}N_1$]indole, indicating that their proposed branches of IAA biosynthesis were either not active in hypocotyls under our conditions or did not proceed from indole or anthranilate precursors. TAM, which we found to be consistently present but not labeled, was previously considered as a possible intermediate in the YUCCA pathway before YUCCA enzymes were known to catalyze the formation of IAA from IPyA (Zhao et al., 2001; Won et al., 2011). TAM has been shown to be synthesized via Trp, but its role in IAA biosynthesis has not been determined (Tivendale et al., 2014). Quittenden et al. (Quittenden et al., 2009) reported that a majority of TAM in pea roots was [$^{2}H_5$]-labeled after incubation with [$^{2}H_5$]Trp, and that a small amount of IAA contained the [$^{2}H_5$]-label after treatment with [$^{2}H_5$]TAM (Quittenden et al., 2009). Cooney and Nonhebel monitored [^{2}H]-incorporation into TAM from $^{2}H_2O$ in tomato shoots and observed increased label incorporation into TAM over time, even as [^{2}H]-incorporation into Trp and IAA eventually declined. This led them to conclude TAM was unlikely to be a major contributor to IAA biosynthesis, and that it could be synthesized from a smaller pool of newly synthesized Trp distinct from that used in IAA biosynthesis (Cooney and Nonhebel, 1991). In contrast, our results in *Arabidopsis* hypocotyls suggest TAM biosynthesis is unlikely to proceed via newly synthesized Trp, as Trp became almost completely labeled through [$^{13}C_6$]anthranilate and [$^{15}N_1$]indole during the labeling treatment while no detectable label was incorporated into TAM (Figures 2-4 and 2-5). The most likely explanation for this observed result is a pool of TAM with very slow turnover.

Isotopic labeling experiments have shown IAM to be a potential IAA biosynthetic intermediate in the IAOx pathway in *Arabidopsis*, through which Trp is converted to IAOx by CYP79B2 and CYP79B3, and IAOx is then converted to IAM and IAN, which can each be converted to IAA (Sugawara et al., 2009). IAM was not consistently present

at detectable levels in our [$^{13}C_6$]anthranilate and [$^{15}N_1$]indole labeling samples, and no label was detected in samples containing measureable IAM. Interestingly, IAOx and IAN both contained significant [$^{13}C_6$]- and [$^{15}N_1$]-labels (Figures 2-4 and 2-5), suggesting the IAOx pathway may bypass IAM as an intermediate in *Arabidopsis* hypocotyls under our conditions.

In summary, dark-grown *Arabidopsis* hypocotyls transferred to red light, conditions that induce adventitious root formation, increase in their endogenous IAA levels over a 4-day period relative to hypocotyls that remain in darkness. Chemical inhibition of the two enzymes of the YUCCA pathway decreases the red light-induced IAA increase over the dark control, and also alters IAA labeling in experiments using multiple labeled precursors so that IAA becomes preferentially labeled through indole relative to anthranilate. Labeling through indolic intermediates of proposed Trp to IAA pathways do not account for the IAA labeling pattern measured, suggesting a route independent of Trp/Ser is likely responsible for the label incorporation measured.

Methods

Plant material and growth conditions

Wild-type Columbia-0 ecotype *Arabidopsis* seeds were surface sterilized by soaking in 20% commercial bleach (Clorox, 6% sodium hypochlorite) for 5 minutes and then rinsing four times with sterile water. Seeds were then imbibed in a sterile solution of 100 μM GA_4 (Valent BioSciences, Libertyville, IL) for 5-10 days at 4°C to promote uniform germination. Seeds were sown in a single row on a 9 cm × 9 cm square of 20 μm nylon mesh (Sefar) atop 0.5X strength Murashige and Skoog (MS) medium with vitamins (Phytotech) containing 1% sucrose and 1% agar (pH 5.7) in 10 cm × 10 cm square Petri plates (Fisherbrand). Plates were placed vertically in a dark room at 20°C for 7 days.

Inhibitor treatment

Nylon mesh and etiolated seedlings were transferred onto 0.5X strength MS media containing 100 μM 5-[2,6-difluorophenyl]-2,4-dihydro-[1,2,4]-triazole-3-thione

(YDF; CAS# 1094690-87-5, custom synthesis by LabSeeker, Wujiang City, China; dissolved in dimethyl sulfoxide and filter sterilized before adding to media) and/or 30 μM 3,4-dichloro-α-[(1,3-dihydro-1,3-dioxo-2H-isoindol-2-yl)oxy]-benzenepropanoic acid, methyl ester (PVM2153/KOK2153; CAS# 1394950-62-9, LabSeeker; dissolved in acetonitrile and filter sterilized), or solvent mock treatment. Plates were placed vertically in a Conviron PGR15 growth chamber equipped with Heliospectra L4A Series 10 lamps, using a 16 h photoperiod and a constant temperature of 21°C. Only the 660 nm LEDs were used, providing 135 μM m^{-2} sec^{-1} red light.

Stable isotope labeling

After three days of growth on inhibitor or mock treatment in the growth chamber, seedlings were bathed (3 mL per plate) for 16 h in labeling solution: 3 mM [$^{13}C_3$]Ser (Cambridge Isotope Laboratories) or 500 μM [$^{13}C_6$]anthranilate (Sigma-Aldrich) plus 500 μM [$^{15}N_1$]indole (Cambridge Isotope Laboratories) in water with 0.5X strength MS salts.

Sample collection

Petri plates were placed on ice and hypoctoyls were dissected with a scalpel. Hypocotyl tissue (5-50 mg) was flash frozen with liquid nitrogen and stored at -80°C until extraction.

Extraction and analysis of IAA and biosynthesis intermediates

For analysis of proposed IAA biosynthesis intermediates (Trp, TAM, IPyA, IAAld, IAOx, IAN, and IAM), samples of 20-50 mg plant tissue were homogenized for 4 min using a Qiagen Mixer-Mill and three 1.6 mm stainless steel balls with 40-100 μL of buffer containing 100 mM methoxylamine hydrochloride (for derivatization of IPyA and IAAld to generate their oximes (IPyA-MeOx and IAAld-MeOx)), 35% 0.2 M imidazole solution in water (pH 7.0), and 65% isopropanol. Homogenized samples were then set on ice for 50 minutes, diluted 10-fold with water, centrifuged to remove solids, and loaded

onto a SPE spin column (TopTips) containing Rensa HLB 2001 resin (MIP Technologies AB) conditioned with acetonitrile followed by 20% acetonitrile in water. Spin columns were washed with 5% acetonitrile and eluted with 80% acetonitrile. Eluted samples were dried to approximately 20 µL using a vacuum concentrator (SpeedVac) prior to LC-MS/MS analysis with a Dionex Ultimate 3000 RSLC HPLC coupled to a hybrid quadrupole Orbitrap Q Exactive mass spectrometer with a heated electrospray ionization (HESI) source (Thermo Scientific). 5-10 µL of prepared sample was injected onto a 50 × 2.1 mm Force C18 HPLC column (Restek) with 0.2 µm precolumn filter (UltraShield). Samples were analyzed using the following mobile phase gradient of 0.1% formic acid in water (Optima LC/MS grade) (A) and 0.1% formic acid in acetonitrile (HPLC Plus, ≥99.9%) (B): 5 %B (-2-1 min), 5-15 %B (1-3 min), 15-30 %B (3-3.5 min), 30 %B (3.5-5 min), 30-39 %B (5-7.5 min), 39-80 %B (7.5-8 min), 80% B (8-10 min) at a flow rate of 0.4 mL per min. Mass spectra were collected using a staggered series of full MS-SIM scans with different scan ranges to target compounds of interest and their isotopomers: 200-213.5 *m/z* (0-2.3 min, Trp), 156-173 *m/z* (2.3-3 min, TAM), 133-148 *m/z* (3-3.85 min, ANT), 170-186 *m/z* (3.5-5.4 min, IAM and IAOx), 152-170 *m/z* (5.25-6.2 min, IAN), 200-245 *m/z* (5.4-6.5 min, IPyA-MeOx), 184-198.5 *m/z* (6.5-8.5 min, IAAld-MeOx). HESI source conditions were as follows: sheath nitrogen gas flow rate 30 units, aux nitrogen gas flow rate 20 units, spray voltage 4 kV, capillary temperature 305 ℃, S-lens RF level 50, aux gas heater temperature 300 ℃. Orbitrap resolution was set to 70,000 full width at half maximum (FWHM) with maximum ionization time of 200 milliseconds and automatic gain control (AGC) of 5×10^5. Retention times and exact mass data from unlabeled compounds were matched to authentic standards that were analyzed using identical LC-MS parameters. Exact mass values of standards, endogenous unlabeled compounds, and labeled isotopomers were within 0.0015 *m/z* of calculated values listed in Table 2-1.

Samples for IAA quantitation by LC-MS/MS were prepared and analyzed essentially as described (Tang et al., 2019). Data points were removed if recovery of internal standard was too low for accurate quantitation, or if the measurement deviated from the mean by more than 10 standard deviations (presumably due to contamination).

Figures

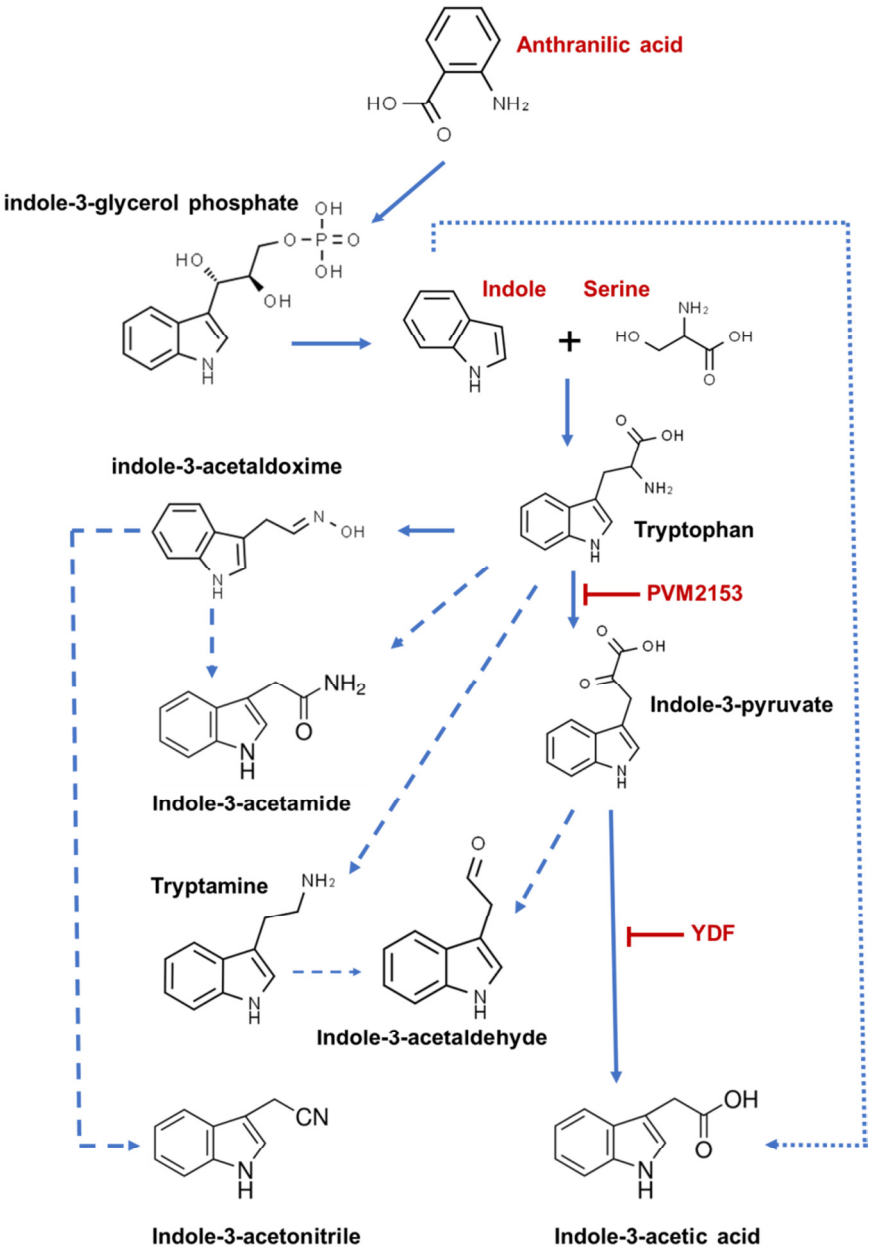

Figure 2-1: Proposed IAA biosynthesis pathways in *Arabidopsis*. Genetically defined pathways are indicated with solid arrows; other proposed pathways are shown with dashed arrows. Reactions inhibited by pyruvamine 2153 (PVM2153) and yucasin DF (YDF) are shown with red lines. Stable isotope labeled compounds used in the experiments (anthranilic acid, serine and indole) are labeled with red type.

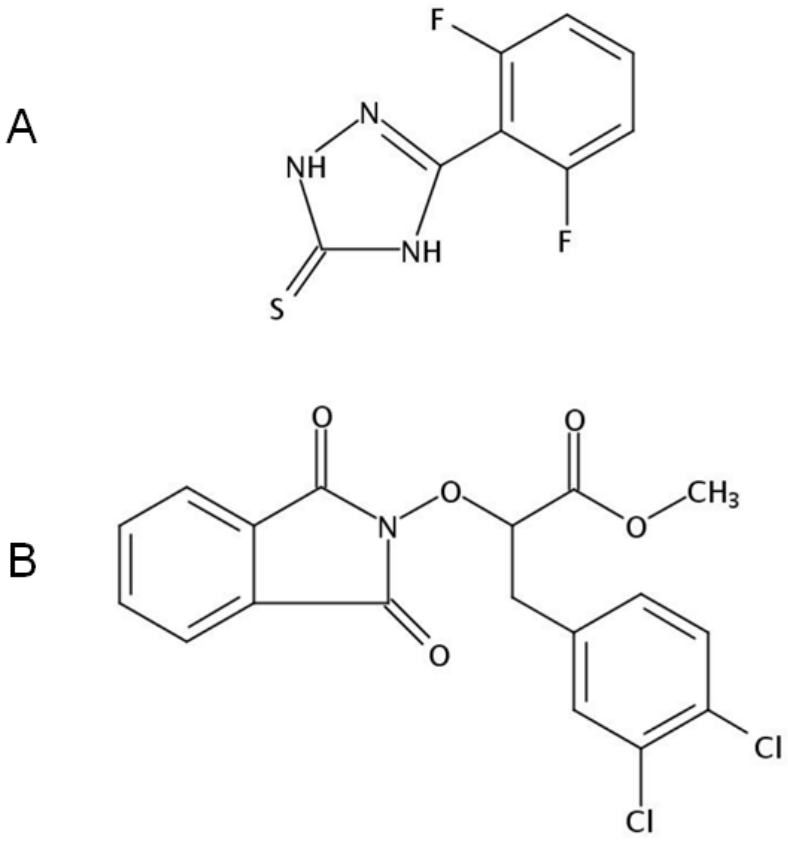

Figure 2-2: Chemical structures of IAA biosynthesis inhibitors. Yucasin DF (YDF; 5-[2,6-difluorophenyl]-2,4-dihydro-[1,2,4]-triazole-3-thione; CAS# 1094690-87-5) (A) and pyruvamine 2153 (PVM2153; 3,4-dichloro-α-[(1,3-dihydro-1,3-dioxo-2H-isoindol-2-yl)oxy]-benzenepropanoic acid, methyl ester; CAS# 1394950-62-9) (B)

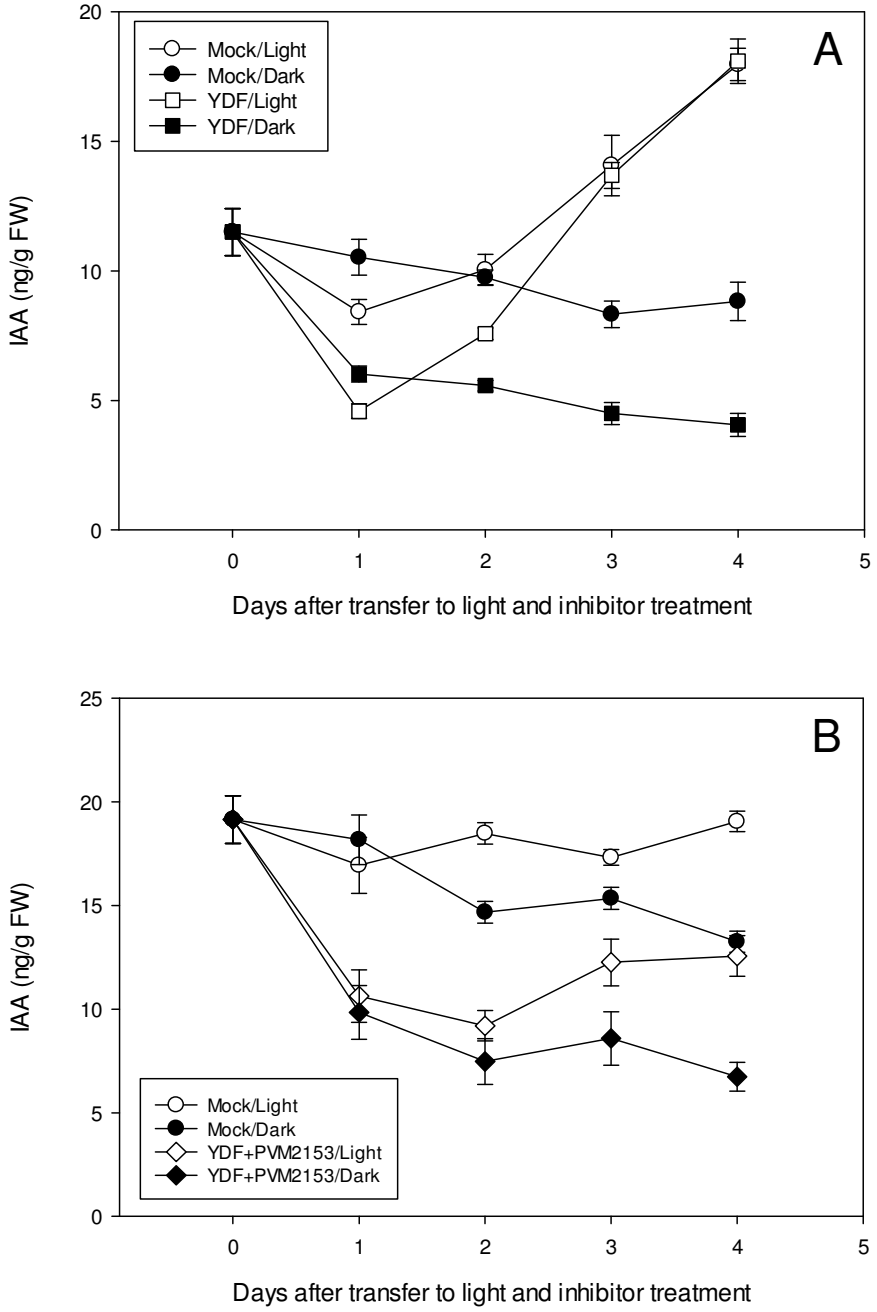

Figure 2-3: Endogenous IAA content in *Arabidopsis* hypocotyls. Seedlings were grown in the dark for 7 d, then transferred onto media containing 100 µM YDF or DMSO (mock) (A), or a combination of 100 µM YDF and 30 µM PVM2153 or DMSO and acetonitrile (mock) (B), and placed in growth chambers where they were exposed to either a 16 h photoperiod of red light (660 nm, 135 µmol m^{-2} s^{-1}) or kept in continued darkness. 5-15 mg samples of hypocotyl tissue were collected immediately before and

each of the 4 days after transfer. Free IAA levels were quantified by isotope dilution LC-MS/MS using [$^{13}C_6$]IAA internal standard. Each point represents the mean of 3-6 biological replicates; error bars represent SE. 10 ng IAA per g FW corresponds to approximately 60 nM.

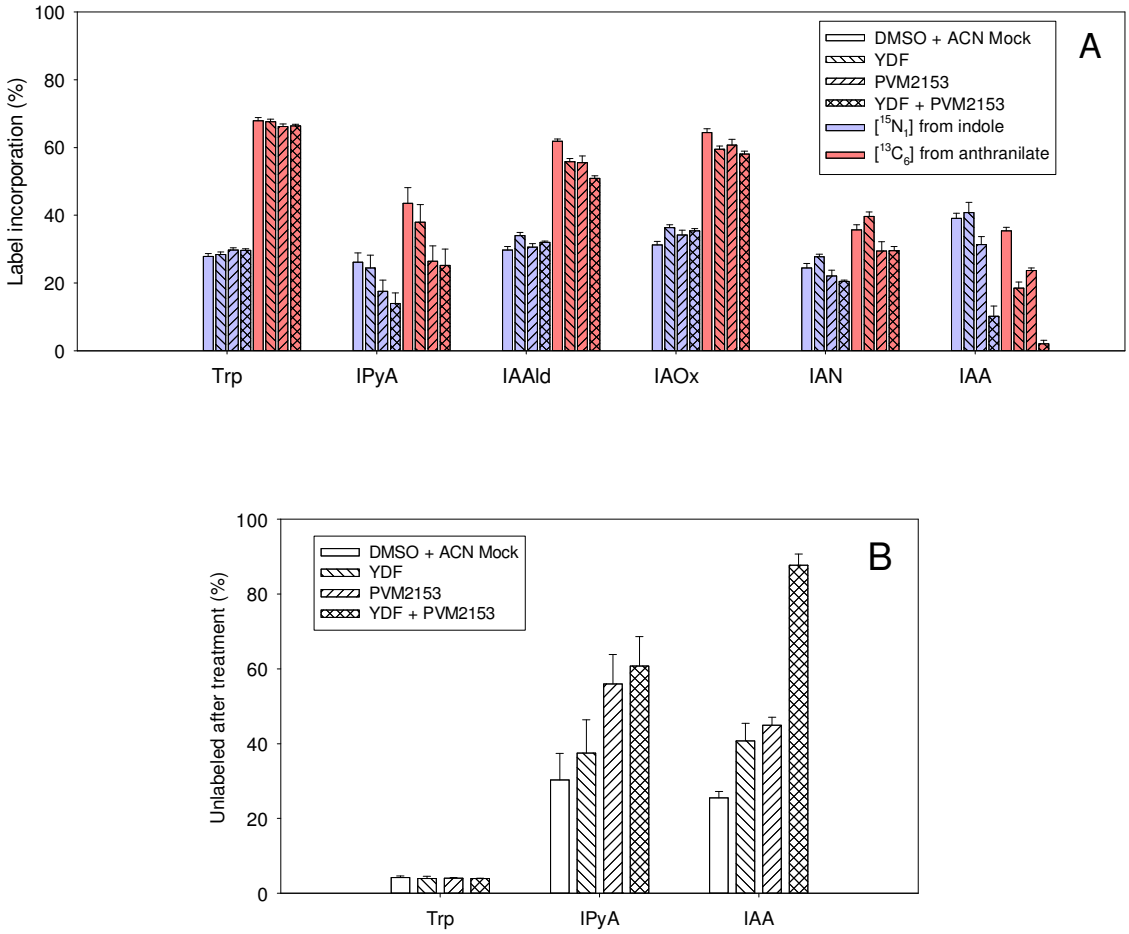

Figure 2-4: [$^{15}N_1$]Indole and [$^{13}C_6$]anthranilate labeling of IAA precursors in *Arabidopsis* hypocotyls in the presence of YUCCA pathway inhibitors. Seedlings were grown in the dark for 7 d, then transferred onto media containing 100 µM YDF and/or 30 µM PVM2153, or DMSO and acetonitrile (mock). Seedlings were then exposed to a 16 h photoperiod of red light (660 nm, 135 µmol m^{-2} s^{-1}) for 3 days, and then treated by applying a solution containing 500 µM [$^{15}N_1$]indole and 500 µM [$^{13}C_6$]anthranilate for 16 hours under red light. Samples containing approximately 20 hypocotyls were collected for LC-MS analysis of isotopic enrichment of IAA and IAA biosynthesis intermediates. Data are expressed as the percentage of total detected compound containing the specified isotopic label (A), or for Trp, IPyA, and IAA the percentage of compound remaining unlabeled after treatment (B) and have been corrected for the natural abundance of ^{15}N. Each bar represents the mean of 5-7 biological replicates; error bars represent SE.

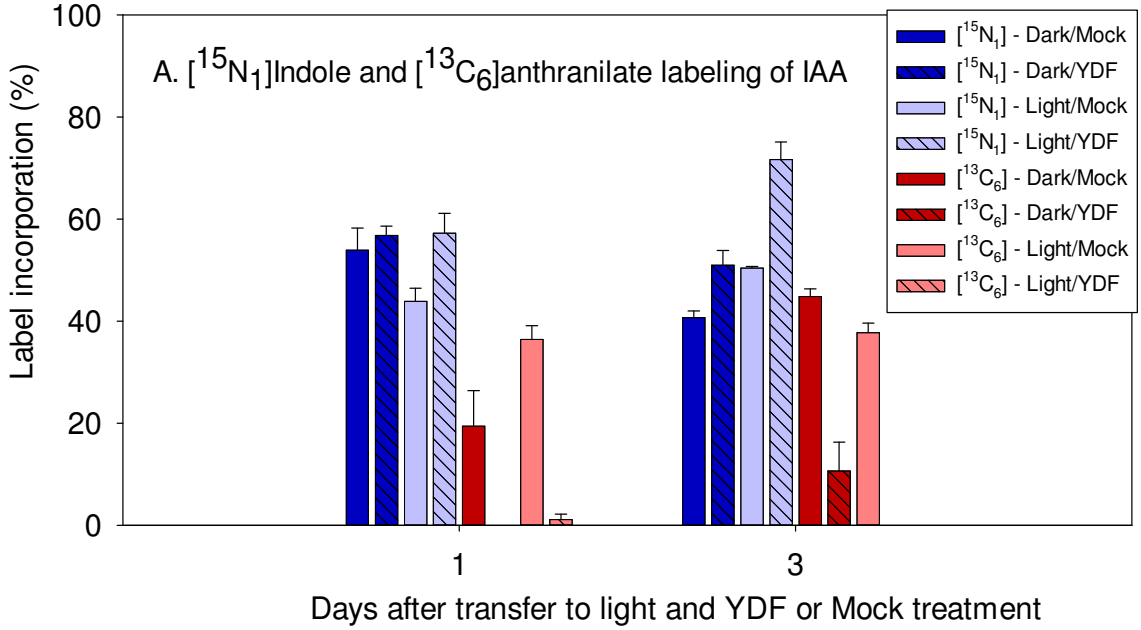
A. [15N1]Indole and [13C6]anthranilate labeling of IAA
Label incorporation (%)
100
80
60
40
20
0
1
3
Days after transfer to light and YDF or Mock treatment
[15N1] - Dark/Mock
[15N1] - Dark/YDF
[15N1] - Light/Mock
[15N1] - Light/YDF
[13C6] - Dark/Mock
[13C6] - Dark/YDF
[13C6] - Light/Mock
[13C6] - Light/YDF

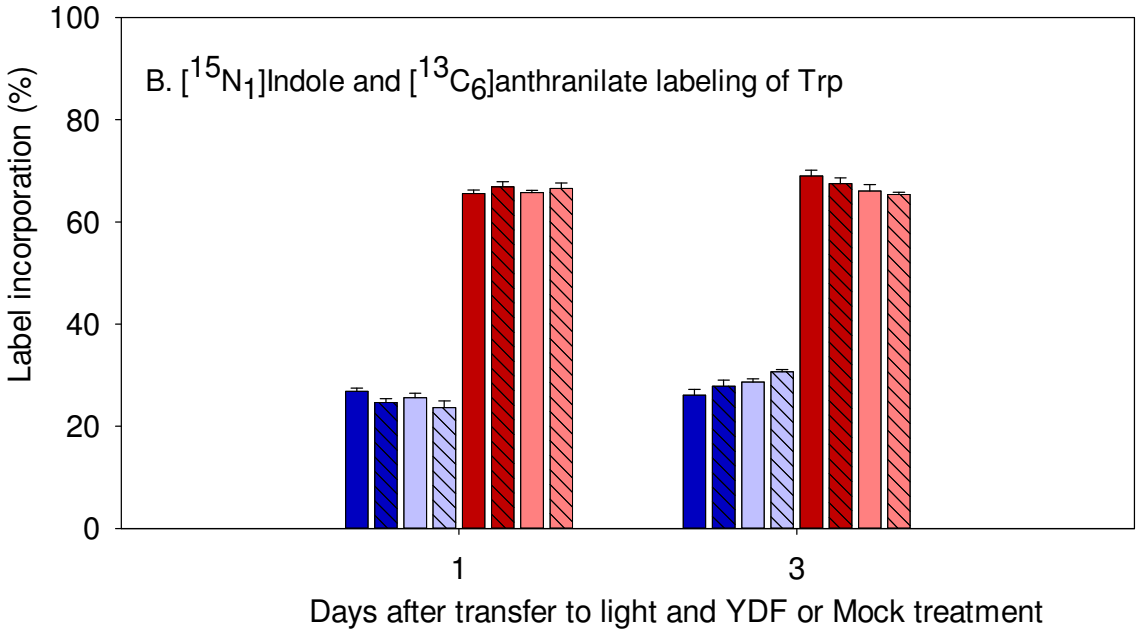
B. [15N1]Indole and [13C6]anthranilate labeling of Trp
Label incorporation (%)
100
80
60
40
20
0
1
3
Days after transfer to light and YDF or Mock treatment

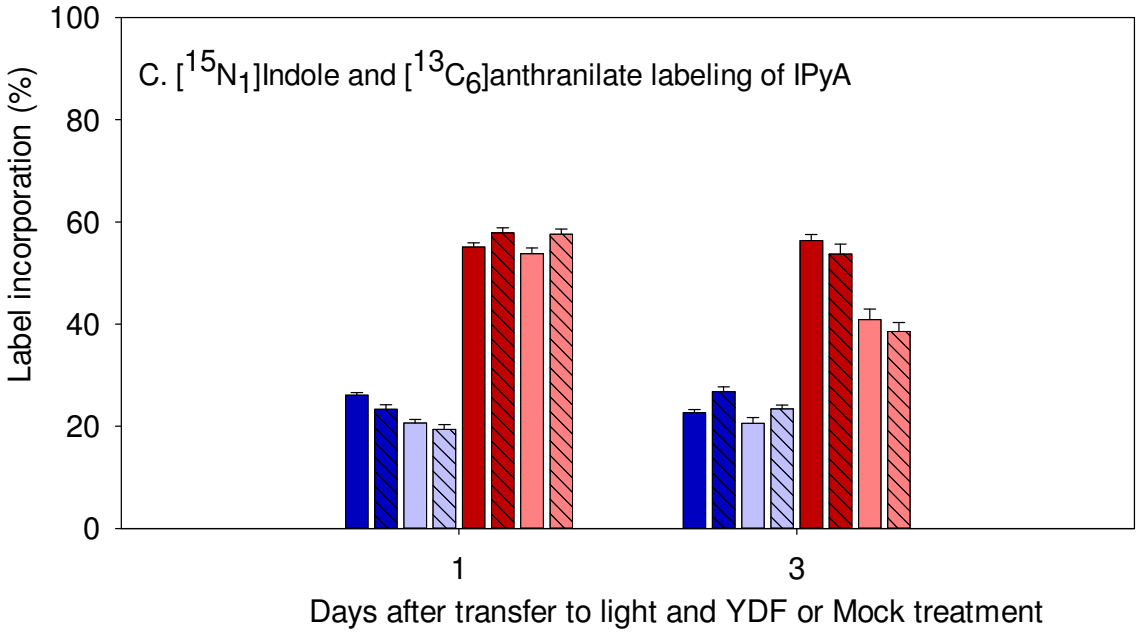
C. [15N1]Indole and [13C6]anthranilate labeling of IPyA
Label incorporation (%)
100
80
60
40
20
0
1
3
Days after transfer to light and YDF or Mock treatment

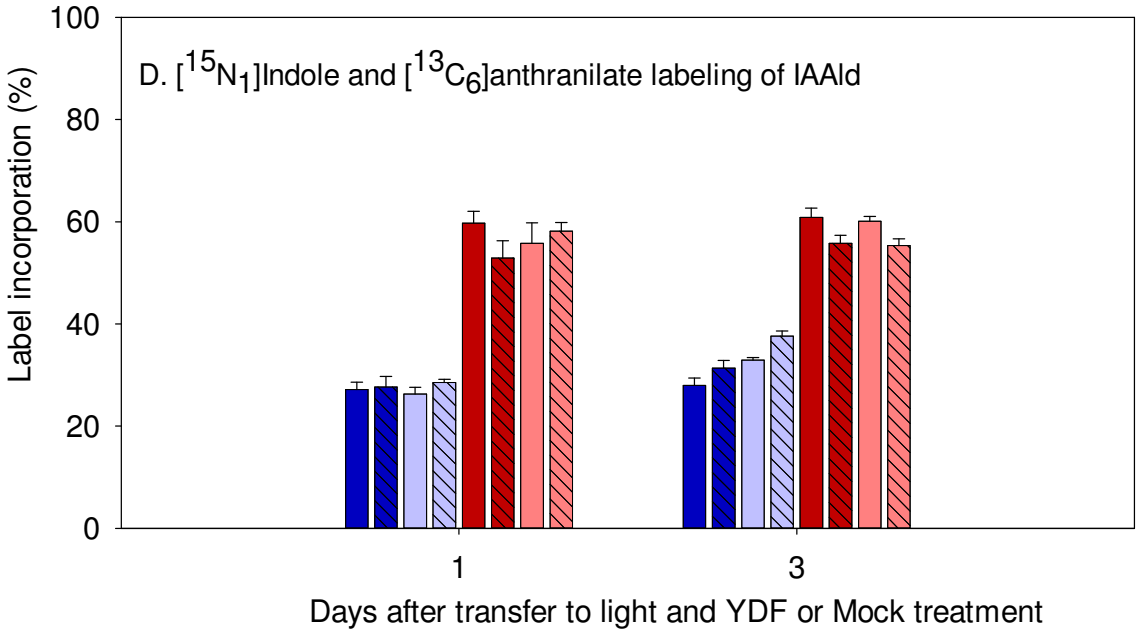
D. [15N1]Indole and [13C6]anthranilate labeling of IAAld
Label incorporation (%)
100
80
60
40
20
0
1
3
Days after transfer to light and YDF or Mock treatment

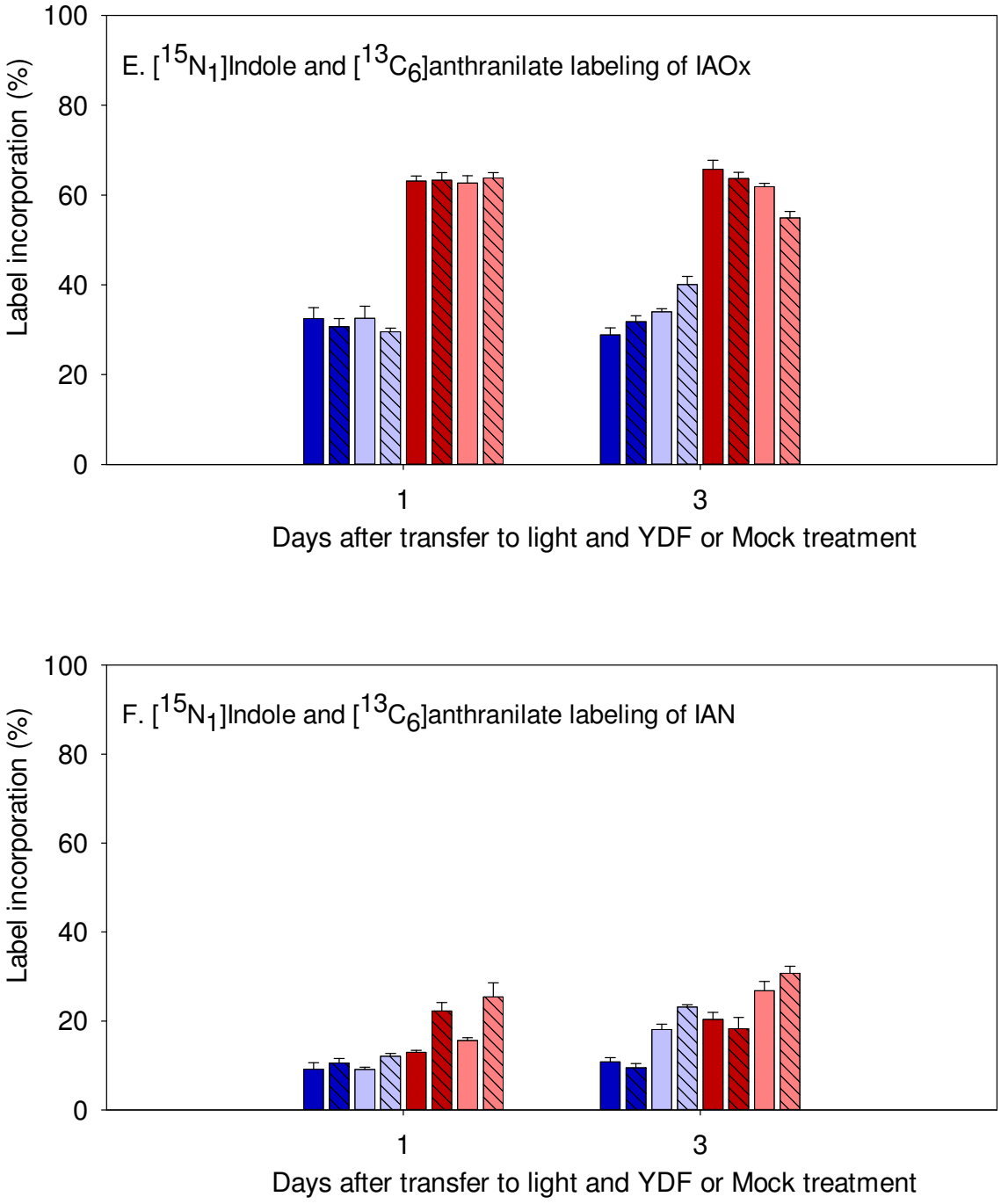

Figure 2-5: [$^{15}N_1$]Indole and [$^{13}C_6$]anthranilate labeling of IAA precursors in *Arabidopsis* hypocotyls treated with YDF under light and dark. Seedlings were grown in the dark for 7 d, then transferred onto media containing 100 μM YDF or DMSO (mock) and exposed to a 16 h photoperiod of red light or continued darkness for 1 or 3

days. Seedlings were then treated by applying a solution containing 500 μM [$^{15}N_1$]indole and 500 μM [$^{13}C_6$]anthranilate for 16 hours. Samples containing approximately 20 hypocotyls were collected for LC-MS analysis of isotopic enrichment of IAA (A) and potential IAA biosynthesis intermediates: Trp (B), IPyA (C), IAAld (D), IAOx (E), IAN (F). Data are expressed as the percentage of total detected compound containing the specified isotopic label and have been corrected for the natural abundance of ^{15}N. Each bar represents the mean of 4 biological replicates; error bars represent SE.

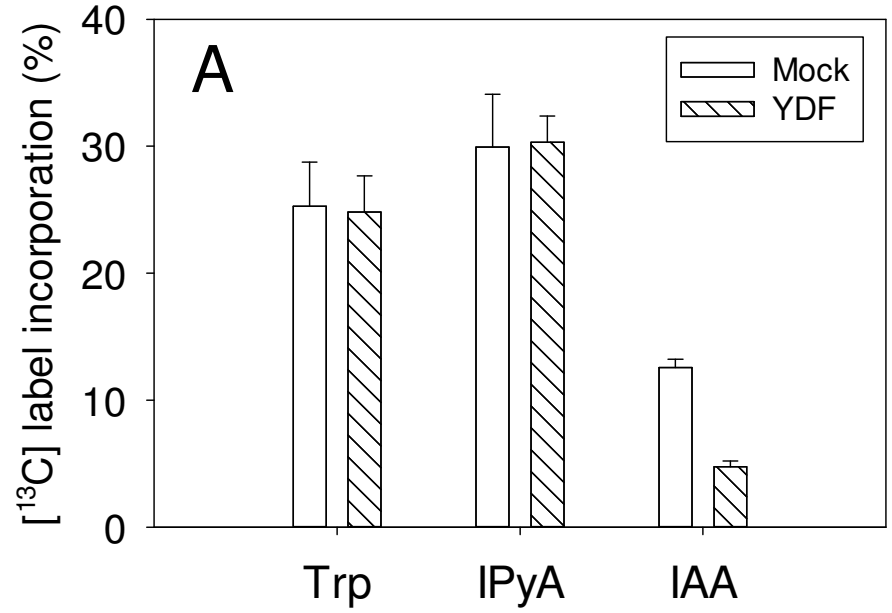
A
Mock
YDF
[13C] label incorporation (%)
40
30
20
10
0
Trp
IPyA
IAA

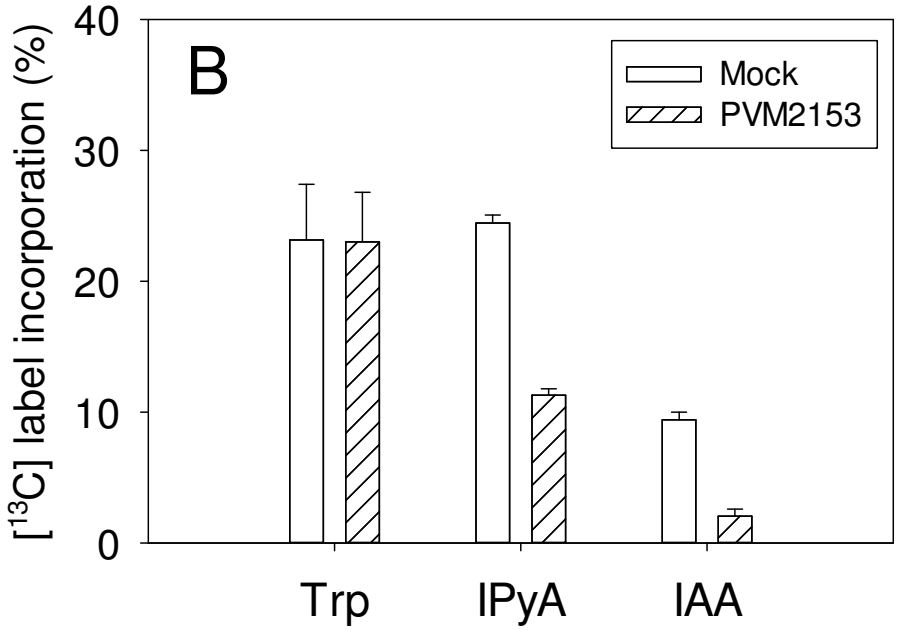
B
Mock
PVM2153
[13C] label incorporation (%)
40
30
20
10
0
Trp
IPyA
IAA

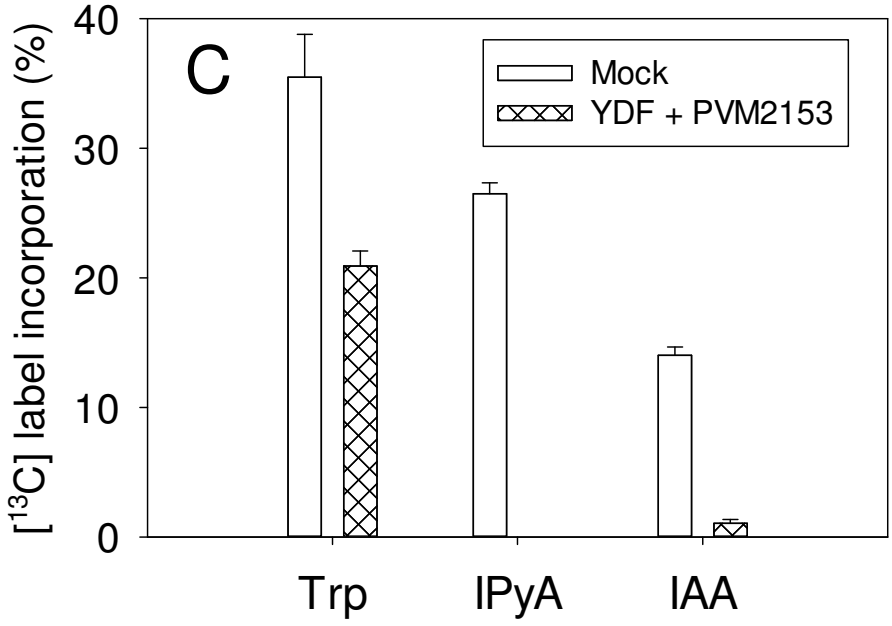

Figure 2-6: [$^{13}C_3$]Serine labeling of YUCCA pathway compounds in *Arabidopsis* hypocotyls in the presence of pathway inhibitors. Seedlings were grown in the dark for 7 d, then transferred onto media containing 100 μM YDF or DMSO (A), 30 μM PVM2153 or acetonitrile (B), or 100 μM YDF with 30 μM PVM2153 or DMSO and acetonitrile (C). Seedlings were then exposed to a 16 h photoperiod of red light for 3 days, and then treated with a solution containing 3 mM [$^{13}C_3$]serine for 16 hours. Samples containing approximately 40 hypocotyls were collected for LC-MS analysis of isotopic enrichment of IAA and IAA biosynthesis intermediates. Each bar represents the mean of 4-9 biological replicates; error bars represent SE. No ^{13}C label was detected in IPyA in the YDF + PVM2153 inhibitor treatment.

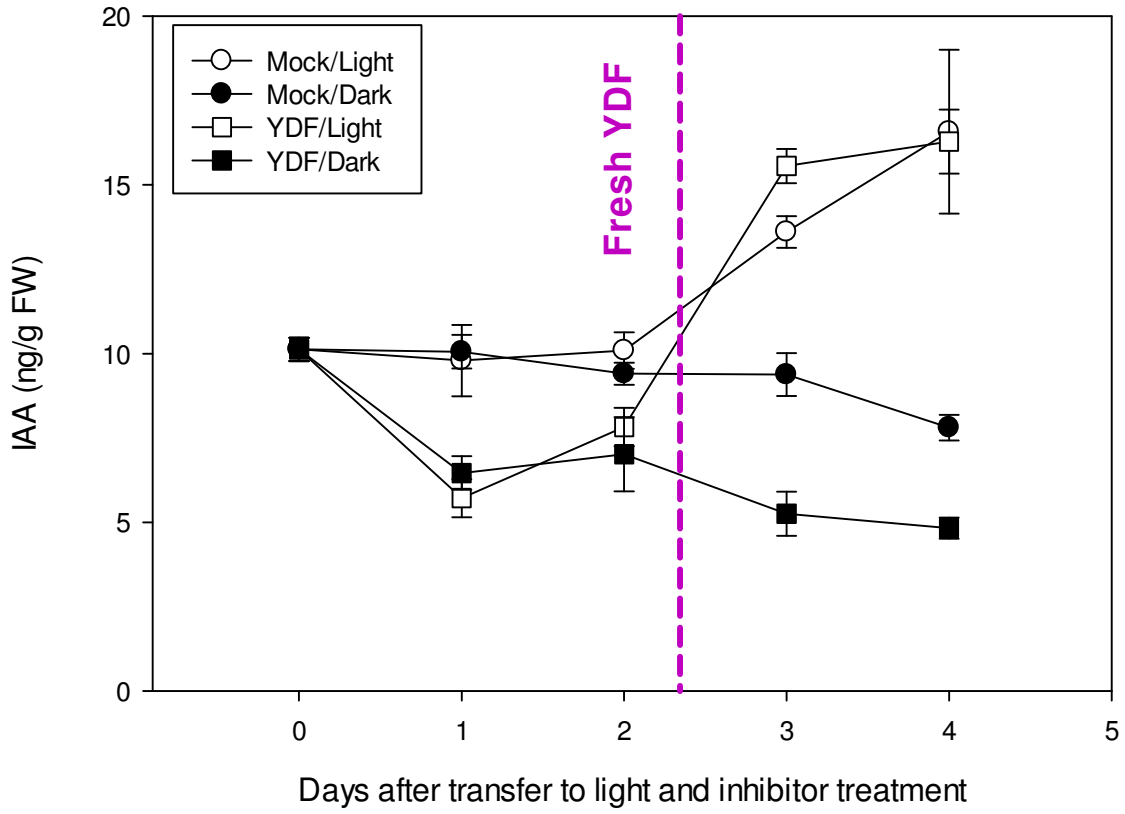

Figure 2-7: Endogenous IAA content in *Arabidopsis* hypocotyls grown on YDF media. Seedlings were grown in the dark for 7 d, then transferred onto media containing 100 µM YDF or DMSO (mock) and placed in growth chambers where they were exposed to either a 16 h photoperiod of red light or kept in continued darkness. After growing on YDF or mock media for 2 days, seedlings were transferred onto fresh media (indicated by dashed line). 5-15 mg samples of hypocotyl tissue were collected immediately before and at each of the 4 days after transfer. Free IAA levels were quantified by isotope dilution LC-MS/MS using [$^{13}C_6$]IAA internal standard. Each point represents the mean of 5-10 biological replicates; error bars represent SE.

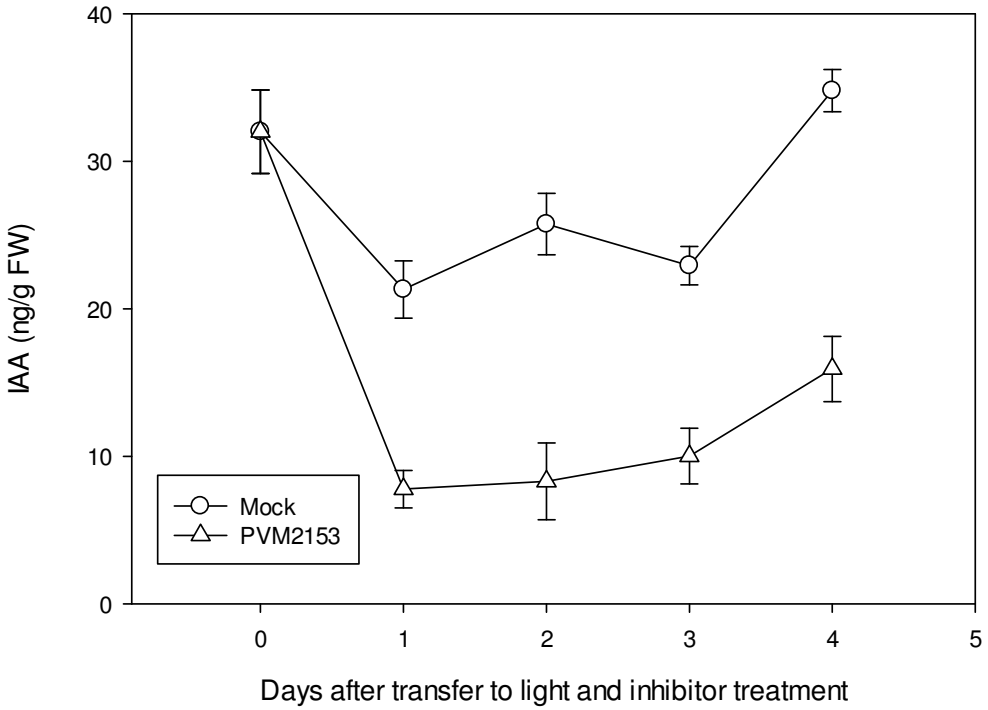

Figure 2-8: Endogenous IAA content in *Arabidopsis* hypocotyls grown on PVM2153 media. Seedlings were grown in the dark for 7 d, then transferred onto media containing 30 μM PVM2153 or acetonitrile (mock) and placed in growth chambers where they were exposed to a 16 h photoperiod of red light. 5-15 mg samples of hypocotyl tissue were collected immediately before and each of the 4 days after transfer. Free IAA levels were quantified by isotope dilution LC-MS/MS using [$^{13}C_6$]IAA internal standard. Each point represents the mean of 4-6 biological replicates; error bars represent SE.

Table 2-1: Retention times, chemical formulas, and calculated *m/z* values of isotopomers of IAA and proposed biosynthesis intermediates. Retention times were determined with authentic standards.

	Retention time (min)	Formula	*m/z* M(+H)	*m/z* $^{15}N_1$	*m/z* $^{13}C_1$	*m/z* $^{13}C_2$	*m/z* $^{13}C_3$	*m/z* $^{13}C_6$
Trp	1.87	$C_{11}H_{12}N_2O_2$	205.0972	206.0942	-	-	208.1072	211.1173
TAM	2.60	$C_{10}H_{12}N_2$	161.1073	162.1044	-	-	-	167.1275
IAOx	5.01/5.17*	$C_{10}H_{10}N_2O$	175.0866	176.0836	-	-	-	181.1067
IAM	3.96	$C_{10}H_{10}N_2O$	175.0866	176.0836	-	-	-	181.1067
IAN	5.87	$C_{10}H_8N_2$	157.0760	158.0731	-	-	-	163.0962
IPyA-MeOx	6.27	$C_{12}H_{12}N_2O_3$	233.0921	234.0891	-	-	236.1021	239.1122
IAAld-MeOx	7.74/8.07*	$C_{11}H_{12}N_2O$	189.1022	190.0993	-	-	-	195.1224
IAA	4.44	$C_{10}H_9NO_2$	176.0706	177.0676	-	178.0773	-	182.0907
Quinolinium ion (IAA)	-	C_9H_7N	130.0651	131.0622	131.0685	-	-	136.0853

*IAOx and IAAld-MeOx each produced two peaks

Chapter 3: Analytical methods for visualizing the indolic precursor network leading to auxin biosynthesis

1. Introduction

Plant life is characterized by strictly regulated developmental events that achieve optimum growth and reproduction. This is accomplished through an extremely complex hormonal signaling network in which the plant growth hormone auxin plays a central and defining role. To this end, auxin helps regulate almost all aspects of plant growth and development including embryogenesis, tissue architecture, and tropic responses (Tivendale et al., 2014). Maintenance of auxin homeostasis involves multiple pathways for the biosynthesis of indole-3-acetic acid (IAA), the principal auxin in plants, and several regulatory pathways as well as subsequent catabolic events. These additional input/output processes include conjugation and hydrolysis of sugar and cyclitol conjugates, amino acid, peptide and protein conjugates, formation and β-oxidation of indole-3-butyric acid, as well as deactivation by ring oxidation of IAA and its amino acid conjugates (Cooke et al., 2002; Woodward and Bartel, 2005). Nevertheless, how much IAA is made and accumulates remains the critical regulatory event in many aspects of plant development (Tivendale and Cohen, 2015).

Although several biosynthetic pathways for the bioactive auxin IAA have been proposed, many of them have not been well defined and flux information is largely lacking (Figure 3-1). The predominant biosynthetic route to IAA in *Arabidopsis thaliana* is widely believed to be through the YUCCA pathway, in which the amino acid tryptophan (Trp) is converted to indole-3-pyruvic acid (IPyA), which is then converted to IAA by YUCCA enzymes (Mashiguchi et al., 2011). Species-specific evidence for the synthesis of IAA from Trp through indole-3-acetaldoxime (IAOx), which is converted to indole-3-acetamide (IAM) and sometimes an indole-3-acetonitrile (IAN) intermediate has been shown in *Arabidopsis* (Sugawara et al., 2009; Nonhebel et al., 2011). Other

potential intermediates of IAA synthesis downstream of Trp have been proposed, such as indole-3-acetaldehyde (IAAld) (Rajagopal, 1971; Koshiba and Matsuyama, 1993; Tsurusaki et al., 1997) and tryptamine (TAM) (Quittenden et al., 2009), though their places within the web of auxin biosynthesis have not been well detailed. A Trp-independent route has also been proposed based on tryptophan synthase mutants, metabolic flux analysis, and *in vitro* analyses, in which indole or another upstream compound serves as the IAA precursor (Wright et al., 1991; Normanly et al., 1993; Östin et al., 1999; Tivendale et al., 2014); however, unbound chemical intermediates, if they are involved in this pathway, have as yet not been identified (Nonhebel, 2015).

Chemical biology approaches are complimentary to genetic and biochemical studies, and are particularly useful in studying IAA biosynthesis. While auxin biosynthesis mutants may have severe developmental defects that alter growth and confound comparisons to wild type plants (Cheng et al., 2007), biosynthetic reactions can be turned off at specific developmental time points with chemical inhibitors. Additionally, genetic redundancy can be overcome by inhibiting an entire enzyme family with a single chemical treatment (Fukui and Hayashi, 2018). Such is the case with inhibitors targeting both steps in the YUCCA pathway. The YUCCA enzymes are encoded by multiple genes in *Arabidopsis thaliana,* and mutations in small sets of these genes encoding the flavin monooxygenase proteins result in significant morphological defects (Cheng et al., 2006). A number of chemical inhibitors have been developed to inhibit the YUCCA pathway of auxin biosynthesis (Table 3-1), providing valuable tools to study the function of this pathway in different plant tissues and environmental conditions. Similarly, TAA1/TAR/ISS1/VAS1 (TRYPTOPHAN AMINOTRANSFERASE OF ARABIDOPSIS 1/ TRYPTOPHAN AMINOTRANSFERASE RELATED/ INDOLE SEVERE SENSITIVE 1/ REVERSAL OF SAV3 PHENOTYPE1) form a set of enzymes with overlapping biochemical functions that catalyze the penultimate step in the IPyA pathway (Pieck et al., 2015). Alternative aromatic amino acid substrates, such as L-kynurenine, can act as competitive inhibitors of tryptophan aminotransferase, and a series of potent inhibitors has been developed to target pyridoxal phosphate-dependent enzymes with enhanced specificity to TAA1 and related enzymes (“pyruvamines”) (Narukawa-Nara et al., 2016).

The issues of redundancy with tryptophan synthase (TS) are a bit different. *Arabidopsis* and maize have two copies of the genes that encode each of the two proteins that form the αββα heterodimeric complex that catalyzes the formation of tryptophan from indole-glycerol-phosphate and serine in the plastids. In addition, maize has genes BX1 and IGL for TSα-like cytosolic enzymes that serve as sources of free indole (Kriechbaumer et al., 2008). *Arabidopsis* also has a cytosolic TSα-like enzyme encoded by the indole synthase (INS) gene (Zhang et al., 2008). TS is, however, a well-researched and highly conserved bi-enzyme complex (Watkins-Dulaney et al., 2020) such that inhibitors are available (Table 3-1) that target specifically TSα and TSβ, as well as the 25-Å long tunnel to the β-subunit where indole diffuses in order to participate in the TSβ pyridoxal 5'-phosphate-mediated β-addition reaction with serine. Mutations in both copies of TSβ are seedling lethal (Wright et al., 1992).

In this chapter, we describe methods utilizing chemical biology coupled with a modified approach of isotope dilution/tracing and liquid chromatography–high resolution-mass spectrometry (LC-HR-MS) for qualitative and quantitative analysis of IAA biosynthesis in *Arabidopsis*. Growing seedlings on fully ^{15}N-labeled media enables accurate quantitation of biosynthetic intermediates by reverse isotope dilution, using unlabeled internal standards which are typically more readily available than isotopically labeled standards (Bloch and Anker, 1948). Seedlings are first germinated on nylon mesh and are easily transferred onto media containing chemical treatments at the desired developmental time point. Next, stable isotope-labeled precursor compounds are fed to the plant. Labeled serine is used as a tracer for Trp-dependent biosynthesis specifically (Erdmann and Schiewer, 1971), while labeled indole and anthranilate can feed into both Trp-dependent and Trp-independent pathways (Rapparini et al., 1999; Rapparini et al., 2002; Pieck et al., 2015) (Figure 3-2).

We also describe a technique for identifying novel intermediates based on the characteristic quinolinium ion produced from MS fragmentation of 3-substituted indolic compounds. This method involves using a series of injections of the same sample with increasingly narrow mass ranges, similar to the methods described by Yu et al. (2014), to target novel indolic compounds. By monitoring exact masses of [$^{13}C_8$, $^{15}N_1$]- and

[$^{15}N_1$]quinolinium ions after treatment with [$^{13}C_8$, $^{15}N_1$]- and [$^{15}N_1$]indole, this method can be used to identify unknown compounds synthesized downstream from indole.

2. Materials

2.1 Growing, labeling, and collecting plant material

- 20 μm nylon mesh (Sefar, 03-20/14), cut into 9 cm × 9 cm squares and autoclave-sterilized with 45 minute sterilization time at 121°C
- Sterile deionized water
- Forceps, flame-sterilized
- 10 cm × 10 cm square Petri dishes (Fisherbrand, FB0875711A)
- Dilute bleach solution for seed sterilization: 20 mL concentrated regular liquid bleach (Clorox), 80 mL deionized water, 20 μL Tween 80 (Sigma-Aldrich, P1754)
- Plant growth medium: ATS (Lincoln et al., 1990)
- KimWipes delicate task wipes (Kimberly-Clark, KC34155EXL)
- 1.5 mL microcentrifuge tubes (Fisherbrand, 05-408-129)
- Liquid nitrogen
- Dry ice
- One or more isotopically labeled precursor solutions in aqueous ATS salts (see Notes 1 and 2; see Table 3-2 for description of example labeling strategies):
    - 3 mM [$^{13}C_3$]L-serine (Cambridge Isotope Laboratories, CLM-1574-H)
    - 500 μM [$^{13}C_6$]anthranilate (Sigma-Aldrich,709530)
    - 500 μM [$^{15}N_1$]indole (Cambridge Isotope Laboratories, NLM-792)
    - 500 μM [$^{13}C_8{}^{15}N_1$]indole (Cambridge Isotope Laboratories, CNLM-4786-0)

2.2 Homogenization and extraction

- Tissue homogenizer (Retsch MM300)
- Microcentrifuge, temperature controlled at 4°C
- Repeater pipette (Eppendorf M4)

- Homogenization buffer: 65% isopropanol, 35% 0.2 M imidazole (pH 7.0), 100 mM methoxyamine hydrochloride (CH_3ONH_2·HCl) (Sigma-Aldrich, 226904) for targeted analysis of IAA and biosynthesis intermediates (see Note 3); 50% isopropanol for analysis of unknown indolic compounds
    - For absolute quantitation, stable isotope internal standard is added into homogenization buffer. The amount of internal standard added to each sample should be similar to the amount of endogenous compound in the plant tissue (*see* Notes 4 and 5)
- Stainless steel beads for homogenization (1.6 mm diameter, Next Advance, SSB16)
- 2 mL screwcap tubes (Fisherbrand, 02-681-343)
- 10-200 μL Empty TopTips (Glygen, TT2EMT) and adaptors provided by Glygen for centrifugation
- Vacuum concentrator (SpeedVac, Savant)
- Additional materials required for specified extraction techniques are described in the sections below:

  2.2.1 IAA extraction
  - Bondesil-NH_2 resin (Agilent, 12213020) suspended in water, 1:4 w:v
  - IAA extraction solvents and solutions as described by Liu et al. (Liu et al., 2012): hexane, acetonitrile, ethyl acetate, methanol, 0.2 M imidazole (pH 7.0), distilled water, 0.25% phosphoric acid (PA), 0.1 M succinic acid (SA, pH 6.0), 5:1 PA:SA solution
  - Macro-prep epoxide support resin (Bio-Rad, 156-0000), suspended in 0.1 M sodium bicarbonate (pH 7.0), 1:4 w:v

  2.2.2 Extraction of proposed IAA biosynthesis intermediates: Anthranilate, Ser, IAAld, IPyA, IAOx, IAN, IAM, indole
  - RENSA HLB resin (MIP Technologies, 92001-0010) suspended in methanol, 1:5 w:v
  - Acetonitrile: 100%, 80%, 20%, and 5% prepared in distilled water

  2.2.3 Indole extraction
  - Pentane

2.3 LC-MS analysis

- Amber autosampler vials (ChromTech, 404810) with 50 μL glass inserts (ChromTech, CTI-2405)
- Liquid chromatograph/mass spectrometer system: Dionex UltiMate 3000 UHPLC, Q Exactive mass spectrometer, Xcalibur software (Thermo Scientific)
- C18 HPLC column, 50 × 2.1 mm (Force, 9634252) with 0.2 μm precolumn filter (UltraShield, 25809)
- Mobile phase: A, 0.1% formic acid in water; B, 0.1% formic acid in acetonitrile. Different LC-MS methods are used to target compounds of interest:
    - IAA analysis*:* Mobile phase gradient of 5% B (-1-0 min), 5-20% B (0-3 min), 20-80% B (3-6 min), 80% B (6-6.5 min) at a flow rate of 0.4 mL•min^{-1}. Mass spectra are collected in positive ion mode in a parallel reaction monitoring (PRM) scan and the inclusion list contains ions of 176, 177, 178, and 182 *m/z*. PRM resolution is 17500 full width at half maximum (FWHM), automatic gain control (AGC) target is 2×10^5, maximum ionization time is 50 milliseconds (ms), isolation window is 2.0 *m/z*, and normalized collision energy (NCE) is 20. Ion source conditions are: spray voltage: 4.00 kV, capillary temperature: 275 ℃, probe heater temperature: 300 ℃, sheath gas: 30 arbitrary units, aux gas: 20 arbitrary units, S-lens RF level: 50.
    - For analysis of all the listed intermediates except indole, inject 5-10 μL plant extract into the LC system with the following mobile phase gradient: 5% B (-2-1 min), 5-15% B (1-3 min), 15-30% B (3-3.5 min), 30% B (3.5-5 min), 30-39% B (5-7.5 min), 39-80% B (7.5-8 min), 80% B (8-8.5 min) at a flow rate of 0.4 mL•min^{-1}. Mass spectra are collected in selected ion monitoring (SIM) mode. SIM resolution is 70,000 FWHM with maximum ionization time of 200 ms and AGC of 5×10^5. Ion source conditions are: spray voltage: 4.00 kV, capillary temperature: 275℃, probe heater temperature: 300 ℃, sheath gas: 30 arbitrary units, aux gas: 20 arbitrary units, S-lens RF level: 50. MS is set to acquire several segments of full scans each targeting 1-3 compounds. The segments are: 200-217 *m/z* (0-2.1 min), 157-173 *m/z* (2.1-3 min), 133-150 *m/z*

(3-3.74 min), 170-188 *m/z* (3.74-5.4 min), 152-170 *m/z* (5.4-6 min), 227-245 *m/z* (6-6.7 min), 184-201 *m/z* (6.7-8.5 min).

- For indole analysis, 5-10 µL plant extract is injected with the following LC mobile phase gradient: 5% B (-1-1 min), 5-30% B (1-3 min), 30-39% B (3-5.5 min), 39-80% B (5.5-6.5 min), 80% B (6.5-7 min) at a flow rate of 0.4 $mL \bullet min^{-1}$. Mass spectra are collected in SIM mode using a mass range of 110-132 *m/z*. SIM resolution is 70,000 FWHM with maximum ionization time of 200 ms and AGC of 5×10^5. Ion source conditions are: spray voltage: 4.00 kV, capillary temperature: 275℃, probe heater temperature: 300℃, sheath gas: 30 arbitrary units, aux gas: 20 arbitrary units, S-lens RF level: 50.
- For analysis of compounds labeled by treatment with $[^{15}N_1]$- and $[^{13}C_8{}^{15}N_1]$indole, multiple injections of the same sample are made using a series of methods (A-D, described below) with different MS parameters. The same mobile phase gradient is used with each method: 5% B (-2-2 min), 5-50% B (2-8 min), 50-85% B (8-10 min), 80% B (10-12 min) at a flow rate of 0.4 $mL \bullet min^{-1}$.
  - Method A: Scan groups consist of one full MS-SIM scan followed by four PRM scans. For the SIM scan, Orbitrap resolution is 70,000 full width at half maximum (FWHM) with maximum ionization time of 200 ms, automatic gain control (AGC) target of 5×10^5, and scan range of 100-400 *m/z*. For the PRM scans, FWHM resolution is set to 17,500, maximum ionization time is 100 ms, AGC target is 2×10^5, normalized collision energy (NCE) is 35, and isolation window is 20 *m/z*. Four variations of this method (used in four separate injections) with different values in the inclusion list are used to cover a range of *m/z* values for potential compounds of interest:
    a) Method A.1: The inclusion list contains *m/z* values beginning at 130 and increasing by increments of 20 to 290 (130, 150, 170,… 250, 270, 290 *m/z*)
    b) A.2: *m/z* values begin at 140 and increase by increments of 20 to 300

c) A.3: *m/z* values begin at 300 and increase by increments of 20 to 460

d) A.4: *m/z* values begin at 310 and increase by increments of 20 to 470

- Method B: LC-MS parameters are nearly identical to Method A, except that the isolation window is changed to 2 *m/z* and the inclusion list is designed to cover a 20 *m/z* range with values increasing by increments of 2 *m/z*. The inclusion list is customized to target features of interest observed using Method A. For example, to investigate a candidate peak identified in the 210 *m/z* scan filter from Method A, the inclusion list for Method B would contain 200, 202, 204, … 216, 218, 220 *m/z*.
- Method C: Again, LC-MS parameters are nearly identical to Methods A and B, except that the isolation window is further narrowed to 1 *m/z* and the inclusion list is customized to isolate the isotopomers of interest observed with Method B. Values within 1-2 *m/z* of the scan range containing features of interest found from Method B are included. For example, to target a peak observed in the 206 *m/z* scan filter from Method B, 205, 206, and 207 *m/z* should be added to the inclusion list of Method C.
- Method D: Scan groups include one full MS- SIM scan followed by one PRM scan. MS parameters are the same as those described above except that the NCE is 15 and the isolation window is ≤1 *m/z*. The inclusion list is customized to contain only the $[^{13}C_8{}^{15}N_1]$-, $[^{15}N_1]$-, and unlabeled molecular ions of interest with as much specificity as possible.

3. Methods

3.1 Growing seedlings with inhibitor and stable isotope precursor treatments

3.1.1 In a laminar flow hood, moisten sterile nylon mesh squares with sterile water and use forceps to place squares flat on germination media (see Note 7 and Table 3-2) in square Petri dishes.

3.1.2 Clean *Arabidopsis* seeds by shaking in 20% bleach solution for 5 minutes and rinsing 4 times with sterile water.

3.1.3 Sow seeds approximately 0.5 cm apart in single row on mesh.

3.1.4 Store plates at 4°C in the dark for 3-7 days to stratify seeds. Remove plates from cold and place vertically in growth conditions.

3.1.5 Transfer seedlings onto inhibitor media (Table 3-1) to begin auxin biosynthesis inhibition treatment (see Note 8). In a laminar flow hood, use forceps to gently lift mesh with seedlings from germination plates and lay flat onto plates containing inhibitor media. Cover plates and place vertically under growth conditions.

3.1.6 Begin isotopic labeling treatments by flooding plates with 3 mL of labeling solution (Table 3-2). Gently rock plate back and forth 5-10 times to ensure labeling solution covers entire mesh square. Cover plates and place flat under growth conditions for 0-24 hours (see Note 8).

3.1.7 Collect samples by gathering 10-50 mg of plant tissue (see Notes 9 and 10), gently blotting away moisture on a KimWipe, and placing in a microcentrifuge tube. Immediately submerge tube in liquid nitrogen to flash freeze and place on dry ice. Store samples at -80°C until extraction.

3.2 Homogenization and extraction

3.2.1 Holding frozen samples on dry ice, add 20 µL of homogenization solution per 10 mg tissue and 2-3 beads to each sample.

3.2.2 Homogenize samples in Geno/Grinder for 4 minutes at 1500 RPM and incubate samples on ice for 1 hour (see Note 11)

3.2.3 Add 90 µL of water to each homogenized sample per 10 µL homogenization buffer and shake tube to mix.

3.2.4 Centrifuge samples at 25000 g for 10 min. at 4°C.

3.2.5 Prepare samples for LC-MS analysis using purification methods specified for compounds of interest:

3.2.5.1 Indole

1) Transfer 200 µL supernatant into a new tube. Add 100 µL pentane and vortex at room temperature for 5 minutes.
2) Spin samples a short time to clearly separate the organic and aqueous phases. Transfer the upper organic layer into a new tube. Save the aqueous

phase for extraction of IAA (section 3.2.2) or auxin intermediates (section 3.2.3).

3) Evaporate pentane with vacuum concentrator and resuspend sample in 20 µL acetonitrile

3.2.5.2 IAA

1) Prepare TopTips with NH_2 resin for solid phase extraction (SPE) according to Liu et al. (2012). Add 20 µL resin suspension per TopTip; wash with 50 µL each: hexane, acetonitrile, ethyl acetate; condition with 50 µL 0.2 M imidazole followed by 2 × 100 µL water
2) Load supernatant from step 3.2.4 onto prepared TopTips. For larger samples, 250 µL of supernatant can be loaded at a time and spun through. Reload and spin until all supernatant has been loaded. Wash with 50 µL methanol.
3) Exchange tubes under TopTip adapters to fresh 2 mL tubes for elution. Elute with 3× 50 µL of PA, then add 25 µL of SA to each sample.
4) Prepare TopTips with PMME resin for solid phase extraction (SPE) according to Liu et al. (2012). Add 75 µL PMME resin suspension per TopTip; wash with 2 × 100 µL methanol; condition with 2 × 100 µL PA:SA.
5) Load samples onto prepared TopTips. Wash with 2 × 50 µL PA:SA.
6) Exchange tubes under TopTip adapters to clean 1.5 mL tubes for elution. Elute with 2 × 50 µL methanol. Reduce volume of each sample to approximately 20 µL with vacuum concentrator.

3.2.5.3 Proposed IAA biosynthesis pathway intermediates: Anthranilate, Ser, IPyA, IAAld, IAOx, IAN, IAM

1) Prepare TopTips with HLB resin for SPE. Add 25 µL resin suspension per TopTip; equilibrate with 2 × 50 µL 100% acetonitrile and 2 × 50 µL 20% acetonitrile.
2) Load supernatant onto prepared TopTips.
3) If sensitive detection and quantification of IAA is required, save 200-300 µL of supernatant for IAA analysis as described in section 3.2.5.2.

4) Wash with 50 µL 5% acetonitrile.
5) Exchange tubes under TopTip adapters to clean 1.5 mL tubes for elution. Elute with 2 × 50 µL 80% acetonitrile. Reduce volume of each sample to approximately 20 µL using vacuum concentrator (about 10-12 minutes).

3.2.5.4. Unknown indolic compounds (double indole labeling samples)

1) Transfer supernatant to a clean tube and centrifuge again at 25000 g for 10 min. at 4°C to remove all debris.

3.3 LC-MS Analysis

3.3.1 Carefully transfer each sample to a 50 µL glass insert so that no air pockets remain at the bottom of the insert. Assemble insert into autosampler vial with cap.

3.3.2 Inject 5-10 µL of sample for LC-MS analysis using methods described in section 2.3.

3.4 Data Analysis

3.4.1 Targeted data analysis

1) Raw data files are converted to mzXML format using the msconvert tool from the ProteoWizzard software (Chambers et al., 2012) prior to input into R. Quantitative data for each indolic compound is extracted using the Metabolite-Turnover script developed in the Hegeman lab (https://github.com/HegemanLab/Metabolite-Turnover, (Evans et al., 2018)). In this script, the ProteinTurnover (Fan et al., 2016) and the XCMS package (Smith et al., 2006) are employed to extract EICs for each isotopmer of IAA and intermediates. This quantification approach using linear regression (Huttlin et al., 2007) is preferred over that using peak area (Cohen et al., 1986) when the MS data have high background noise due to low analyte abundance.
2) Exact masses for isotopomers of interest are calculated using the University of Wisconsin—Madison Biological Magnetic Resonance Data Bank exact mass calculator (http://www.bmrb.wisc.edu/metabolomics/mol_mass.php).

Isotopomers of proposed IAA biosynthetic intermediates derived from several isotopic labeling strategies are listed in Table 3-3. (See Note 12)

3) In the data output csv files, the slope of each linear regression line represents the ratio of the respective isotopic trace to its monoisotopmer. This ratio is used to calculate the relative abundance of labeled compounds, allowing us to track label incorporation from upstream precursors into IAA intermediates through multiple pathways.

3.4.2 Double indole labeling analysis

1) Use LC-MS method A1 described in section 2.3 to identify potential features producing [$^{15}N_1$]- and [$^{13}C_8{}^{15}N_1$]quinolinium ions.
   a) Under the "Ranges" tab in "Chromatogram Ranges" in Xcalibur, set the chromatogram viewing options to display three mass ranges: 130.0641 - 130.0661 (corresponding to unlabeled quinolinium ion), 131.0612 - 131.0632 ([$^{15}N_1$]quinolinium), and 139.0880-139.0900 ([$^{13}C_8{}^{15}N_1$]quinolinium).
   b) Set "Scan Filter" to display chromatogram from the first ion of the inclusion list. Note any coeluting peaks present in both the [$^{15}N_1$]quinolinium and [$^{13}C_8{}^{15}N_1$]quinolinium mass ranges. Ions producing these peaks may have incorporated label from the indole treatments.
   c) View chromatograms through each Scan Filter, keeping the same mass ranges specified above, and continue to note any candidate peaks with matching retention times.
2) Repeat workflow described in step 1 with method A2 to identify additional candidate features.
3) Perform subsequent injection with method B, aiming to narrow *m/z* windows containing the parent ions. View data using the same settings in Xcalibur that were used in step 1, taking note of retention times and scan windows that show the presence of coeluting peaks for both quinolinium labeled mass ranges.

4) Perform subsequent injection with method C to progress toward pinpointing molecular ions. This method should be tailored to candidate peaks that were identified in steps 1-3.
    a) Using the same mass ranges settings to target quinolinium ion isotopomers, view EIC through each scan filter to identify the filter range containing the strongest quinolinium signal. The molecular ion is expected to be near (within 1 *m/z*) this value.
5) Customize method D to include approximate molecular ion values identified in step 3 in the inclusion list. Run sample using this method to obtain exact mass spectra.
6) Compare spectra produced from each of the three ions in the inclusion list of method D, taking note of exact mass differences between the major ions of different spectra. Exact mass differences of 0.9970, 9.0239, and 8.0268 *m/z* correspond to the differences between $^{15}N_1$ and unlabeled, $^{13}C_8{}^{15}N_1$ and unlabeled, and $^{13}C_8{}^{15}N_1$ and $^{15}N_1$, respectively.
7) If no molecular ions are observed, NCE settings in method D can be set to a lower intensity to preserve a greater abundance of molecular ion.
8) Unlabeled molecular ion and spectral data can be searched against mass spectral databases to identify potential compound identities: MassBank, METLIN, NIST Tandem Mass Spectral Library, *m/z*Cloud, MS-DIAL.
9) Confirm compound identities by comparing retention time and mass spectral data against authentic standards.

Notes

1. 500 μM [$^2H_5$]Trp (or other labeled forms of Trp) may also be used as a labeled precursor treatment (Baldi et al., 1991; Wright et al., 1991; Östin et al., 1999; Rapparini et al., 1999; Mashiguchi et al., 2011); however, results should be examined cautiously as high levels of exogenous Trp will feedback inhibit anthranilate synthase and anthranilate phosphoribosyltransferase (Sugimoto and Shiio, 1983; Niyogi and Fink, 1992; Poulsen et al., 1993), which may confound results.

2. To improve solubility, labeled indole can first be dissolved in a small volume of acetonitrile; anthranilate can first be dissolved in a small volume of isopropanol.
3. IPyA and IAAld degrade quickly and need to be derivatized with CH_3ONH_2 to generate their oximes (IPyA-MeOx and IAAld-MeOx). Standards should be derivatized and prepared freshly.
4. For IAA quantitation by isotope dilution, mix 10 ng of stable isotope labeled-IAA per 1 mL homogenization buffer. We recommend using [$^{13}C_6$]IAA (Cambridge Isotope Laboratories, CLM-1896) in experiments where other [$^{13}C_6$]-labeled precursors (such as [$^{13}C_6$]anthranilate) are not used.
5. For reverse isotope dilution quantitation, use unlabeled internal standards as endogenous compounds are [^{15}N]-labeled in plants germinated and grown on [^{15}N]ATS media. Add 50 nM ANT, 500 nM indole, 5 μM Trp, 1 nM IAM, 2.5 μM IAN, 100 nM IPyA, 10 nM IAAld, 10 nM IAA, 1 nM TAM, 10 nM IAOx, and 100 mM freshly prepared methoxylamine hydrochloride (CH3ONH2 · HCl) into homogenization buffer. In the data analysis output for reverse isotope dilution samples, the slope of each linear regression line represents the ratio of the respective isotopic trace (labeled compounds) to its monoisotopomer (unlabeled internal standard added) and is used to quantify the isotopic traces.
6. Although MS parameters are altered in subsequent injections, it is important to keep the LC gradient consistent with method A so that retention times are consistent across injections.
7. For absolute quantitation of compounds by reverse isotope dilution, use fully [^{15}N]-labeled salts in both germination and inhibitor media. If only relative label incorporation data are needed, unlabeled media can be used.
8. Timing for inhibitor treatments, isotopic labeling, and sample collection can be adapted to study auxin biosynthesis at different developmental stages. Significant IAA biosynthesis inhibition can be observed in 12-day seedlings after 20 hours on 100 μM YDF and 30 μM PVM2153 media with 30 minutes labeling treatment.
9. For absolute quantitation, record fresh weight of harvested tissues. These data are later used for isotope dilution calculations.

10. Recommended amounts for tissue collection: 40-50 mg per sample for [$^{13}C_3$]serine labeling or double indole labeling; 10-30 mg for indole/anthranilate labeling experiments. More tissue may be needed depending on plant tissue type and inhibitor treatment
11. Plant tissue should be completely pulverized after homogenization. If significant plant material remains intact, repeat Geno/Grinder homogenization.
12. We recommend using a mass range window of the calculated *m/z* value +/- 0.003.

Figures

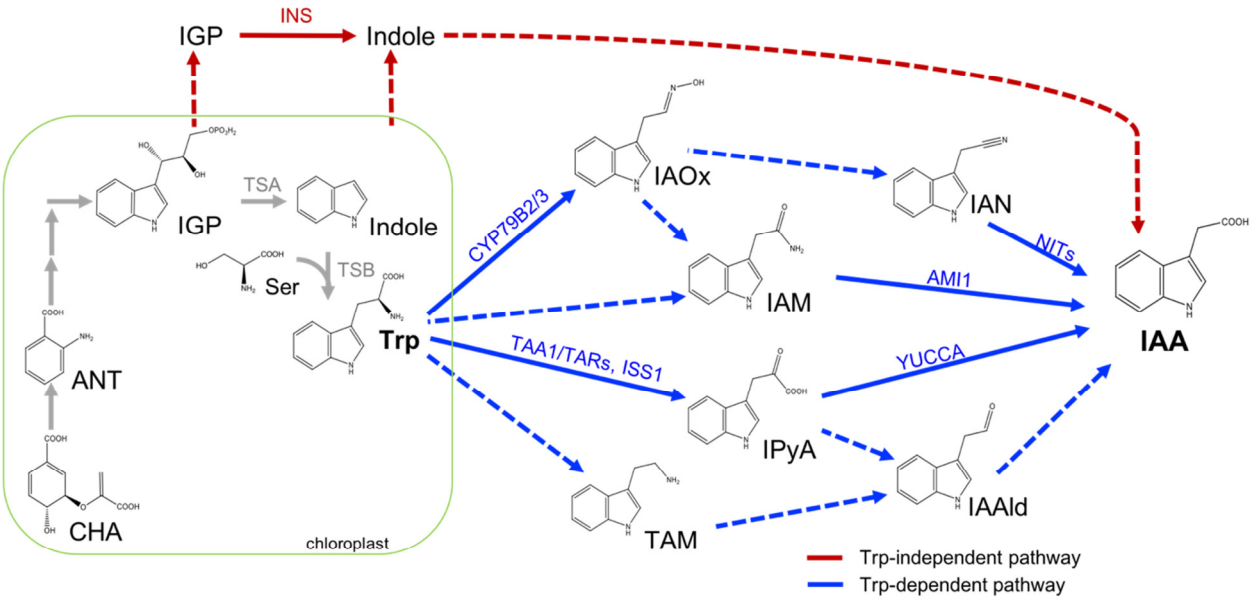

Figure 3-1: Major pathways for IAA biosynthesis. Solid arrows refer to pathways with enzymes identified in at least one species, and dashed arrows to undefined ones. AMI1, indole-3-acetamide hydrolase-1; ANT, anthranilate; CHA, chorismic acid; IAAld, indole-3-acetaldehyde; CYP79B2/3, cytochrome P450 (79B2/3); IAM, indole-3-acetamide; IAN, indole-3-acetonitrile; IAOx, indole-3-acetaldoxime; IGP, indole-3-glycerol phosphate; INS, indole synthase; IPyA, indole-3-pyruvic acid; ISS1, Indole Severe Sensitive 1; NIT, nitrilase; TAA1, TRYPTOPHAN AMINOTRANSFERASE OF ARABIDOPSIS 1; TAR, TRYPTOPHAN AMINOTRANSFERASE-RELATED; TAM, tryptamine; TSA, TRYPTOPHAN SYNTHASE α; TSB, TRYPTOPHAN SYNTHASE β; YUCCA, *Arabidopsis* flavin monooxygenase

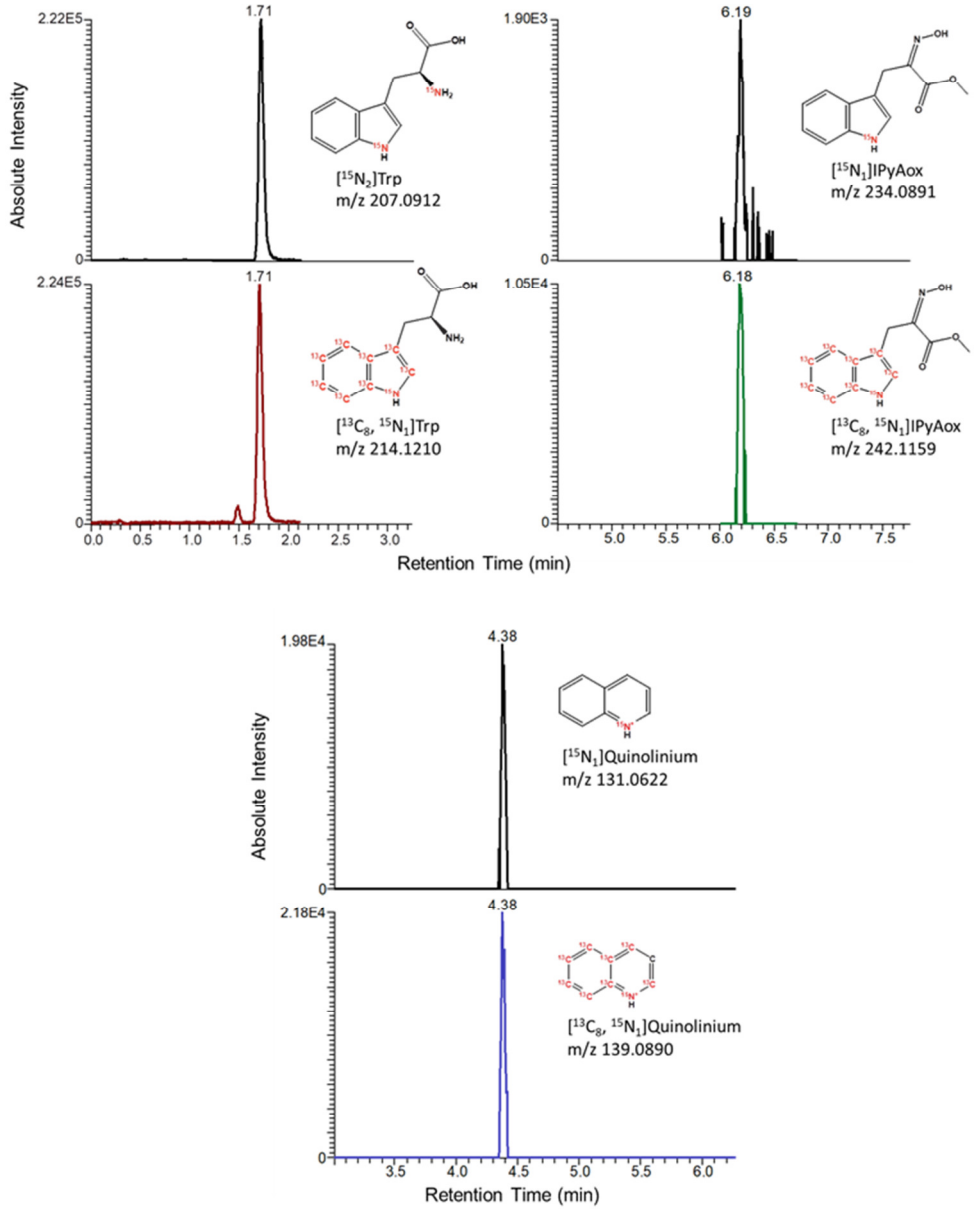

Figure 3-2: Representative results from analysis of Trp, IPyA, and IAA. 13-day-old seedlings grown on ^{15}N media were subjected to mock inhibitor treatment (DMSO+ACN) for 22h, then labeled with 500 µM [$^{13}C_8$, $^{15}N_1$] indole for 1h. [$^{15}N_2$]Trp, [$^{13}C_8$, $^{15}N_1$]Trp, [$^{15}N_1$]IPyAox, and [$^{13}C_8$, $^{15}N_1$]IPyAox were monitored in SIM mode. [$^{15}N_1$] IAA →[$^{15}N_1$]quinolinium and [$^{13}C_8$, $^{15}N_1$]IAA → [$^{13}C_8$, $^{15}N_1$]quinolinium transitions were monitored in PRM mode.

Table 3-1: Some chemical inhibitors of auxin biosynthesis

Inhibitor name	Representative Structure(s)	Target	Mode of action	Reference
BBo	3-chlorophenylboronic acid, 4-biphenylboronic acid	YUCCA	Competitive inhibitor	(Kakei et al., 2015)
PPBo	4-phenoxyphenyl- boronic acid	YUCCA	Competitive inhibitor	(Kakei et al., 2015)
Ponalrestat	2-(3-(4-Bromo-2-fluorobenzyl)-4-oxo-3,4-dihydrophthalazin-1-yl)acetic acid	YUCCA	Substrate antagonist	(Zhu et al., 2019)
Yucasin	5-(4-chlorophenyl)-4H-1,2,4-triazole-3-thione	YUCCA	Competitive inhibitor	(Nishimura et al., 2014)
Yucasin DF (YDF)	5-[2,6-difluorophenyl]-2,4-dihydro-[1,2,4]-triazole-3-thione	YUCCA	Competitive inhibitor	(Tsugafune et al., 2017)
Pyruvamines (PVM) "Type I compounds"	PVM1169; L-alpha-(aminooxy)-3-(naphthalen-2-yl)propanoic acid	TAA1	Competitive inhibitor	(Narukawa-Nara et al., 2016)
Pyruvamines (PVM) "Type II compounds" (Derivatives of Type I compounds)	PVM2153; Benzene propanoic acid, 3,4-dichloro-α-[(1,3-dihydro-1,3-dioxo-2H-isoindol-2-yl)oxy]-, methyl ester	TAA1	Competitive inhibitor	(Narukawa-Nara et al., 2016)
L-Kynurenine (Kyn)	(2S)-2-Amino-4-(2-aminophenyl)-4-oxobutanoic acid	TAA1	Alternative substrate/ Competitive inhibitor	(He et al., 2011)
AVG	Aminoethoxyvinyl-glycine	TAA1	Slow-binding inhibition	(Soeno et al., 2010)
AOPP	L-aminooxyphenyl-propionic acid	TAA1	Competitive inhibitor	(Soeno et al., 2010)
AOA	Amino-oxyacetic acid	TAA1		(Soeno et al., 2010)
AOIBA	2-amino-oxyisobutyric acid	TAA1		(Soeno et al., 2010)

Indoleacrylic acid	trans-indole-3-acrylic acid	Trp synthase β and α	Allosteric inhibitor	(Matchett, 1972); (Marabotti et al., 2000)
(1-Fluorovinyl)glycine	α-(1′-fluoro)vinyl glycine	Trp synthase β	PLP-enzyme mechanism-based inhibitor	(Xu and Abeles, 1993)
Arylsulfide phosphonates	[4-[(2-aminophenyl) sulfanyl]butyl] phosphonic acid	Trp synthase α	Transition state analog	(Finn et al., 1999); (Dias et al., 2006)
Indoline-5-sulfonamides	1-(2-Fluorobenzoyl)-N-methyl-5-indoline sulfonamide N-Methyl-1-[(5-methyl-2-thienyl)carbonyl]-5-indolinesulfonamide	Trp synthaseinter-subunit interface	Allosteric inhibitor	(Abrahams et al., 2017)
sulfolane and indole-5-sulfonamide	GSK1, (3R,4R)-4-[4-(2-chlorophenyl)piperazin-1-yl]-1,1-dioxothiolan-3-ol); GSK2, (1-[2-fluorobenzoyl]-N-methyl-2,-3-dihydro-1H-indole-5-sulfonamide)	Trp synthaseinter-subunit interface	Allosteric inhibitor	(Michalska et al., 2020)
Aryl sulfonamides	[F9]; N-(4'-Trifluoromethoxy benzenesulfonyl)-2-aminoethyl phosphate	Trp synthase β	α-Site allosteric ligand	(Ngo et al., 2007)
Benzamide	N-(4-Carbamoyl benzyl)-5-(3-chloro phenyl)-1,2-oxazole-3-carboxamide	Trp synthase α	α-Site ligand	(Naz et al., 2019)

Table 3-2: Labeling precursors used for different applications. Example labeling strategies employing different stable isotope-labeled precursors for studying IAA biosynthesis. These strategies can be used in combination with various inhibitors (Table 3-1) for targeted analysis of specific routes of IAA biosynthesis.

Labeled Precursor Treatment	**Germination Media**	**Purpose/Description**
3 mM [$^{13}C_3$]Serine	[^{14}N] ATS	Traces synthesis of Trp and Trp-dependent pathway intermediates. [$^{13}C_3$]Ser is condensed with indole to give [$^{13}C_3$]Trp ([$^{13}C_3$]-label is incorporated into Trp sidechain).
500 µM [$^{13}C_6$]anthranilate and 500 µM [$^{15}N_1$]indole	[^{14}N] ATS	Multiple auxin precursors upstream of Trp are applied to monitor label incorporation into various intermediates through multiple pathways.
500 µM [$^{13}C_8{}^{15}N_1$]indole and 500 µM [$^{15}N_1$]indole	[^{14}N] ATS	Multiple labeled forms of indole are applied to label indole-derived metabolites and potential IAA biosynthesis intermediates. LC-MS/MS analysis workflow for identifying candidate compounds is described in Section 2.3.
500 µM [$^{13}C_6$]anthranilate and 500 µM [$^{13}C_8{}^{15}N_1$]indole	[^{15}N] ATS	Growing seedlings on [^{15}N] ATS media enables rapid [^{15}N]-labeling of newly synthesized IAA and biosynthesis intermediates during early seedling development. Unlabeled internal standards may be used for quantitation of IAA and biosynthetic intermediates in plant tissue grown on [^{15}N] ATS (reverse isotope dilution quantitation).

Table 3-3: *m/z* values of isotopomers measured in IAA and intermediates analyses.

	M(+H)	$^{15}N_1$	$^{13}C_1$	$^{15}N_2$	$^{13}C_1{}^{15}N_1$	$^{13}C_1{}^{15}N_2$
ANT	138.0550	139.0520	139.0583		140.0553	
IND	118.0651	119.0622	119.0685		120.0655	
Trp	205.0972	206.0942	206.1005	207.0912		
Ser	106.0499	107.0469	107.0532			
TAM	161.1073	162.1044	162.1107	163.1014	163.1077	164.1047
IAOx	175.0866	176.0836	176.0899	177.0807	177.0870	178.0840
IAM	175.0866	176.0836	176.0899	177.0807	177.0870	178.0840
IAN	157.0760	158.0731	158.0794	159.0701		160.0734
IPyA-MeOx	233.0921	234.0891	234.0954		235.0925	
IAAld-MeOx	189.1022	190.0993	190.1056		191.1026	
IAA	176.0706	177.0676	177.0740		178.0710	
Quinolinium	130.0651	131.0622	131.0685			
	$^{2}H_4$	$^{13}C_6$	$^{13}C_6{}^{15}N_1$	$^{13}C_7$	$^{13}C_7{}^{15}N_1$	$^{13}C_8{}^{15}N_1$
ANT		144.0751	145.0721	145.0784		147.0788
IND		124.0853	125.0823	125.0886		127.0890
Trp		211.1173	212.1143		213.1177	214.1210
Ser						
TAM			168.1245		169.1278	170.1312
IAOx			182.1038		183.1071	184.1105
IAM			182.1038		183.1071	184.1105
IAN			164.0932		165.0965	166.0999
IPyA-MeOx		239.1122	240.1092	240.1156		242.1159
IAAld-MeOx		195.1224	196.1194	196.1257		198.1261
IAA	180.0957	182.0907	183.0878	183.0941		185.0945
Quinolinium	134.0902	136.0853				139.0890

Chapter 4: Conclusion

The plant hormone auxin plays a central role in development and its concentration in plant tissues must therefore be tightly regulated through transport, metabolism, and biosynthesis. Substantial progress has been made in recent years toward deciphering biochemical pathways leading to auxin. One especially important development has been the elucidation of the pathway through Trp and IPyA involving tryptophan aminotransferases and YUCCA flavin monooxygenases in *Arabidopsis* (Mashiguchi et al., 2011; Stepanova et al., 2011; Tivendale et al., 2014). Despite such progress, uncertainties remain regarding the utilization of various proposed intermediates and the prevalence of different pathways in specific tissues or during particular developmental time points. A proposed Trp-independent biosynthesis pathway has been particularly elusive. Outstanding questions remain unanswered regarding the enzymes and intermediates involved in this segment of the auxin biosynthesis web, creating some skepticism over its utilization in plants (Nonhebel, 2015). The data presented in Chapter 2 suggest that the YUCCA pathway is a significant contributor to auxin biosynthesis during light-induced adventitious root formation, and also provide new evidence for operation of a Trp-independent pathway through indole. These findings demonstrate the need for future research to examine Trp-independent contributions to auxin biosynthesis and to further describe the steps involved in this pathway. It is possible that previous studies have overestimated Trp-dependent contributions to auxin biosynthesis by using labeled Trp as a tracer, because Trp has been shown to feedback inhibit upstream reactions involved in auxin biosynthesis. In Chapter 3, I describe methods for using stable isotope labeled Serine as an alternative to labeled Trp, which will be useful in future investigations into the role of Trp as an intermediate in IAA biosynthesis. Altogether, the approach to visualizing the auxin biosynthesis network described in this thesis reveals the complexity of IAA biosynthesis, and can be used to further investigate the roles of different pathways in various aspects of plant growth.

Future Directions

The research I describe in Chapter 2 and Appendix A provides new insight into the process of light-induced adventitious root formation which may have useful implications in agriculture, particularly for vegetative propagation. Future work may further investigate the genetic factors controlling light-induced AR formation. The results presented in Appendix A suggest this response can be induced by multiple different wavelengths of light and that may be negatively regulated by signaling pathways known to function in plant responses to light.

As mass spectrometry and other analytical methods become increasingly sensitive and are coupled with increasingly sophisticated dissection techniques, they can also be used to characterize in greater detail the tissue-specific hormonal changes driving developmental events. In Appendix Section B.2, we quantified auxin levels in laser capture microdissected tissue samples during abscission zone development. Such approaches could be used to describe the precise oscillations in auxin levels and changes in biosynthesis occurring in adventitious root primordia during root initiation, and many other developmental events and environmental responses.

Future research aiming to describe the auxin biosynthesis network in *Arabidopsis* may employ analytical techniques described in Chapter 3 to identify novel intermediates. This could be done using the double indole labeling and analysis method described in Chapter 3, and/or by supplying other labeled forms of suspected precursors. Use of chemical inhibitors can aid in this area of research by redirecting biosynthesis of IAA toward pathways of interest, and are especially important tools for use when mutations in specific genes are lethal and/or developmentally limiting and thus would prevent the necessary studies from being carried out.

Bibliography

Abrahams KA, Cox JA, Fütterer K, Rullas J, Ortega-Muro F, Loman NJ, Moynihan PJ, Pérez-Herrán E, Jiménez E, Esquivias J (2017) Inhibiting mycobacterial tryptophan synthase by targeting the inter-subunit interface. Scientific Reports **7:** 1-15

Anderson K, Miles E, Johnson K (1991) Serine modulates substrate channeling in tryptophan synthase: A novel intersubunit triggering mechanism. Journal of Biological Chemistry **266:** 8020-8033

Baldi BG, Maher BR, Slovin JP, Cohen JD (1991) Stable isotope labeling, in vivo, of D-and L-tryptophan pools in *Lemna gibba* and the low incorporation of label into indole-3-acetic acid. Plant Physiology **95:** 1203-1208

Barkawi LS, Tam Y-Y, Tillman JA, Normanly J, Cohen JD (2010) A high-throughput method for the quantitative analysis of auxins. Nature Protocols **5:** 1609-1618

Barkawi LS, Tam Y-Y, Tillman JA, Pederson B, Calio J, Al-Amier H, Emerick M, Normanly J, Cohen JD (2008) A high-throughput method for the quantitative analysis of indole-3-acetic acid and other auxins from plant tissue. Analytical Biochemistry **372:** 177-188

Bellini C, Pacurar DI, Perrone I (2014) Adventitious roots and lateral roots: similarities and differences. Annual Review of Plant Biology **65:** 639-666

Berlyn MB, Last RL, Fink GR (1989) A gene encoding the tryptophan synthase beta subunit of *Arabidopsis thaliana*. Proceedings of the National Academy of Sciences **86:** 4604-4608

Bialek K, Meudt WJ, Cohen JD (1983) Indole-3-acetic acid (IAA) and IAA conjugates applied to bean stem sections: IAA content and the growth response. Plant Physiology **73:** 130-134

Bloch K, Anker H (1948) An extension of the isotope dilution method. Science (Washington) **107**

Brumos J, Robles LM, Yun J, Vu TC, Jackson S, Alonso JM, Stepanova AN (2018) Local auxin biosynthesis is a key regulator of plant development. Developmental Cell **47:** 306-318. e305

Cano A, Sánchez-García AB, Albacete A, González-Bayón R, Justamante MS, Ibáñez S, Acosta M, Pérez-Pérez JM (2018) Enhanced conjugation of auxin by GH3 enzymes leads to poor adventitious rooting in carnation stem cuttings. Frontiers in Plant Science **9:** 566

Chambers MC, Maclean B, Burke R, Amodei D, Ruderman DL, Neumann S, Gatto L, Fischer B, Pratt B, Egertson J (2012) A cross-platform toolkit for mass spectrometry and proteomics. Nature Biotechnology **30:** 918-920

Chandler JW (2009) Local auxin production: a small contribution to a big field. Bioessays **31:** 60-70

Chen J (2017) The study of Tryptophan-Dependent Indole-3-Acetic Acid Biosynthesis pathways in Maize Endosperm. University of Minnesota PhD dissertation. Retrieved from the University of Minnesota Digital Conservancy, http://hdl.handle.net/11299/191384

Chen L, Tong J, Xiao L, Ruan Y, Liu J, Zeng M, Huang H, Wang J-W, Xu L (2016) YUCCA-mediated auxin biogenesis is required for cell fate transition occurring during de novo root organogenesis in Arabidopsis. Journal of Experimental Botany **67:** 4273-4284

Cheng Y, Dai X, Zhao Y (2006) Auxin biosynthesis by the YUCCA flavin monooxygenases controls the formation of floral organs and vascular tissues in Arabidopsis. Genes & Development **20:** 1790-1799

Cheng Y, Dai X, Zhao Y (2007) Auxin synthesized by the YUCCA flavin monooxygenases is essential for embryogenesis and leaf formation in Arabidopsis. The Plant Cell **19:** 2430-2439

Cohen JD, Baldi BG, Slovin JP (1986) $^{13}C_6$-[Benzene Ring]-indole-3-acetic acid a new internal standard for quantitative mass spectral analysis of indole-3-acetic acid in plants. Plant Physiology **80:** 14-19

Cooke TJ, Poli D, Sztein AE, Cohen JD (2002) Evolutionary patterns in auxin action. *In* Auxin Molecular Biology. Springer, pp 319-338

Cooney TP, Nonhebel HM (1989) The measurement and mass spectral identification of indole-3-pyruvate from tomato shoots. Biochemical and Biophysical Research Communications **162:** 761-766

Cooney TP, Nonhebel HM (1991) Biosynthesis of indole-3-acetic acid in tomato shoots: Measurement, mass-spectral identification and incorporation of ^2H from ^2H_2O into indole-3-acetic acid, D-and L-tryptophan, indole-3-pyruvate and tryptamine. Planta **184:** 368-376

da Costa CT, Gaeta ML, de Araujo Mariath JE, Offringa R, Fett-Neto AG (2018) Comparative adventitious root development in pre-etiolated and flooded Arabidopsis hypocotyls exposed to different auxins. Plant Physiology and Biochemistry **127:** 161-168

da Rocha Correa L, Troleis J, Mastroberti A, Mariath J, Fett-Neto A (2012) Distinct modes of adventitious rooting in Arabidopsis thaliana. Plant Biology **14:** 100-109

Della Rovere F, Fattorini L, D'angeli S, Veloccia A, Falasca G, Altamura M (2013) Auxin and cytokinin control formation of the quiescent centre in the adventitious root apex of Arabidopsis. Annals of Botany **112:** 1395-1407

Dias MVB, Canduri F, da Silveira NJF, Czekster CM, Basso LA, Palma MS, Santos DS, de Azevedo WF (2006) Molecular models of tryptophan synthase from Mycobacterium tuberculosis complexed with inhibitors. Cell Biochemistry and Biophysics **44:** 375-384

Ding Z, Wang B, Moreno I, Dupláková N, Simon S, Carraro N, Reemmer J, Pěnčík A, Chen X, Tejos R (2012) ER-localized auxin transporter PIN8 regulates auxin

homeostasis and male gametophyte development in Arabidopsis. Nature Communications **3:** 1-11

Epstein E, Chen K-H, Cohen JD (1989) Identification of indole-3-butyric acid as an endogenous constituent of maize kernels and leaves. Plant Growth Regulation **8:** 215-223

Epstein E, Cohen JD, Slovin JP (2002) The biosynthetic pathway for indole-3-acetic acid changes during tomato fruit development. Plant Growth Regulation **38:** 15-20

Erdmann N, Schiewer U (1971) Tryptophan-dependent indoleacetic-acid biosynthesis from indole, demonstrated by double-labelling experiments. Planta **97:** 135-141

Evans EM, Freund DM, Sondervan VM, Cohen JD, Hegeman AD (2018) Metabolic patterns in Spirodela polyrhiza revealed by 15N stable isotope labeling of amino acids in photoautotrophic, heterotrophic, and mixotrophic growth conditions. Frontiers in Chemistry **6:** 191

Fan K-T, Rendahl AK, Chen W-P, Freund DM, Gray WM, Cohen JD, Hegeman AD (2016) Proteome scale-protein turnover analysis using high resolution mass spectrometric data from stable-isotope labeled plants. Journal of Proteome Research **15:** 851-867

Finn J, Langevine C, Birk I, Birk J, Nickerson K, Rodaway S (1999) Rational herbicide design by inhibition of tryptophan biosynthesis. Bioorganic & Medicinal Chemistry Letters **9:** 2297-2302

Fukui K, Hayashi K-i (2018) Manipulation and sensing of auxin metabolism, transport and signaling. Plant and Cell Physiology **59:** 1500-1510

Gleeson M, Mitter N, Carroll B (2014) Etiolation-mediated regulation of adventitious rooting in avocado. *In* XXIX International Horticultural Congress on Horticulture: Sustaining Lives, Livelihoods and Landscapes (IHC2014): 1110, pp 35-40

He W, Brumos J, Li H, Ji Y, Ke M, Gong X, Zeng Q, Li W, Zhang X, An F (2011) A small-molecule screen identifies L-kynurenine as a competitive inhibitor of

TAA1/TAR activity in ethylene-directed auxin biosynthesis and root growth in Arabidopsis. The Plant Cell **23:** 3944-3960

Howard B, Ridout M (1992) A mechanism to explain increased rooting in leafy cuttings of Syringa vulgaris 'Madame Lemoine' following dark-treatment of the stockplant. Journal of Horticultural Science **67:** 103-114

Huttlin EL, Hegeman AD, Harms AC, Sussman MR (2007) Comparison of full versus partial metabolic labeling for quantitative proteomics analysis in Arabidopsis thaliana. Molecular & Cellular Proteomics **6:** 860-881

Kakei Y, Yamazaki C, Suzuki M, Nakamura A, Sato A, Ishida Y, Kikuchi R, Higashi S, Kokudo Y, Ishii T (2015) Small-molecule auxin inhibitors that target YUCCA are powerful tools for studying auxin function. The Plant Journal **84:** 827-837

Kasahara H (2016) Current aspects of auxin biosynthesis in plants. Bioscience, Biotechnology, and Biochemistry **80:** 34-42

Klopotek Y, Haensch K-T, Hause B, Hajirezaei M-R, Druege U (2010) Dark exposure of petunia cuttings strongly improves adventitious root formation and enhances carbohydrate availability during rooting in the light. Journal of Plant Physiology **167:** 547-554

Korasick DA, Enders TA, Strader LC (2013) Auxin biosynthesis and storage forms. Journal of Experimental Botany **64:** 2541-2555

Koshiba T, Matsuyama H (1993) An in vitro system of indole-3-acetic acid formation from tryptophan in maize (*Zea mays*) coleoptile extracts. Plant Physiology **102:** 1319-1324

Kreiser M, Giblin C, Murphy R, Fiesel P, Braun L, Johnson G, Wyse D, Cohen JD (2016) Conversion of indole-3-butyric acid to indole-3-acetic acid in shoot tissue of hazelnut (*Corylus*) and elm (*Ulmus*). Journal of Plant Growth Regulation **35:** 710-721

Kriechbaumer V, Botchway SW, Hawes C (2017) Localization and interactions between Arabidopsis auxin biosynthetic enzymes in the TAA/YUC-dependent pathway. Journal of Experimental Botany **68:** 4195-4207

Kriechbaumer V, Wang P, Hawes C, Abell BM (2012) Alternative splicing of the auxin biosynthesis gene YUCCA4 determines its subcellular compartmentation. The Plant Journal **70:** 292-302

Kriechbaumer V, Weigang L, Fießelmann A, Letzel T, Frey M, Gierl A, Glawischnig E (2008) Characterisation of the tryptophan synthase alpha subunit in maize. BMC Plant Biology **8:** 44

Li J, Last RL (1996) The *Arabidopsis thaliana trp5* mutant has a feedback-resistant anthranilate synthase and elevated soluble tryptophan. Plant Physiology **110:** 51-59

Lincoln C, Britton JH, Estelle M (1990) Growth and development of the *axr1* mutants of Arabidopsis. The Plant Cell **2:** 1071-1080

Liu J, Sheng L, Xu Y, Li J, Yang Z, Huang H, Xu L (2014) WOX11 and 12 are involved in the first-step cell fate transition during de novo root organogenesis in Arabidopsis. The Plant Cell **26:** 1081-1093

Liu X, Barkawi L, Gardner G, Cohen JD (2012) Transport of indole-3-butyric acid and indole-3-acetic acid in Arabidopsis hypocotyls using stable isotope labeling. Plant Physiology **158:** 1988-2000

Liu X, Hegeman AD, Gardner G, Cohen JD (2012) Protocol: high-throughput and quantitative assays of auxin and auxin precursors from minute tissue samples. Plant Methods **8:** 1-17

Ljung K, Hull AK, Celenza J, Yamada M, Estelle M, Normanly J, Sandberg G (2005) Sites and regulation of auxin biosynthesis in Arabidopsis roots. The Plant Cell **17:** 1090-1104

Malamy JE, Benfey PN (1997) Organization and cell differentiation in lateral roots of Arabidopsis thaliana. Development **124:** 33-44

Marabotti A, Cozzini P, Mozzarelli A (2000) Novel allosteric effectors of the tryptophan synthase α2β2 complex identified by computer-assisted molecular modeling. Biochimica et Biophysica Acta (BBA)-Protein Structure and Molecular Enzymology **1476:** 287-299

Mashiguchi K, Tanaka K, Sakai T, Sugawara S, Kawaide H, Natsume M, Hanada A, Yaeno T, Shirasu K, Yao H (2011) The main auxin biosynthesis pathway in Arabidopsis. Proceedings of the National Academy of Sciences **108:** 18512-18517

Matchett WH (1972) Inhibition of tryptophan synthetase by indoleacrylic acid. Journal of Bacteriology **110:** 146-154

Matsui K, Miwa K, Sano K (1987) Two single-base-pair substitutions causing desensitization to tryptophan feedback inhibition of anthranilate synthase and enhanced expression of tryptophan genes of *Brevibacterium lactofermentum*. Journal of Bacteriology **169:** 5330-5332

Michalczuk L, Ribnicky DM, Cooke TJ, Cohen JD (1992) Regulation of indole-3-acetic acid biosynthetic pathways in carrot cell cultures. Plant Physiology **100:** 1346-1353

Michalska K, Chang C, Maltseva NI, Jedrzejczak R, Robertson GT, Gusovsky F, McCarren P, Schreiber SL, Nag PP, Joachimiak A (2020) Allosteric inhibitors of Mycobacterium tuberculosis tryptophan synthase. Protein Science **29:** 779-788

Müller-Moulé P, Nozue K, Pytlak ML, Palmer CM, Covington MF, Wallace AD, Harmer SL, Maloof JN (2016) YUCCA auxin biosynthetic genes are required for Arabidopsis shade avoidance. PeerJ **4:** e2574

Muñoz-Sanhueza LG, Lee Y, Tillmann M, Cohen JD, Hvoslef-Eide AK (2018) Auxin analysis using laser microdissected plant tissues sections. BMC Plant Biology **18:** 133

Narukawa-Nara M, Nakamura A, Kikuzato K, Kakei Y, Sato A, Mitani Y, Yamasaki-Kokudo Y, Ishii T, Hayashi Ki, Asami T (2016) Aminooxy-

naphthylpropionic acid and its derivatives are inhibitors of auxin biosynthesis targeting l-tryptophan aminotransferase: structure–activity relationships. The Plant Journal **87:** 245-257

Naz S, Farooq U, Ali S, Sarwar R, Khan S, Abagyan R (2019) Identification of new benzamide inhibitor against α-subunit of tryptophan synthase from Mycobacterium tuberculosis through structure-based virtual screening, anti-tuberculosis activity and molecular dynamics simulations. Journal of Biomolecular Structure and Dynamics **37:** 1043-1053

Ngo H, Harris R, Kimmich N, Casino P, Niks D, Blumenstein L, Barends TR, Kulik V, Weyand M, Schlichting I (2007) Synthesis and characterization of allosteric probes of substrate channeling in the tryptophan synthase bienzyme complex. Biochemistry **46:** 7713-7727

Nishimura T, Hayashi Ki, Suzuki H, Gyohda A, Takaoka C, Sakaguchi Y, Matsumoto S, Kasahara H, Sakai T, Kato Ji (2014) Yucasin is a potent inhibitor of YUCCA, a key enzyme in auxin biosynthesis. The Plant Journal **77:** 352-366

Niyogi KK, Fink GR (1992) Two anthranilate synthase genes in Arabidopsis: defense-related regulation of the tryptophan pathway. The Plant Cell **4:** 721-733

Nonhebel H, Yuan Y, Al-Amier H, Pieck M, Akor E, Ahamed A, Cohen JD, Celenza JL, Normanly J (2011) Redirection of tryptophan metabolism in tobacco by ectopic expression of an Arabidopsis indolic glucosinolate biosynthetic gene. Phytochemistry **72:** 37-48

Nonhebel HM (2015) Tryptophan-independent indole-3-acetic acid synthesis: Critical evaluation of the evidence. Plant Physiology **169:** 1001-1005

Normanly J (2010) Approaching cellular and molecular resolution of auxin biosynthesis and metabolism. Cold Spring Harbor Perspectives in Biology **2:** a001594

Normanly J, Cohen JD, Fink GR (1993) *Arabidopsis thaliana* auxotrophs reveal a tryptophan-independent biosynthetic pathway for indole-3-acetic acid. Proceedings of the National Academy of Sciences **90:** 10355-10359

Novák O, Hényková E, Sairanen I, Kowalczyk M, Pospíšil T, Ljung K (2012) Tissue-specific profiling of the Arabidopsis thaliana auxin metabolome. The Plant Journal **72:** 523-536

Novák O, Pěnčík A, Blahoušek O, Ljung K (2017) Quantitative auxin metabolite profiling using stable isotope dilution UHPLC-MS/MS. Current Protocols in Plant Biology **1:** 419-430

Östin A, Ilić N, Cohen JD (1999) An in vitro system from maize seedlings for tryptophan-independent indole-3-acetic acid biosynthesis. Plant Physiology **119:** 173-178

Overvoorde P, Fukaki H, Beeckman T (2010) Auxin control of root development. Cold Spring Harbor Perspectives in Biology **2:** a001537

Pengelly WL, Bandurski RS (1983) Analysis of indole-3-acetic acid metabolism in Zea mays using deuterium oxide as a tracer. Plant Physiology **73:** 445-449

Phillips KA, Skirpan AL, Liu X, Christensen A, Slewinski TL, Hudson C, Barazesh S, Cohen JD, Malcomber S, McSteen P (2011) vanishing tassel2 encodes a grass-specific tryptophan aminotransferase required for vegetative and reproductive development in maize. The Plant Cell **23:** 550-566

Pieck M, Yuan Y, Godfrey J, Fisher C, Zolj S, Vaughan D, Thomas N, Wu C, Ramos J, Lee N (2015) Auxin and tryptophan homeostasis are facilitated by the ISS1/VAS1 aromatic aminotransferase in Arabidopsis. Genetics **201:** 185-199

Poulsen C, Bongaerts RJ, Verpoorte R (1993) Purification and characterization of anthranilate synthase from *Catharanthus roseus*. European Journal of Biochemistry **212:** 431-440

Quittenden LJ, Davies NW, Smith JA, Molesworth PP, Tivendale ND, Ross JJ (2009) Auxin biosynthesis in pea: characterization of the tryptamine pathway. Plant Physiology **151:** 1130-1138

Rajagopal R (1971) Metabolism of indole-3-acetaldehyde. III. Some characteristics of the aldehyde oxidase of Avena coleoptiles. Physiologia Plantarum **24:** 272-281

Rapparini F, Cohen JD, Slovin JP (1999) Indole-3-acetic acid biosynthesis in *Lemna gibba* studied using stable isotope labeled anthranilate and tryptophan. Plant Growth Regulation **27:** 139-144

Rapparini F, Tam YY, Cohen JD, Slovin JP (2002) Indole-3-acetic acid metabolism in *Lemna gibba* undergoes dynamic changes in response to growth temperature. Plant Physiology **128:** 1410-1416

Rittenberg D, Foster G (1940) A new procedure for quantitative analysis by isotope dilution, with application to the determination of amino acids and fatty acids. Journal of Biological Chemistry **133:** 737-744

Sang YL, Cheng ZJ, Zhang XS (2016) Endogenous auxin biosynthesis and de novo root organogenesis. Journal of Experimental Botany **67:** 4011

Seidel C, Walz A, Park S, Cohen JD, Ludwig-Müller J (2006) Indole-3-acetic acid protein conjugates: novel players in auxin homeostasis. Plant Biology **8:** 340-345

Seo M, Akaba S, Oritani T, Delarue M, Bellini C, Caboche M, Koshiba T (1998) Higher activity of an aldehyde oxidase in the auxin-overproducing *superroot1* mutant of *Arabidopsis thaliana*. Plant Physiology **116:** 687-693

Shrestha B (2020) Ten Major Future Challenges in Single-Cell Metabolomics. *In* Single Cell Metabolism. Springer, pp 219-223

Smith CA, Want EJ, O'Maille G, Abagyan R, Siuzdak G (2006) XCMS: processing mass spectrometry data for metabolite profiling using nonlinear peak alignment, matching, and identification. Analytical Chemistry **78:** 779-787

Soeno K, Goda H, Ishii T, Ogura T, Tachikawa T, Sasaki E, Yoshida S, Fujioka S, Asami T, Shimada Y (2010) Auxin biosynthesis inhibitors, identified by a genomics-based approach, provide insights into auxin biosynthesis. Plant and Cell Physiology **51:** 524-536

Sorin C, Bussell JD, Camus I, Ljung K, Kowalczyk M, Geiss G, McKhann H, Garcion C, Vaucheret H, Sandberg G (2005) Auxin and light control of adventitious rooting in Arabidopsis require ARGONAUTE1. The Plant Cell **17:** 1343-1359

Sorin C, Negroni L, Balliau T, Corti H, Jacquemot MP, Davanture M, Sandberg G, Zivy M, Bellini C (2006) Proteomic analysis of different mutant genotypes of Arabidopsis led to the identification of 11 proteins correlating with adventitious root development. Plant Physiology **140:** 349-364

Steffens B, Rasmussen A (2016) The physiology of adventitious roots. Plant Physiology **170:** 603-617

Stepanova AN, Robertson-Hoyt J, Yun J, Benavente LM, Xie D-Y, Doležal K, Schlereth A, Jürgens G, Alonso JM (2008) TAA1-mediated auxin biosynthesis is essential for hormone crosstalk and plant development. Cell **133:** 177-191

Stepanova AN, Yun J, Robles LM, Novak O, He W, Guo H, Ljung K, Alonso JM (2011) The Arabidopsis YUCCA1 flavin monooxygenase functions in the indole-3-pyruvic acid branch of auxin biosynthesis. The Plant Cell **23:** 3961-3973

Strader LC, Wheeler DL, Christensen SE, Berens JC, Cohen JD, Rampey RA, Bartel B (2011) Multiple facets of Arabidopsis seedling development require indole-3-butyric acid–derived auxin. The Plant Cell Online **23:** 984-999

Sugawara S, Hishiyama S, Jikumaru Y, Hanada A, Nishimura T, Koshiba T, Zhao Y, Kamiya Y, Kasahara H (2009) Biochemical analyses of indole-3-acetaldoxime-dependent auxin biosynthesis in Arabidopsis. Proceedings of the National Academy of Sciences **106:** 5430-5435

Sugimoto S-i, Shiio I (1983) Regulation of tryptophan biosynthesis by feedback inhibition of the second-step enzyme, anthranilate phosphoribosyl-transferase, in *Brevibacterium flavum*. Agricultural and Biological Chemistry **47:** 2295-2305

Tang Q, Yu P, Tillmann M, Cohen JD, Slovin JP (2019) Indole-3-acetylaspartate and indole-3-acetylglutamate, the IAA-amide conjugates in the diploid strawberry achene, are hydrolyzed in growing seedlings. Planta **249:** 1073-1085

Tao Y, Ferrer J-L, Ljung K, Pojer F, Hong F, Long JA, Li L, Moreno JE, Bowman ME, Ivans LJ (2008) Rapid synthesis of auxin via a new tryptophan-dependent pathway is required for shade avoidance in plants. Cell **133:** 164-176

Tivendale ND, Cohen JD (2015) Analytical history of auxin. Journal of Plant Growth Regulation **34:** 708-722

Tivendale ND, Davies NW, Molesworth PP, Davidson SE, Smith JA, Lowe EK, Reid JB, Ross JJ (2010) Reassessing the role of N-hydroxytryptamine in auxin biosynthesis. Plant Physiology **154:** 1957-1965

Tivendale ND, Ross JJ, Cohen JD (2014) The shifting paradigms of auxin biosynthesis. Trends in Plant Science **19:** 44-51

Tsugafune S, Mashiguchi K, Fukui K, Takebayashi Y, Nishimura T, Sakai T, Shimada Y, Kasahara H, Koshiba T, Hayashi K-i (2017) Yucasin DF, a potent and persistent inhibitor of auxin biosynthesis in plants. Scientific Reports **7:** 13992

Tsurusaki K-i, Takeda K, Sakurai N (1997) Conversion of indole-3-acetaldehyde to indole-3-acetic acid in cell-wall fraction of barley (*Hordeum vulgare*) seedlings. Plant and Cell Physiology **38:** 268-273

Wang B, Chu J, Yu T, Xu Q, Sun X, Yuan J, Xiong G, Wang G, Wang Y, Li J (2015) Tryptophan-independent auxin biosynthesis contributes to early embryogenesis in Arabidopsis. Proceedings of the National Academy of Sciences **112:** 4821-4826

Watkins-Dulaney E, Straathof S, Arnold F (2020) Tryptophan synthase: Biocatalyst Extraordinaire. ChemBioChem

Winter A (1966) A hypothetical route for the biogenisis of IAA. Planta **71:** 229-239

Won C, Shen X, Mashiguchi K, Zheng Z, Dai X, Cheng Y, Kasahara H, Kamiya Y, Chory J, Zhao Y (2011) Conversion of tryptophan to indole-3-acetic acid by TRYPTOPHAN AMINOTRANSFERASES OF ARABIDOPSIS and YUCCAs in Arabidopsis. Proceedings of the National Academy of Sciences **108:** 18518-18523

Woodward AW, Bartel B (2005) Auxin: Regulation, action, and interaction. Annals of Botany **95:** 707-735

Wright AD, Moehlenkamp CA, Perrot GH, Neuffer MG, Cone KC (1992) The maize auxotrophic mutant orange pericarp is defective in duplicate genes for tryptophan synthase beta. The Plant Cell **4:** 711-719

Wright AD, Sampson MB, Neuffer MG, Michalczuk L, Slovin JP, Cohen JD (1991) Indole-3-acetic acid biosynthesis in the mutant maize *orange pericarp*, a tryptophan auxotroph. Science **254:** 998-1000

Xu Y, Abeles RH (1993) Inhibition of tryptophan synthase by (1-fluorovinyl) glycine. Biochemistry **32:** 806-811

Yang H, Klopotek Y, Hajirezaei MR, Zerche S, Franken P, Druege U (2019) Role of auxin homeostasis and response in nitrogen limitation and dark stimulation of adventitious root formation in petunia cuttings. Annals of Botany **124:** 1053-1066

Yang XY, Chen WP, Rendahl AK, Hegeman AD, Gray WM, Cohen JD (2010) Measuring the turnover rates of Arabidopsis proteins using deuterium oxide: an auxin signaling case study. The Plant Journal **63:** 680-695

Yang Z-B, Geng X, He C, Zhang F, Wang R, Horst WJ, Ding Z (2014) TAA1-regulated local auxin biosynthesis in the root-apex transition zone mediates the aluminum-induced inhibition of root growth in Arabidopsis. The Plant Cell **26:** 2889-2904

Yu P, Hegeman AD, Cohen JD (2014) A facile means for the identification of indolic compounds from plant tissues. The Plant Journal **79:** 1065-1075

Zhang R, Wang B, Ouyang J, Li J, Wang Y (2008) Arabidopsis indole synthase, a homolog of tryptophan synthase alpha, is an enzyme involved in the trp-independent indole-containing metabolite biosynthesis. Journal of Integrative Plant Biology **50:** 1070-1077

Zhao J, Last RL (1995) Immunological characterization and chloroplast localization of the tryptophan biosynthetic enzymes of the flowering plant Arabidopsis thaliana. Journal of Biological Chemistry **270:** 6081-6087

Zhao Y (2018) Essential roles of local auxin biosynthesis in plant development and in adaptation to environmental changes. Annual Review of Plant Biology **69:** 417-435

Zhao Y, Christensen SK, Fankhauser C, Cashman JR, Cohen JD, Weigel D, Chory J (2001) A role for flavin monooxygenase-like enzymes in auxin biosynthesis. Science **291:** 306-309

Zhu Y, Li H-j, Su Q, Wen J, Wang Y, Song W, Xie Y, He W, Yang Z, Jiang K (2019) A phenotype-directed chemical screen identifies ponalrestat as an inhibitor of the plant flavin monooxygenase YUCCA in auxin biosynthesis. Journal of Biological Chemistry **294:** 19923-19933

Appendix A: Light quality, quantity, and duration and genotype effects on adventitious root formation in *Arabidopsis*.

Adventitious root formation is an important developmental process affecting the productivity of a wide range of agricultural plants; however, it is not as thoroughly understood as lateral root development (referring to roots that originate from existing roots) (Bellini et al., 2014). The root systems of major monocotyledonous crop species such as corn, rice, and wheat are mainly comprised of adventitious roots in the form of brace or crown roots (Atkinson et al., 2014). These crops provide more than half of the calories consumed by people worldwide (Awika, 2011), making their ability to obtain adequate water and nutrients from the soil through adventitious roots a critical factor for world food security (Steffens and Rasmussen, 2016). Understanding the basis of adventitious root formation is especially relevant in addressing major limitations of crop productivity relating to water and nutrient acquisition, such as drought and nitrogen deficiency. Additionally, horticultural species such as apple, citrus, pear, grape and plum are often propagated by taking shoots of high-performing parents and stimulating them to form adventitious roots, resulting in a new plant that is a genetic copy (Dirr and Heuser, 1987). Light quality, intensity, and photoperiod are important environmental variables affecting adventitious rooting (Christiaens et al., 2016), but rooting responses of various species to even simple dark-light transitions have not been widely explored. Petunia cuttings exposed to a 7 day dark treatment showed a greater than three-fold increase in adventitious root number (Klopotek et al., 2010; Zerche et al., 2016). This dramatic improvement in rooting efficiency, using the results in petunia as an example, demonstrates that dark-light transitions, perhaps optimized using light of a specific wavelength, may be a cost-effective way to improve plant propagation.

Etiolated (dark-grown) seedlings of the reference species *Arabidopsis thaliana* grown in the dark for several days can form adventitious roots upon transfer to light (Sorin et al., 2005). It is not yet entirely clear how transitioning seedlings from darkness into light leads to adventitious root induction, and Takahashi et al. (2003) noted that, in

regard to adventitious rooting in etiolated seedlings, “It will be important to unveil what kind of photo-response is involved in the photo-inhibition of adventitious root initiation.” The following experiments explore the light and hormonal signaling mechanisms regulating adventitious rooting, providing information which may be useful toward improving root development in agriculturally, environmentally, and historically important species. We observed root formation under various light conditions in a number of light signaling mutants to provide insight into the plant photoreceptors and signaling pathways that may regulate light-induced adventitious root formation. We also quantified auxin levels in hypocotyl sections and observed effects of exogenous hormone treatments, as well as inhibitors of IAA biosynthesis and transport, to determine the tissue-specific hormonal changes stimulating light-induced adventitious root formation. A brief summary of our findings from each experiment is included below the figure captions.

Table A-1: *Arabidopsis* genotypes used in adventitious rooting experiments

Name	Description	Locus
ago1	*argonaute 1* mutant (*ago 1-46* allele and CS319294 accession used)	AT1G48410
Col-0	Wild type (WT) Columbia-0 ecotype	
cry1cry2	*cryptochrome 1, cryptochrome 2* double mutant	AT4G08920, AT1G04400
cry1cry2phyA	*cryptochrome 1, cryptochrome 2, phytochrome A* triple mutant	AT4G08920, AT1G04400, AT1G09570
cry1cry2phyB	*cryptochrome 1, cryptochrome 2, phytochrome B-9* triple mutant	AT4G08920, AT1G04400, AT2G18790
dao1	*dioxygenase for auxin oxidation 1-1* mutant	AT1G14130
ech2ibr10	*enoyl-coA hydratase 2, indole-3-butyric acid response 10* double mutant	AT1G76150, AT4G14430
hfr1	*long hypocotyl in far-red* mutant	AT1G02340
hrdl	Unknown mutant in Ler background (***h****igh* ***r****oot formation* ***d****ark to* ***l****ight transition*)	unknown
hy5	*elongated hypocotyl 5* mutant	AT5G11260
hyh	*hy5-homolog* mutant	AT3G17609
Ler	Wild type Landsberg ecotype	
lrb1lrb2	*light-response BTB 1, light-response BTB2* mutant	AT2G46260, AT3G61600
max2	*more axillary branches 2 mutant* (*max 2-1* and *max 2-2* alleles used)	AT2G42620
phot1phot2	*phototropin 1, phototropin 2* double mutant	AT3G45780, AT5G58140
phyA	*phytochrome A* mutant	AT1G09570

phyABDE	*phytochrome A, phytochrome B-9, phytochrome D-2, phytochrome E* quadruple mutant	AT1G09570, AT2G18790, AT4G16250, AT4G18130
phyAphyB	*phytochrome A, phytochrome B-9* double mutant	AT1G09570, AT2G18790
phyB	*phytochrome B-9* mutant	AT2G18790
phyBlrb1lrb2	*phytochrome B-9, light-response BTB 1-1, light-response BTB 2-1* triple mutant	AT2G18790, AT2G46260, AT3G61600
PHYB-OE	PHYTOCHROME B overexpressor line	AT2G18790
phyBphyDlrb1lrb2	*phytochrome B-9, phytochrome D-2, light-response BTB 1-1, light-response BTB 2-1* quadruple mutant	AT2G18790, AT4G16250, AT2G46260, AT3G61600
phyC	*phytochrome C* mutant	AT5G35840
phyD	*phytochrome D-2* mutant	AT4G16250
phyDlrb1lrb2	*phytochrome D-2, light-response BTB 1-1, light-response BTB 2-1* triple mutant	AT4G16250, AT2G46260, AT3G61600
pif7	*phytochrome-interacting factor 7-1* mutant	AT5G61270
pifQ	*phytochrome-interacting factor (pif)1-1, pif3-3, pif4-2, pif5-3* quadruple mutant	AT2G20180, AT1G09530, AT2G43010, AT3G59060
RLD	Wild type RLD ecotype	
rty1wei2	*rooty 1-1, weakly ethylene insensitive 2-1* double mutant	AT2G20610, AT5G05730
sth2	*salt tolerance homolog 2* mutant (also called *bbx21; sth 2-1* and *sth2-2* alleles used)	AT1G75540

sur2	*superroot* mutant	AT4G31500
tir2	*transport inhibitor response 2* mutant	AT1G70560
tt4	*transparent testa 4* mutant	AT5G13930
tt7	*transparent testa 7* mutant	AT5G07990
Ws	Wild type Wassilewskija ecotype	

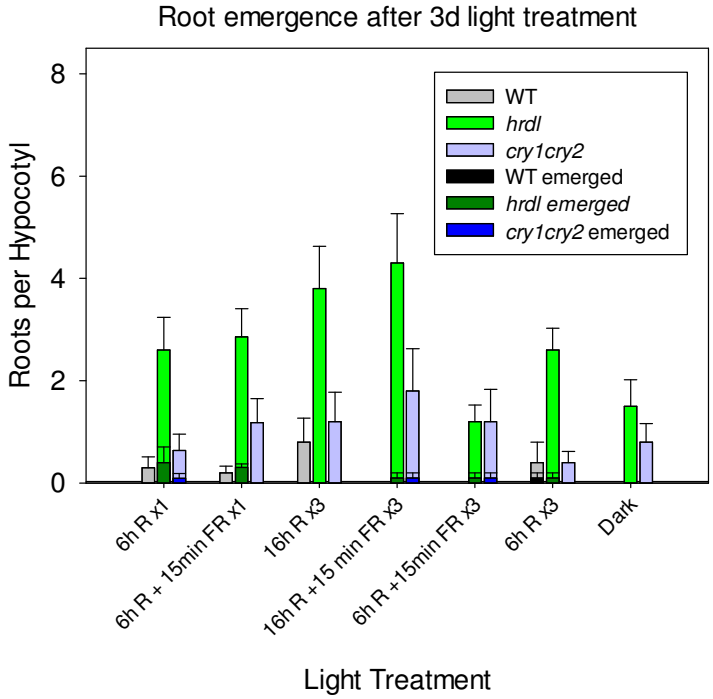
Root emergence after 3d light treatment
Roots per Hypocotyl
0
2
4
6
8
WT
hrdl
cry1cry2
WT emerged
hrdl emerged
cry1cry2 emerged
6h R x1
6h R + 15min FR x1
16h R x3
16h R +15 min FR x3
6h R +15min FR x3
6h R x3
Dark
Light Treatment

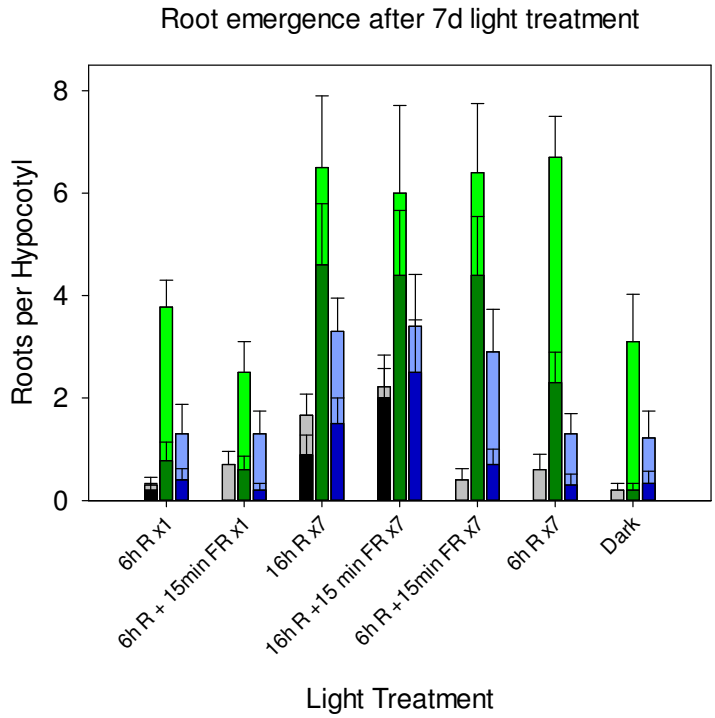
Root emergence after 7d light treatment
Roots per Hypocotyl
0
2
4
6
8
6h R x1
6h R + 15min FR x1
16h R x7
16h R +15 min FR x7
6h R +15min FR x7
6h R x7
Dark
Light Treatment

Figure A-1: Adventitious root primordia formation and emergence from hypocotyls after 3- and 7- day light treatments. *Arabidopsis* seeds were surface sterilized, suspended in a 100 μM gibberellic acid 4 (GA_4) solution, and sown on square Petri plates containing 0.5X strength MS medium with 3% sucrose. Plates were stored vertically in darkness at 20°C for 7 d, then transferred to Conviron PGR15 growth chambers equipped with Heliospectra L4A Series 10 LED lamps where they were exposed to one of the following light conditions (all with 100 μmol m^{-2} s^{-1} intensity): a one-time 6 h pulse of red light (R) supplied by 660 nm LEDs only, a one-time 6 h pulse of R followed by 15 min of far red light (FR) supplied by 730 nm LEDs only, a 16 h photoperiod of R (16 h R: 8 h Dark), a 16 h photoperiod of R followed by 15 min FR before the dark period, a 6 h photoperiod of R (6 h R: 18 h Dark), a 6 h photoperiod of R followed by 15 min FR before the dark period, or continued darkness. Hypocotyls were inspected under a light microscope after 3 and 7 days of light treatment to count the number of emerged adventitious roots and developing primordia. Error bars represent ±SE.

Adventitious roots begin to emerge after approximately 3 days in some light treatments and continue to develop in following days. Adventitious root emergence is increased following light treatments in *hrdl* and *cry1cry2* mutants. The *hrdl* line was previously misidentified as *phyB* and consistently showed increased light-dependent adventitious root formation through two generations of propagation. Multiple day light treatments induce formation of more adventitious roots compared to a single 6 h pulse.

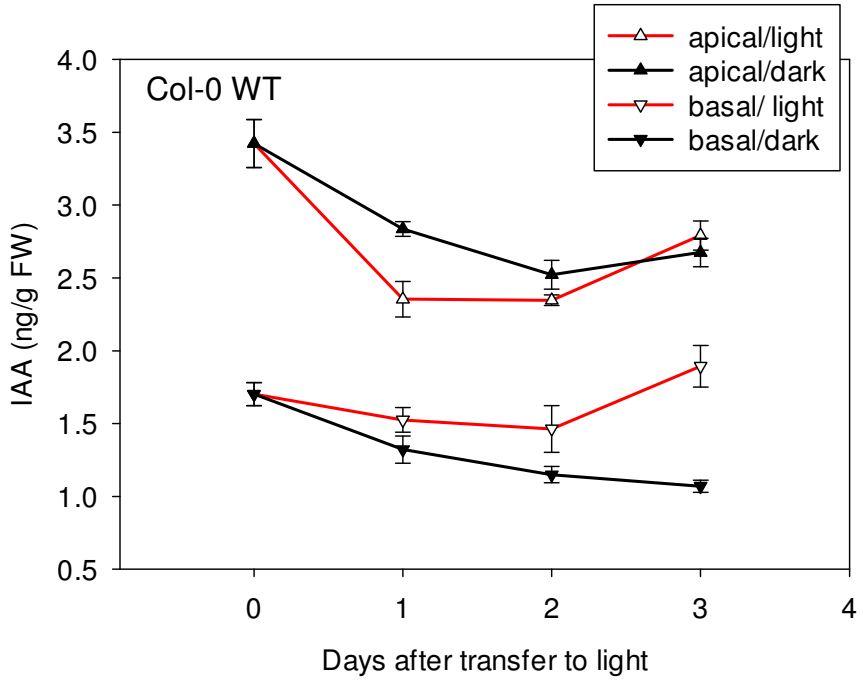

Figure A-2: Free IAA levels in hypocotyl sections on media containing 1% sucrose. Wild-type Col-0 seeds were surface sterilized and imbibed in a 100 µM gibberellic acid 4 (GA_4) solution for one week at 4°C, and then sown on square Petri plates containing 0.5X strength MS medium with 1% sucrose. Plates were stored vertically in darkness at 20°C for 7 d, then transferred to Conviron PGR15 growth chambers equipped with Heliospectra L4A Series 10 LED lamps where they were exposed to either a 16 h photoperiod of red light (660 nm, 135 µmol m^{-2} s^{-1}) or kept in continued darkness. 5-15 mg samples of hypocotyl tissue were collected immediately before and each of the 4 days after transfer. Hypocotyls (approximately 5-15 mm) were divided into apical and basal halves which were pooled into separate samples. Free indole-3-acetic acid (IAA) levels were quantified by isotope dilution LC-MS/MS using [$^{13}C_6$]IAA as an internal standard. Each point represents the mean of 5-6 biological replicates; error bars represent SE.

On 1% sucrose media, red light treatment resulted in higher free IAA levels in basal hypocotyl sections compared to dark control after 3 days. IAA content was higher in apical sections compared to basal sections.

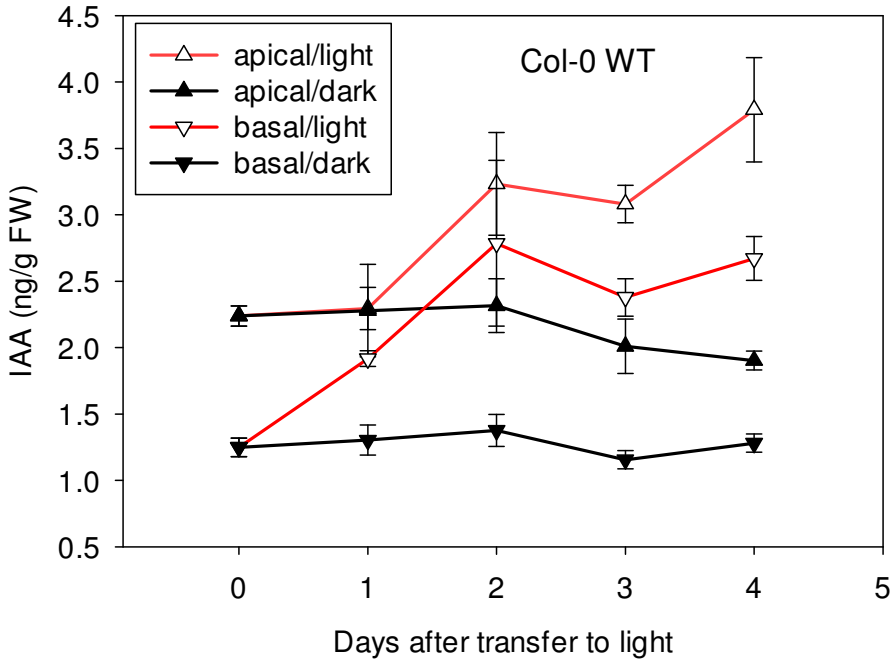

Figure A-3: Free IAA levels in hypocotyl sections on media containing 3% sucrose. Wild-type Col-0 seeds were surface sterilized and imbibed in a 100 µM gibberellic acid 4 (GA_4) solution for one week at 4°C, and then sown on square Petri plates containing 0.5X strength MS medium with 3% sucrose. Plates were stored vertically in darkness at 20°C for 7 d, then transferred to Conviron PGR15 growth chambers equipped with Heliospectra L4A Series 10 LED lamps where they were exposed to either a 16 h photoperiod of red light (660 nm, 135 µmol m^{-2} s^{-1}) or kept in continued darkness. 5-15 mg samples of hypocotyl tissue were collected immediately before and each of the 4 days after transfer. Hypocotyls were divided into apical and basal halves which were pooled into separate samples. Free IAA levels were quantified by isotope dilution LC-MS/MS using [$^{13}C_6$]IAA as an internal standard. Each point represents the mean of 5-6 biological replicates; error bars represent SE.

On 3% sucrose media, red light treatment resulted in higher free IAA levels in apical and basal hypocotyl sections compared to dark control after 2-4 days.

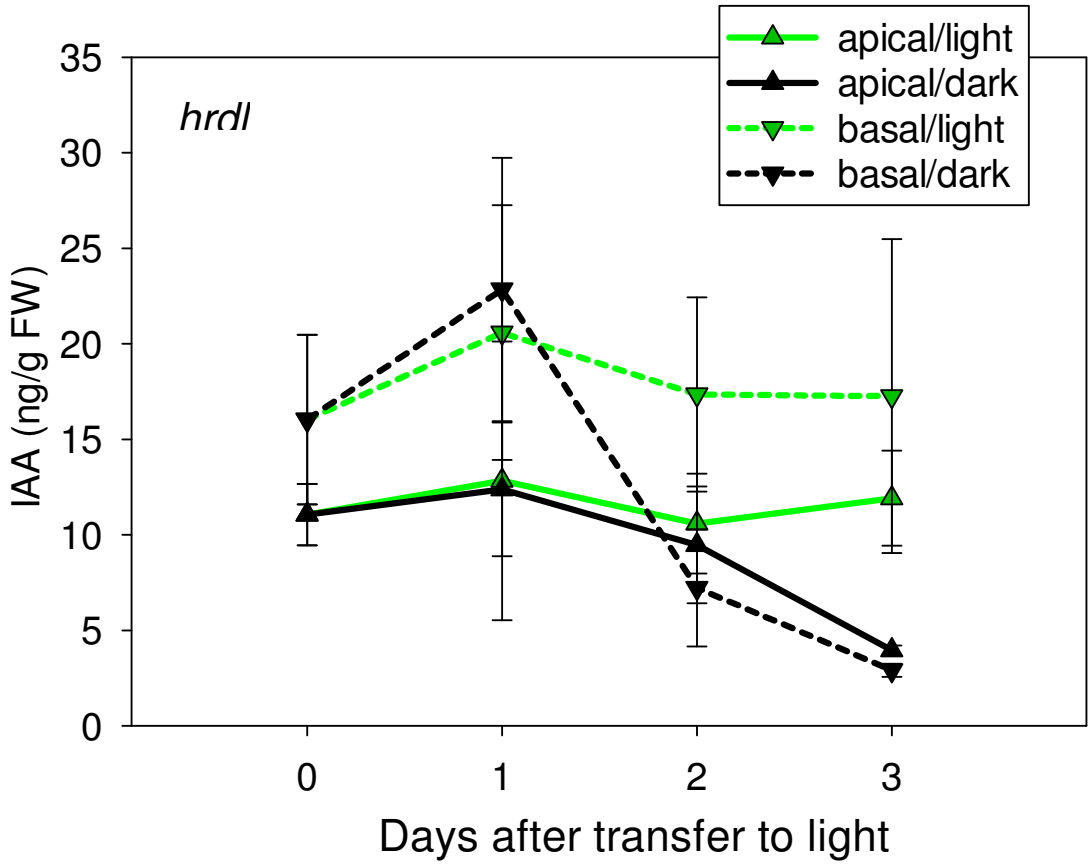

Figure A-4: Free IAA levels in *hrdl* hypocotyl sections. *hrdl* seeds were surface sterilized, suspended in a 100 µM gibberellic acid 4 (GA_4) solution, and sown on square Petri plates containing 0.5X strength MS medium with 3% sucrose. Plates were stored vertically in darkness at 20°C for 7 d, then transferred to Conviron PGR15 growth chambers equipped with Heliospectra L4A Series 10 LED lamps where they were exposed to either a 16 h photoperiod of red light (660 nm, 100 µmol m^{-2} s^{-1}) or kept in continued darkness. 5-15 mg samples of hypocotyl tissue were collected immediately before and each of the 4 days after transfer. Hypocotyls were divided into apical and basal halves which were pooled into separate samples. Free IAA levels were quantified by isotope dilution GC-MS/MS using [$^{13}C_6$]IAA as an internal standard. Each point represents the mean of 3-6 biological replicates; error bars represent SE.

In etiolated *hrdl* seedlings, red light treatment resulted in higher free IAA levels in apical and basal hypocotyl sections compared to dark control after 2-3 days.

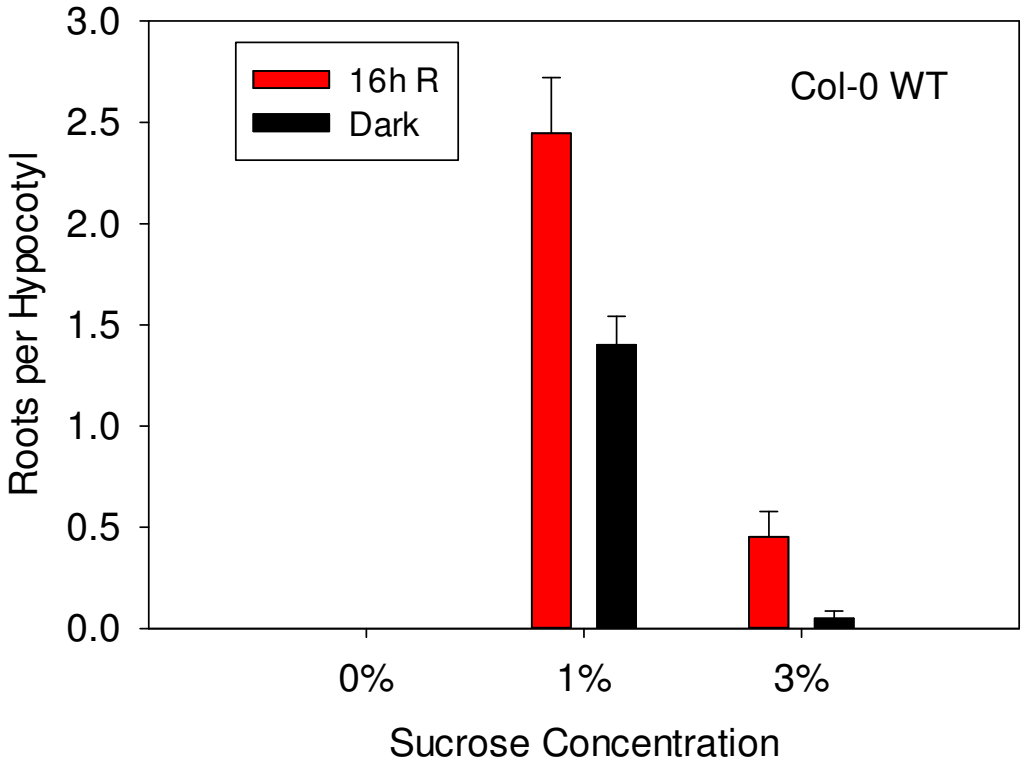

Figure A-5: Adventitious root formation in the presence of different sucrose concentrations. Wild-type Col-0 seeds were surface sterilized, suspended in a 100 µM gibberellic acid 4 (GA_4) solution, and sown on square Petri plates containing 0.5X strength MS medium with 0, 1%, or 3% sucrose. Plates were stored vertically in darkness at 20°C for 7 d, then transferred to Conviron PGR15 growth chambers equipped with Heliospectra L4A Series 10 LED lamps where they were exposed to either a 16 h photoperiod of red light (660 nm, 100 µmol m^{-2} s^{-1}) or kept in continued darkness. The number of adventitious roots visibly emerged from hypocotyls was counted after 7 d of light treatment.

Adventitious roots were only observed in etiolated seedlings grown on media containing sucrose, with more roots forming on 1% compared to 3% sucrose.

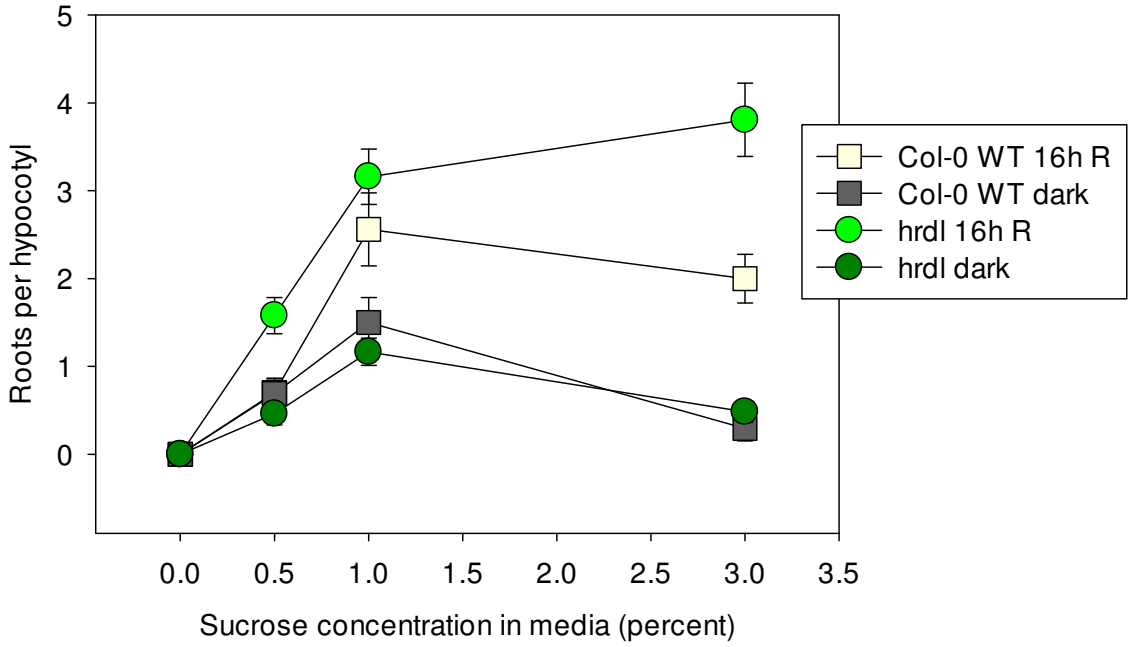

Figure A-6: Adventitious root formation in the presence of different sucrose concentrations. Wild-type Col-0 and *hrdl* seeds were surface sterilized, suspended in a 100 µM gibberellic acid 4 (GA_4) solution, and sown on square Petri plates containing 0.5X strength MS medium with 0, 0.5%, 1%, or 3% sucrose. Plates were stored vertically in darkness at 20°C for 7 d, then transferred to Conviron PGR15 growth chambers equipped with Heliospectra L4A Series 10 LED lamps where they were exposed to either a 16 h photoperiod of red light (660 nm, 100 µmol m^{-2} s^{-1}) or kept in continued darkness. The number of adventitious roots visibly emerged from hypocotyls was counted after 7 d of light treatment.

Adventitious roots were only observed in etiolated seedlings grown on media containing sucrose. Optimal sucrose concentrations for root induction differed between *hrdl* and Col-0 WT.

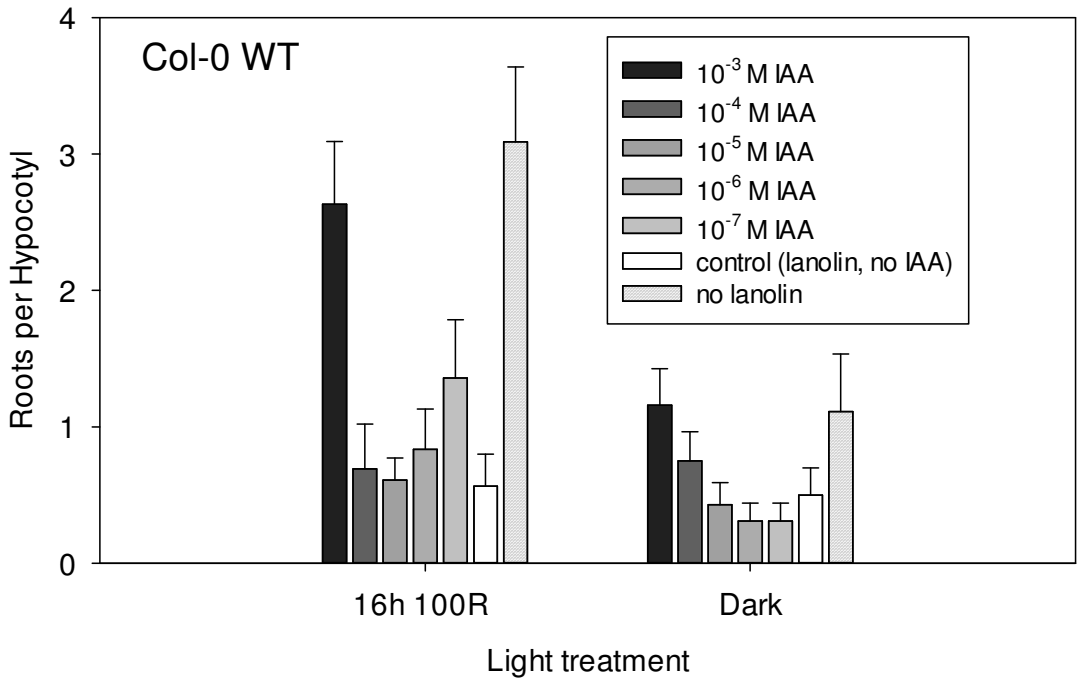

Figure A-7. Effect of IAA treatment administered in lanolin droplets on adventitious root formation. Wild-type Col-0 seeds were surface sterilized, suspended in a 100 μM gibberellic acid 4 (GA_4) solution, and sown on square Petri plates containing 0.5X strength MS medium with 3% sucrose. Plates were stored vertically in darkness at 20°C for 7 d, then a droplet of approximately 10 μL lanolin containing 0, 10^{-3} M, 10^{-4} M, 10^{-5} M, 10^{-6} M, or 10^{-7} M IAA was placed on the apical hook of each etiolated seedling; seedlings without lanolin droplet treatment were also included for comparison. Seedlings were transferred to Conviron PGR15 growth chambers equipped with Heliospectra L4A Series 10 LED lamps where they were exposed to either a 16 h photoperiod of red light (660 nm, 100 μmol m^{-2} s^{-1}) or kept in continued darkness. The number of adventitious roots visibly emerged from hypocotyls was counted after 7 d of light treatment.

Lanolin droplets alone showed a strong inhibitory effect on root formation and thus are not well suited for administering IAA treatments on etiolated seedlings.

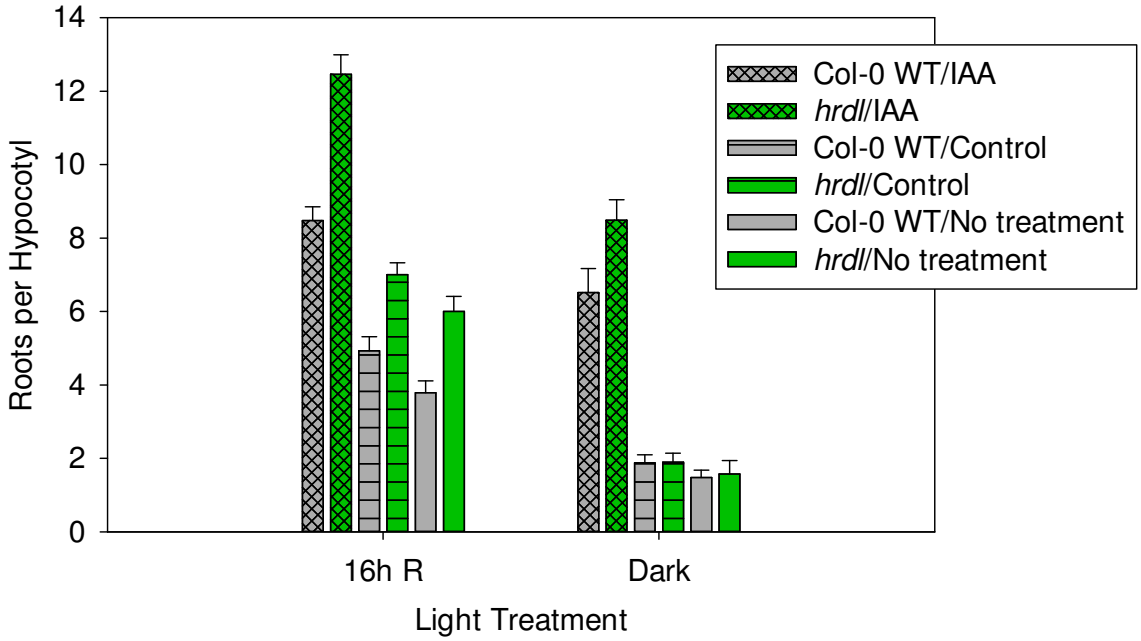

Figure A-8. Effect of IAA treatment administered in agarose droplets on adventitious root formation. Wild-type Col-0 seeds were surface sterilized, suspended in a 100 µM gibberellic acid 4 (GA_4) solution, and sown on square Petri plates containing 0.5X strength MS medium with 3% sucrose. Plates were stored vertically in darkness at 20°C for 7 d, then a 10 µL agarose droplet containing 0 or 10^{-3} M IAA was placed on the apical hook of each seedling; seedlings without agarose droplet treatment were also included for comparison. Seedlings were transferred to Conviron PGR15 growth chambers equipped with Heliospectra L4A Series 10 LED lamps where they were exposed to either a 16 h photoperiod of red light (660 nm, 100 µmol m^{-2} s^{-1}) or kept in continued darkness. The number of adventitious roots visibly emerged from hypocotyls was counted after 7 d of light treatment.

IAA treatment applied to apical hooks had a positive effect on adventitious root formation. Agarose droplets without IAA showed minimal effects on root formation, in contrast to what was shown using lanolin (Figure A.7).

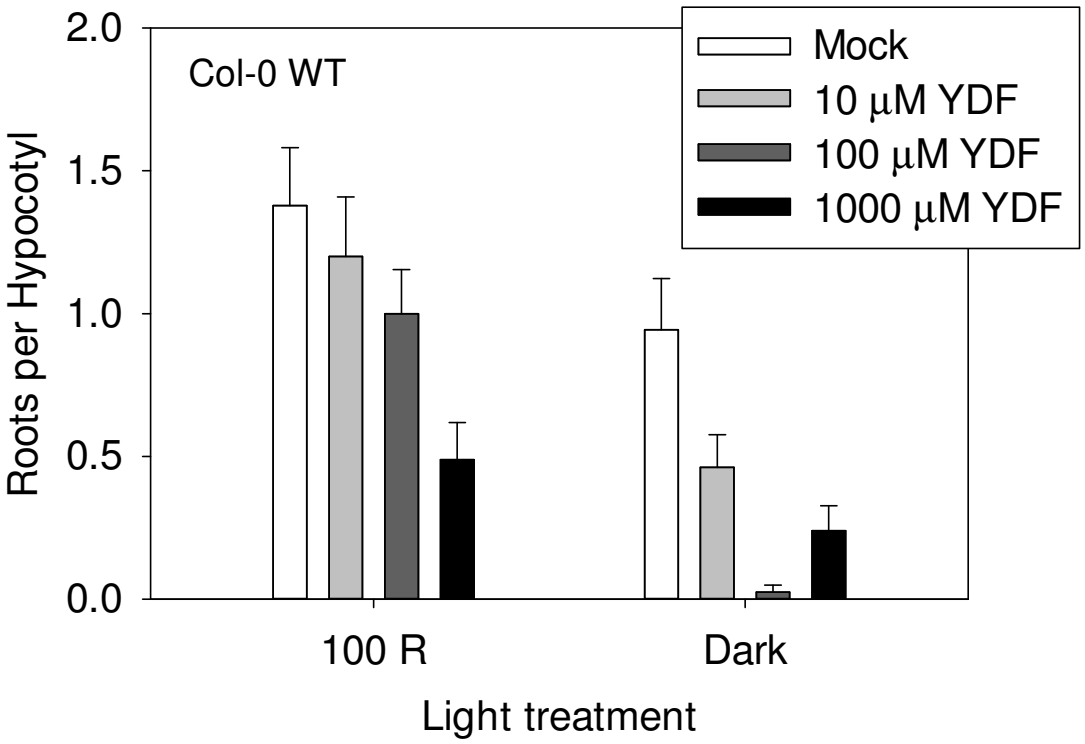

Figure A-9. Effect of YDF treatment on adventitious root formation. Wild-type Col-0 seeds were surface sterilized and imbibed in a 100 μM gibberellic acid 4 (GA_4) solution for one week at 4°C, and then sown on nylon mesh atop 0.5X strength MS medium with 1% sucrose in square Petri plates. Plates were stored vertically in darkness at 20°C for 7 d, after which the mesh with seedlings were transferred to media containing 0, 10, 100, or 1000 μM Yucasin DF (YDF) and transferred to Conviron PGR15 growth chambers equipped with Heliospectra L4A Series 10 LED lamps where they were exposed to either a 16 h photoperiod of red light (660 nm, 135 μmol m^{-2} s^{-1}) or kept in continued darkness. The number of adventitious roots visibly emerged from hypocotyls was counted after 7 d of light treatment.

Seedlings treated with YDF (a potent inhibitor of EC 1.14.13.168 - indole-3-pyruvate monooxygenase) formed fewer adventitious roots compared to control treatments, especially in the dark.

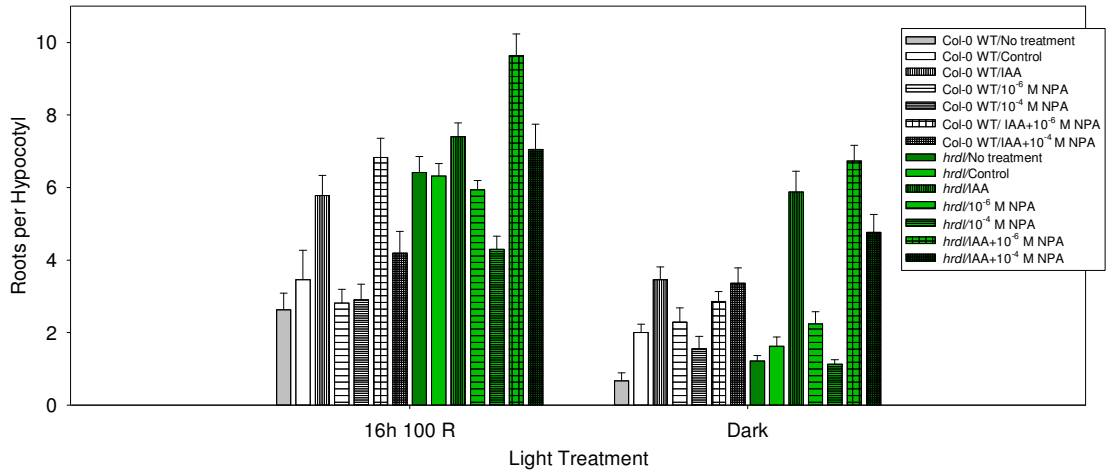

Figure A-10. Effects of IAA and NPA treatments on adventitious root formation. Wild-type Col-0 seeds were surface sterilized, suspended in a 100 µM gibberellic acid 4 (GA_4) solution, and sown on square Petri plates containing 0.5X strength MS medium with 3% sucrose. Plates were stored vertically in darkness at 20°C for 7 d, then a 10 µL agarose droplet containing IAA, N-1-naphthylphthalamic acid (NPA), or a mock treatment was placed on the apical hook of each seedling; seedlings without agarose droplet treatment were also included for comparison. Seedlings were transferred to Conviron PGR15 growth chambers equipped with Heliospectra L4A Series 10 LED lamps where they were exposed to either a 16 h photoperiod of red light (660 nm, 100 µmol m^{-2} s^{-1}) or kept in continued darkness. The number of adventitious roots visibly emerged from hypocotyls was counted after 7 d of light treatment.

IAA treatments applied to apical hooks had a positive effect on adventitious root formation. The positive effect of applied IAA was partially reversed by NPA, an inhibitor of polar auxin transport.

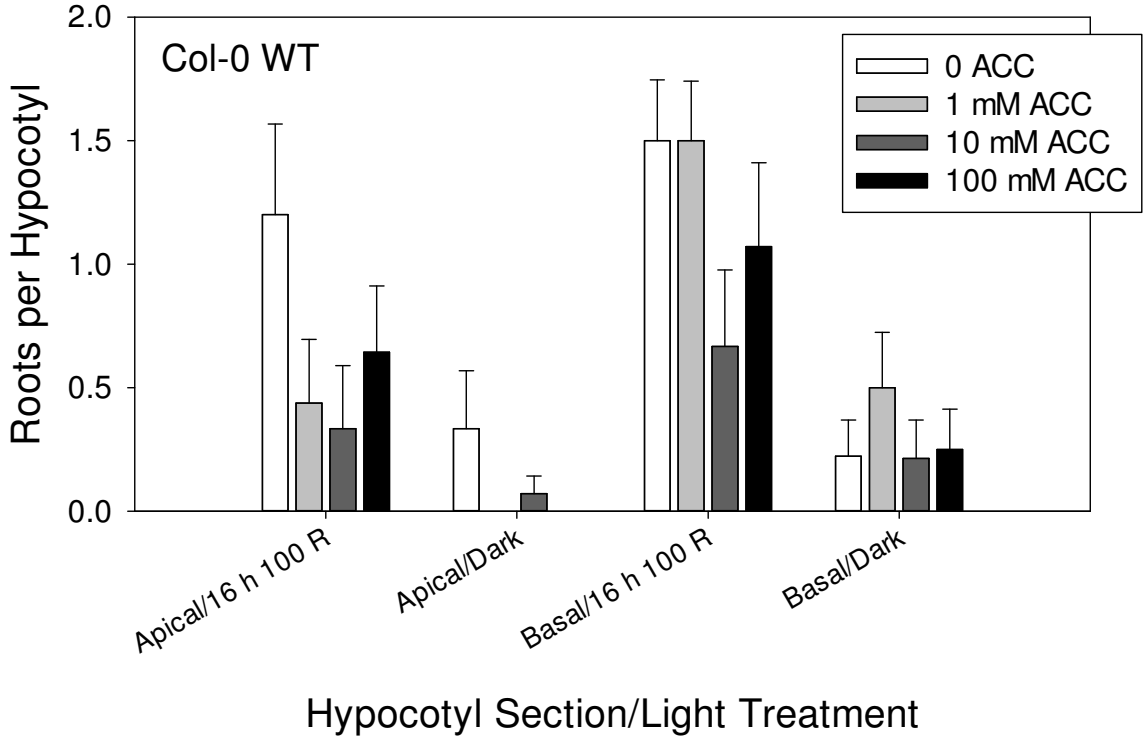

Figure A-11. Effects of ACC treatment on adventitious root formation in apical and basal hypocotyl sections. Wild-type Col-0 seeds were surface sterilized, suspended in a 100 µM gibberellic acid 4 (GA_4) solution, and sown on square Petri plates containing 0.5X strength MS medium with 3% sucrose and varying concentrations (0-100 mM) of 1-aminocyclopropane-1-carboxylic acid (ACC). Plates were stored vertically in darkness at 20°C for 7 d, then transferred to Conviron PGR15 growth chambers equipped with Heliospectra L4A Series 10 LED lamps where they were exposed to either a 16 h photoperiod of red light (660 nm, 100 µmol m^{-2} s^{-1}) or kept in continued darkness. The number of adventitious roots visibly emerged from apical and basal halves of hypocotyls was counted after 7 d of light treatment.

ACC treatment may affect adventitious root formation in the apical section of hypocotyls.

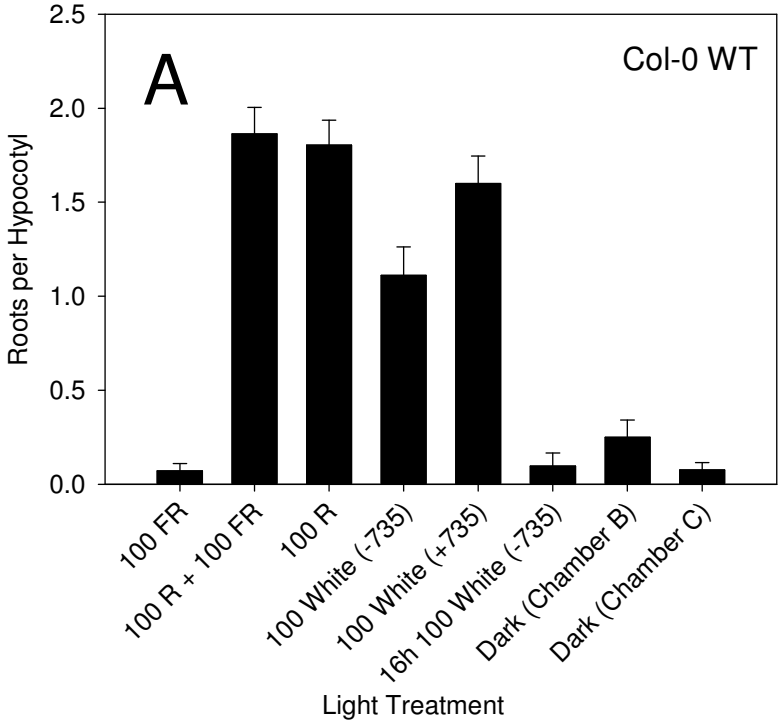
A
Col-0 WT
Roots per Hypocotyl
2.5
2.0
1.5
1.0
0.5
0.0
100 FR
100 R + 100 FR
100 R
100 White (-735)
100 White (+735)
16h 100 White (-735)
Dark (Chamber B)
Dark (Chamber C)
Light Treatment

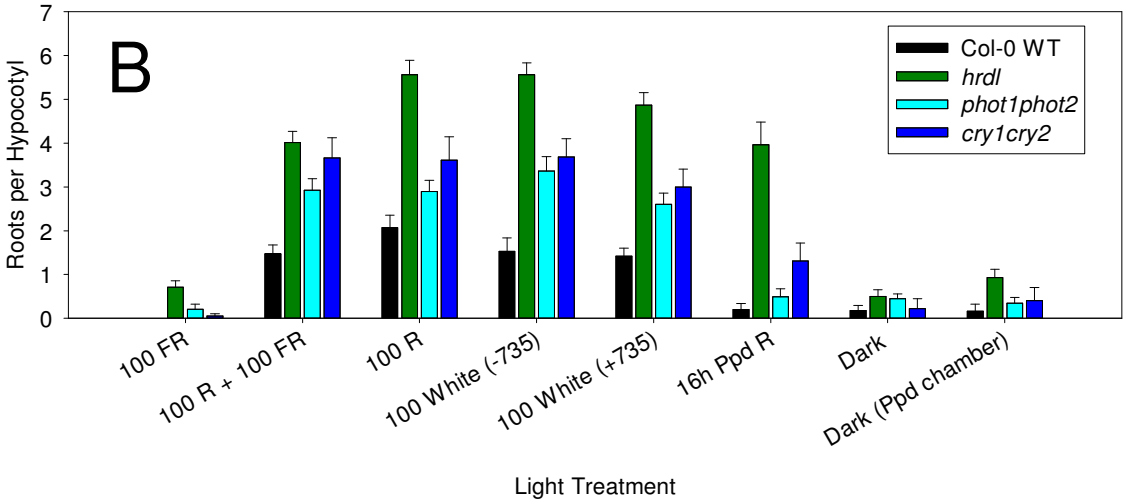
B
Col-0 WT
hrdl
phot1phot2
cry1cry2
Roots per Hypocotyl
7
6
5
4
3
2
1
0
100 FR
100 R + 100 FR
100 R
100 White (-735)
100 White (+735)
16h Ppd R
Dark
Dark (Ppd chamber)
Light Treatment

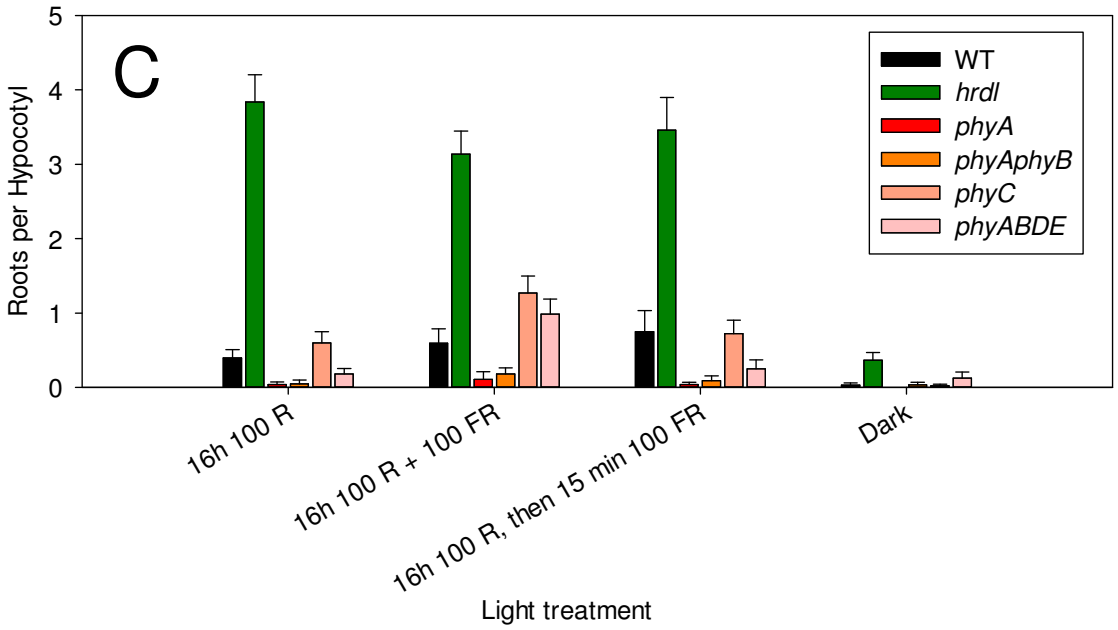
C
Roots per Hypocotyl
0
1
2
3
4
5
WT
hrdl
phyA
phyAphyB
phyC
phyABDE
16h 100 R
16h 100 R + 100 FR
16h 100 R, then 15 min 100 FR
Dark
Light treatment

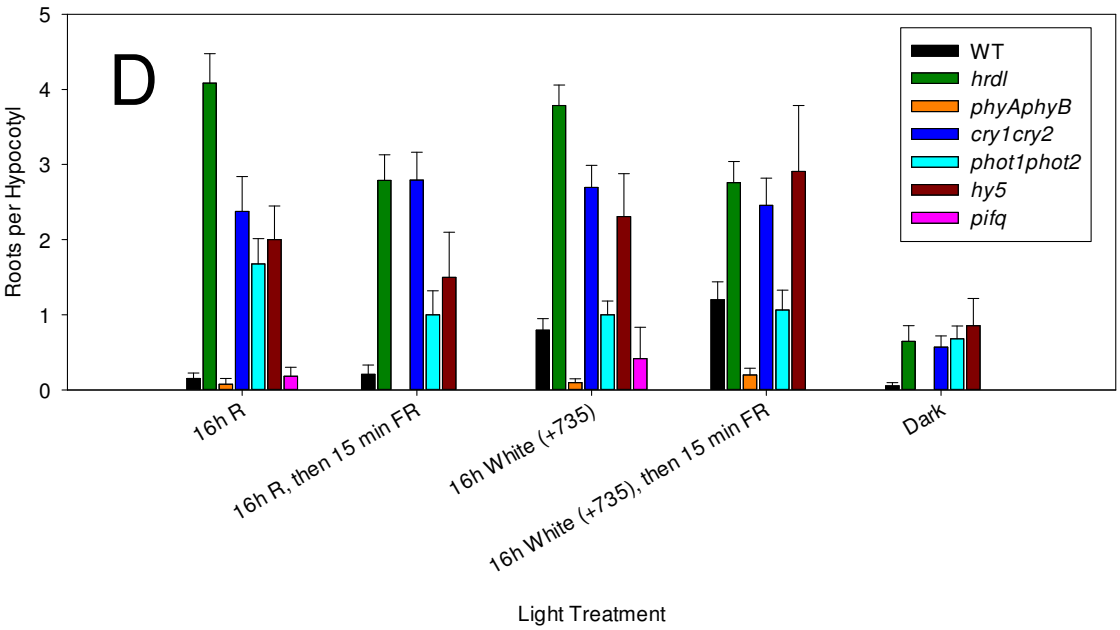
D
Roots per Hypocotyl
0
1
2
3
4
5
WT
hrdl
phyAphyB
cry1cry2
phot1phot2
hy5
pifq
16h R
16h R, then 15 min FR
16h White (+735)
16h White (+735), then 15 min FR
Dark
Light Treatment

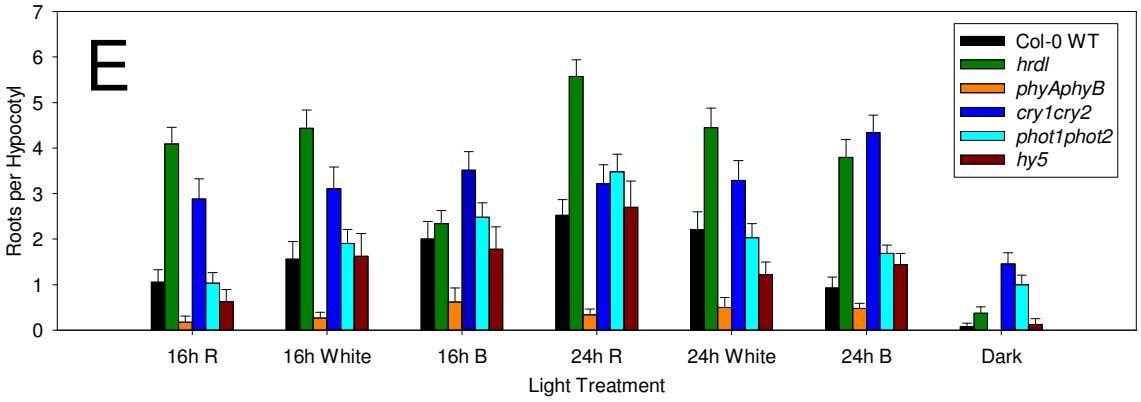
E
Col-0 WT
hrdl
phyAphyB
cry1cry2
phot1phot2
hy5
Roots per Hypocotyl
0
1
2
3
4
5
6
7
16h R
16h White
16h B
24h R
24h White
24h B
Dark
Light Treatment

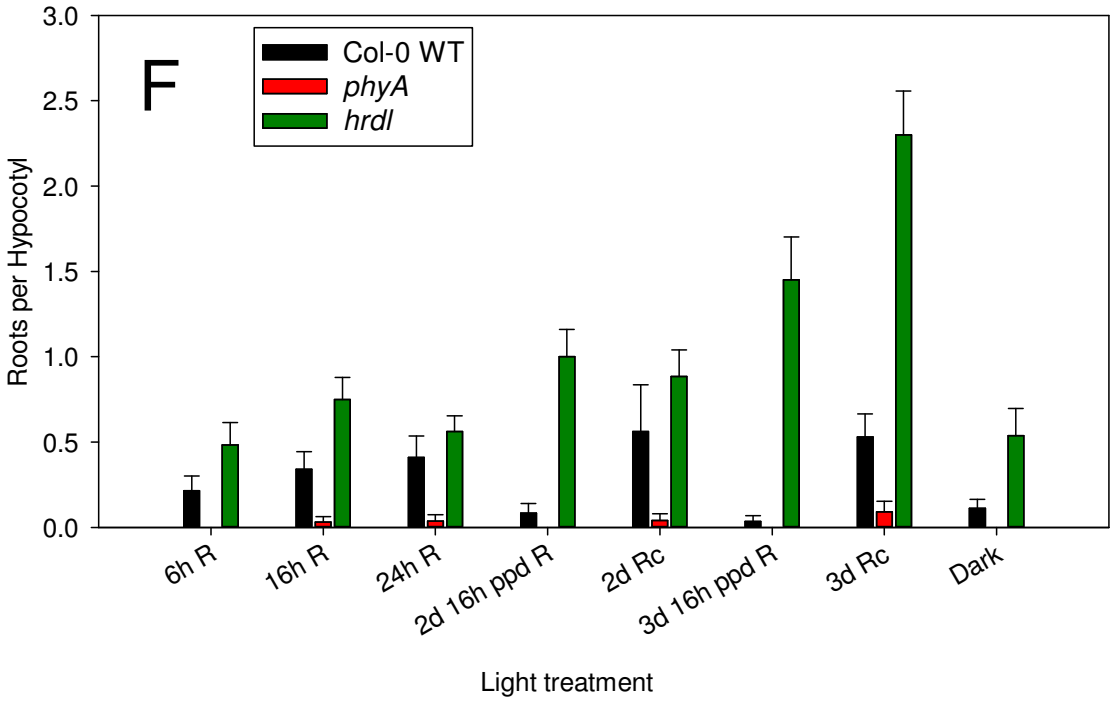
F
Col-0 WT
phyA
hrdl
Roots per Hypocotyl
0.0
0.5
1.0
1.5
2.0
2.5
3.0
6h R
16h R
24h R
2d 16h ppd R
2d Rc
3d 16h ppd R
3d Rc
Dark
Light treatment

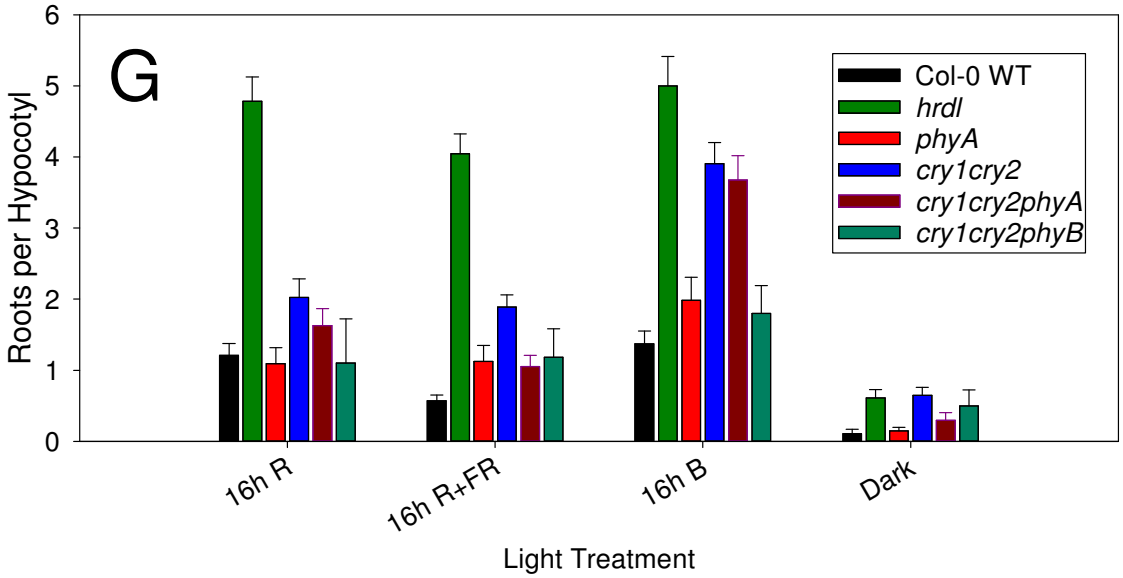
G
Roots per Hypocotyl
0
1
2
3
4
5
6
Col-0 WT
hrdl
phyA
cry1cry2
cry1cry2phyA
cry1cry2phyB
16h R
16h R+FR
16h B
Dark
Light Treatment

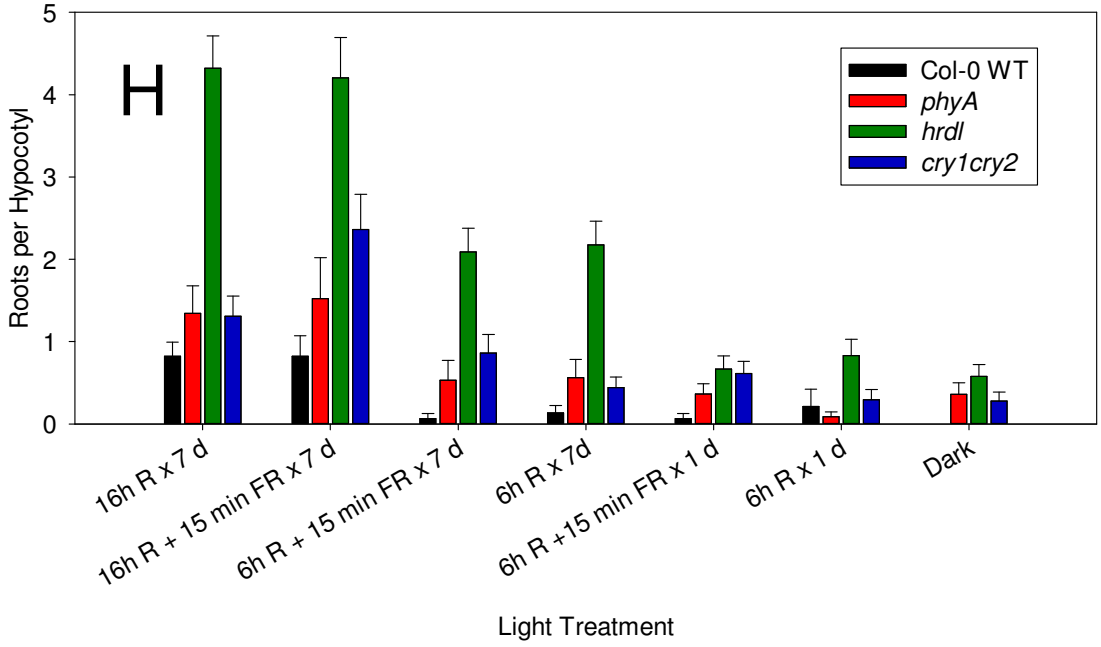
H
Roots per Hypocotyl
0
1
2
3
4
5
Col-0 WT
phyA
hrdl
cry1cry2
16h R x 7 d
16h R + 15 min FR x 7 d
6h R + 15 min FR x 7 d
6h R x 7d
6h R +15 min FR x 1 d
6h R x 1 d
Dark
Light Treatment

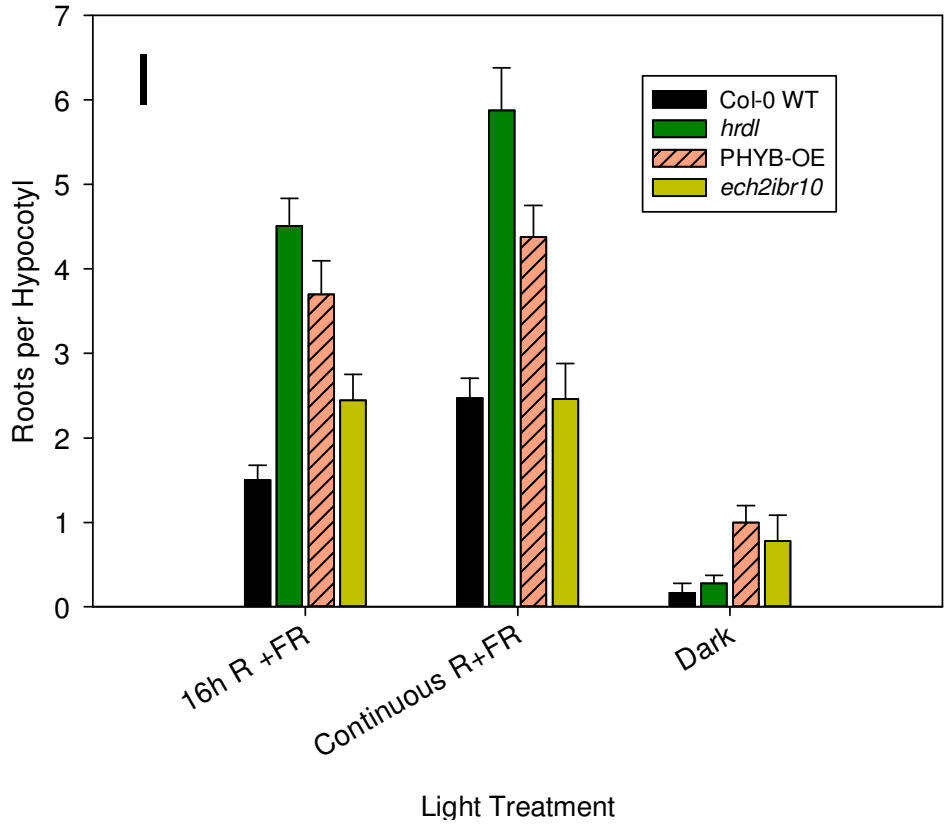
I
Col-0 WT
hrdl
PHYB-OE
ech2ibr10
Roots per Hypocotyl
0
1
2
3
4
5
6
7
16h R +FR
Continuous R+FR
Dark
Light Treatment

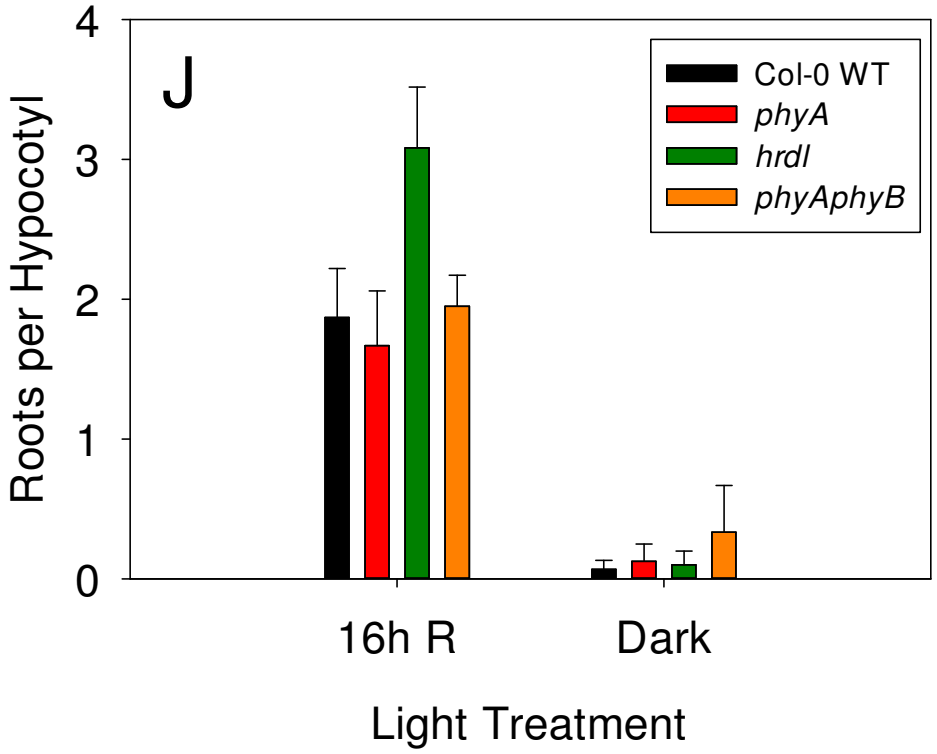
J
Col-0 WT
phyA
hrdl
phyAphyB
Roots per Hypocotyl
0
1
2
3
4
16h R
Dark
Light Treatment

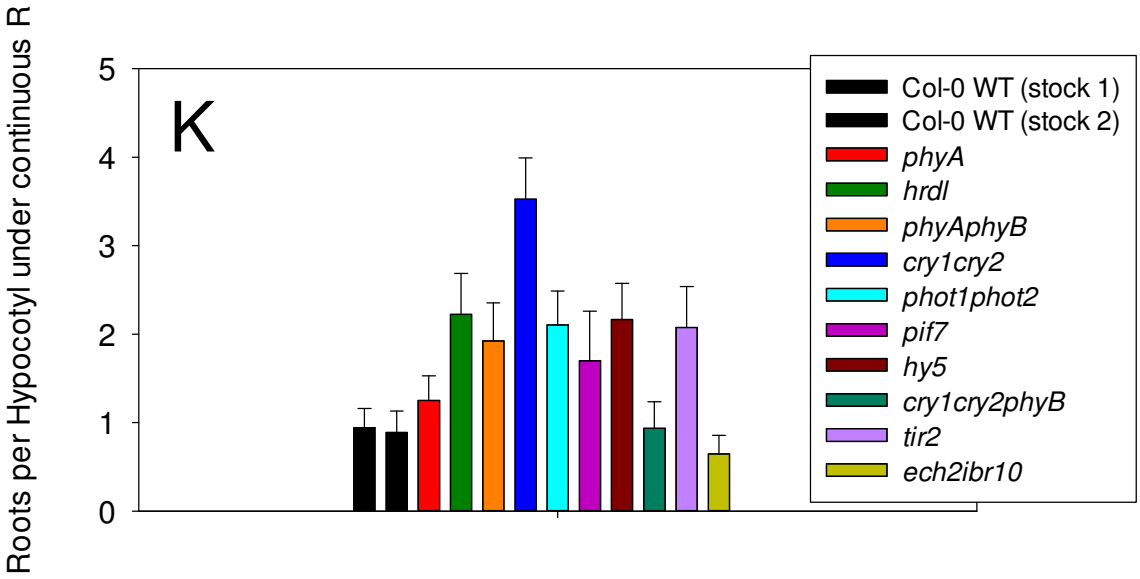
K
Roots per Hypocotyl under continuous R
0
1
2
3
4
5
Col-0 WT (stock 1)
Col-0 WT (stock 2)
phyA
hrdl
phyAphyB
cry1cry2
phot1phot2
pif7
hy5
cry1cry2phyB
tir2
ech2ibr10

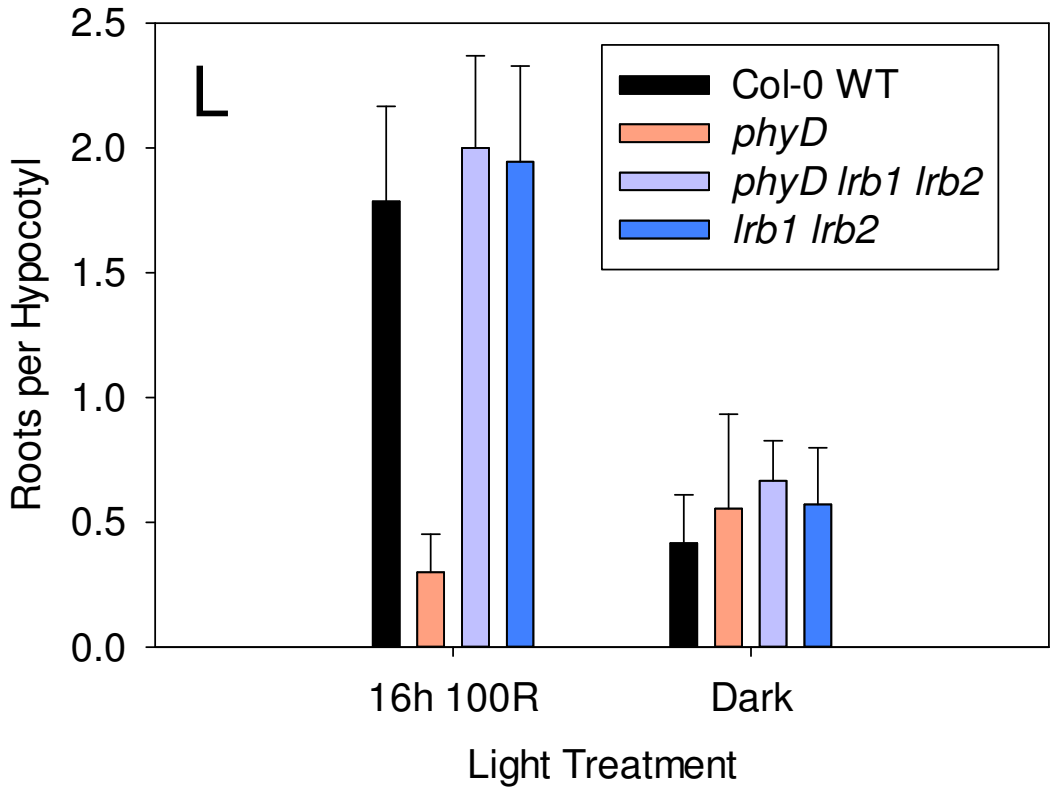
L
Roots per Hypocotyl
0.0
0.5
1.0
1.5
2.0
2.5
Col-0 WT
phyD
phyD lrb1 lrb2
lrb1 lrb2
16h 100R
Dark
Light Treatment

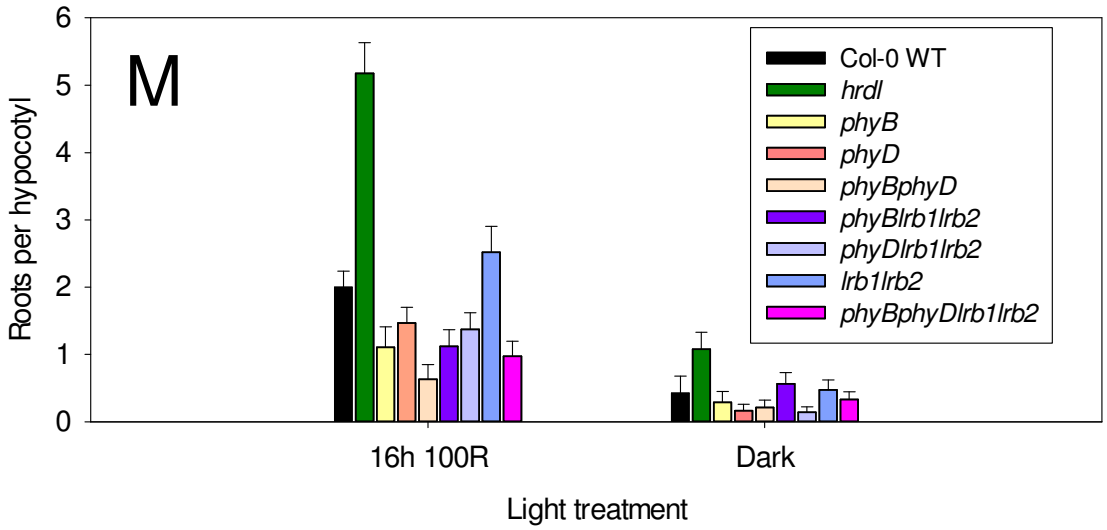
M
Roots per hypocotyl
0
1
2
3
4
5
6
16h 100R
Dark
Light treatment
Col-0 WT
hrdl
phyB
phyD
phyBphyD
phyBlrb1lrb2
phyDlrb1lrb2
lrb1lrb2
phyBphyDlrb1lrb2

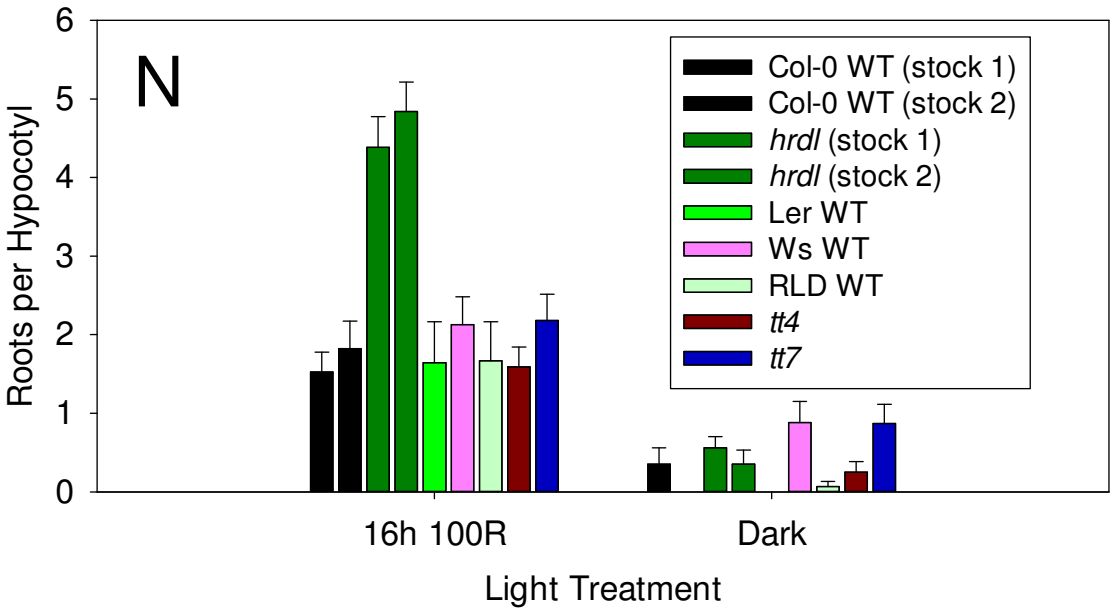
N
Roots per Hypocotyl
0
1
2
3
4
5
6
16h 100R
Dark
Light Treatment
Col-0 WT (stock 1)
Col-0 WT (stock 2)
hrdl (stock 1)
hrdl (stock 2)
Ler WT
Ws WT
RLD WT
tt4
tt7

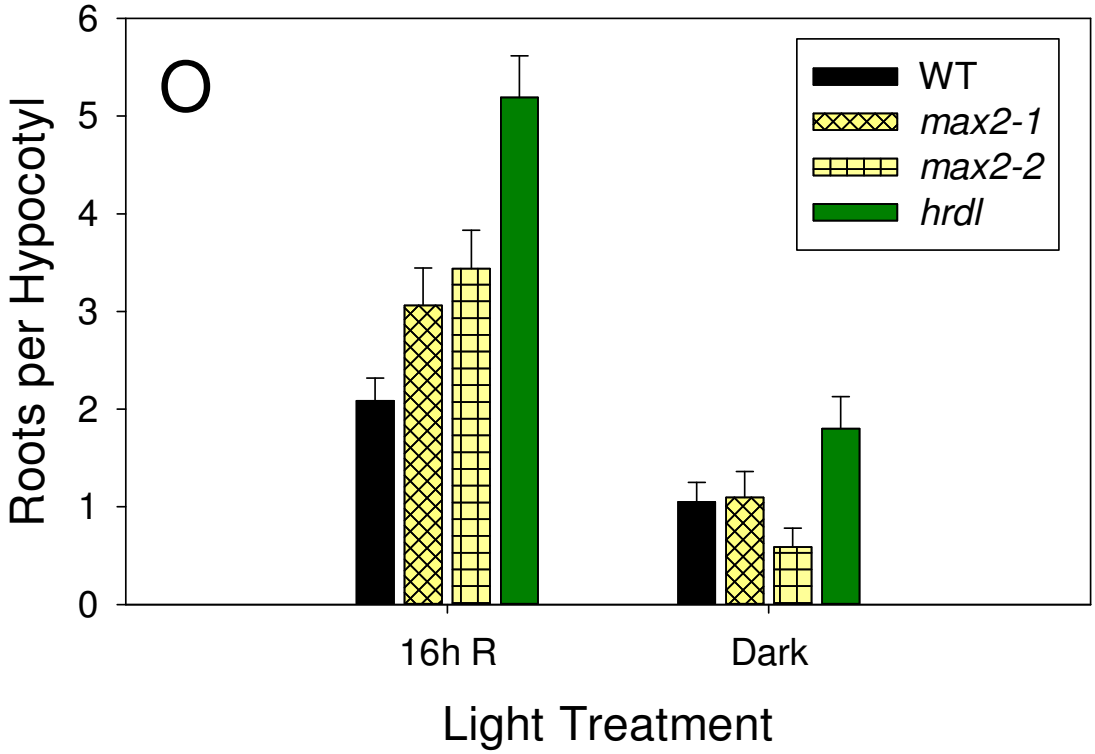
O
Roots per Hypocotyl
0
1
2
3
4
5
6
WT
max2-1
max2-2
hrdl
16h R
Dark
Light Treatment

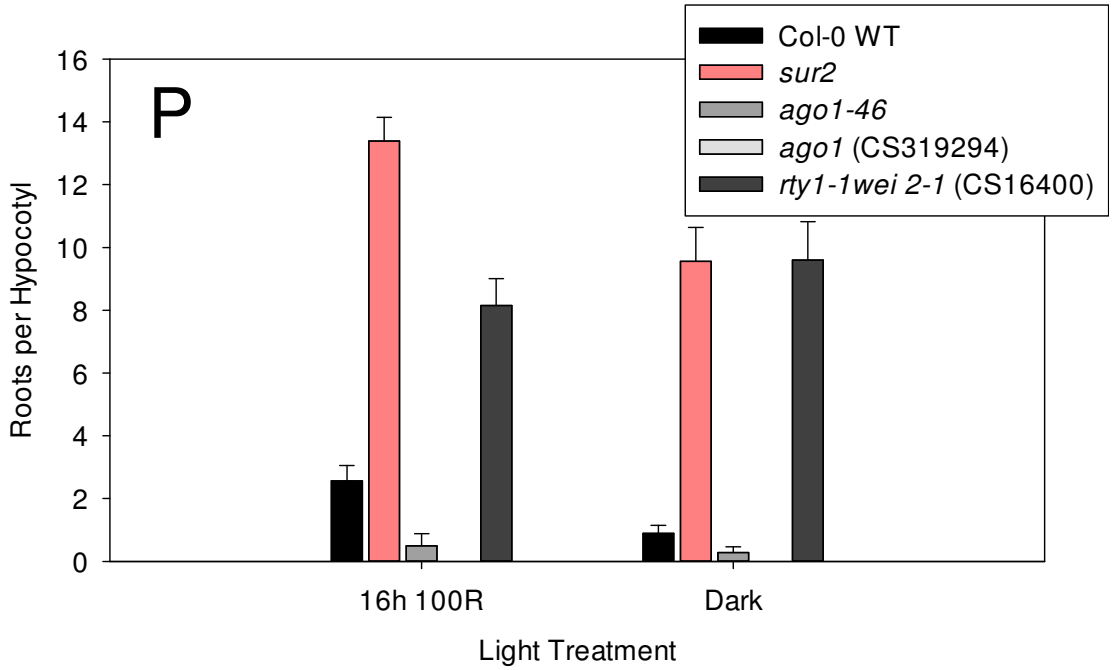
P
Roots per Hypocotyl
0
2
4
6
8
10
12
14
16
Col-0 WT
sur2
ago1-46
ago1 (CS319294)
rty1-1wei 2-1 (CS16400)
16h 100R
Dark
Light Treatment

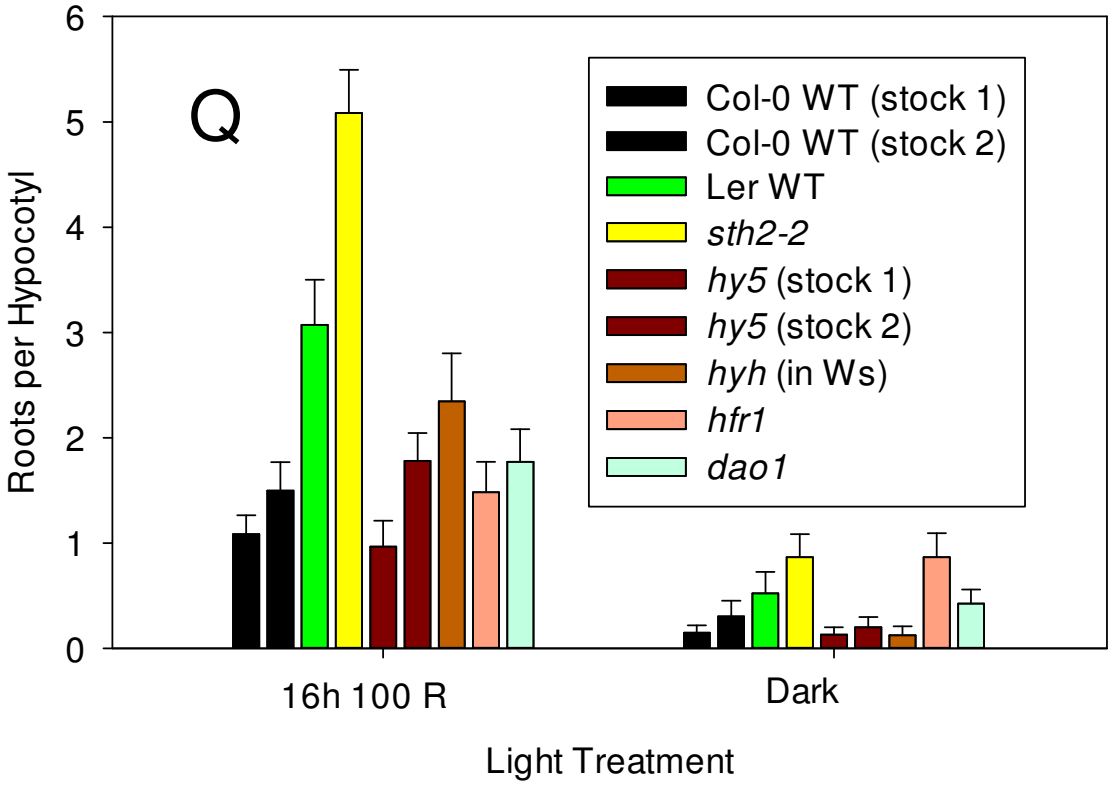
Q
Roots per Hypocotyl
0
1
2
3
4
5
6
Col-0 WT (stock 1)
Col-0 WT (stock 2)
Ler WT
sth2-2
hy5 (stock 1)
hy5 (stock 2)
hyh (in Ws)
hfr1
dao1
16h 100 R
Dark
Light Treatment

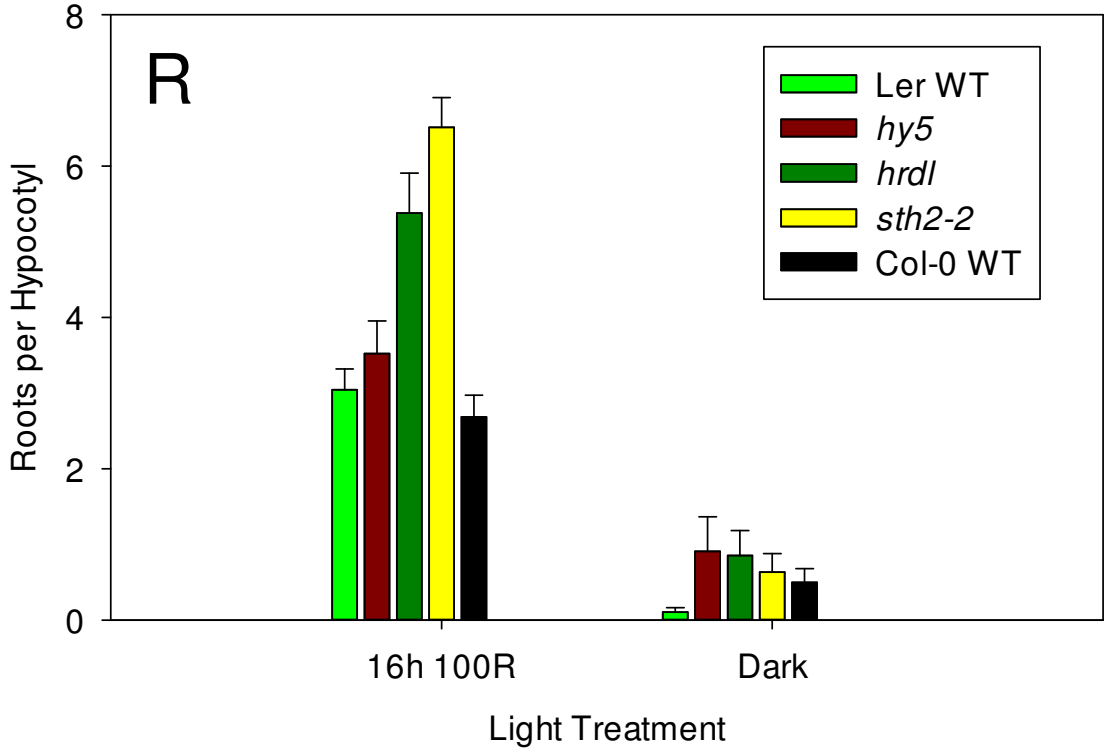
R
Roots per Hypocotyl
0
2
4
6
8
Ler WT
hy5
hrdl
sth2-2
Col-0 WT
16h 100R
Dark
Light Treatment

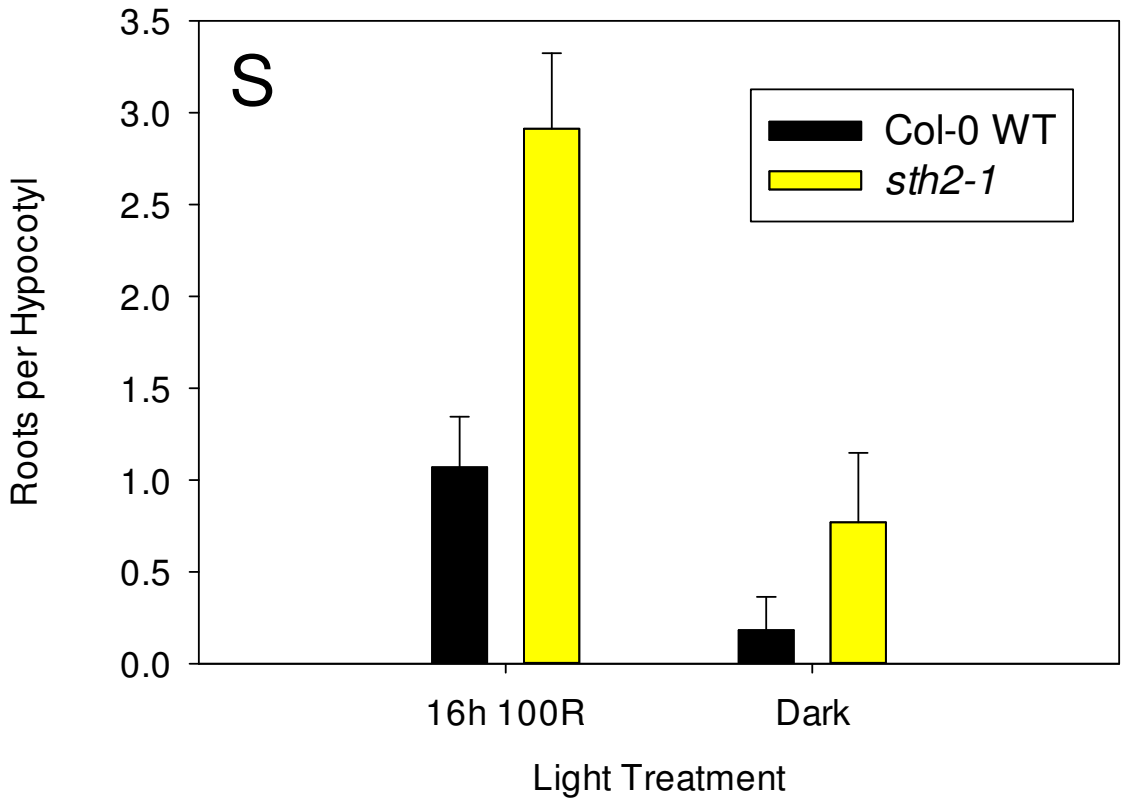
S
Roots per Hypocotyl
3.5
3.0
2.5
2.0
1.5
1.0
0.5
0.0
Col-0 WT
sth2-1
16h 100R
Dark
Light Treatment

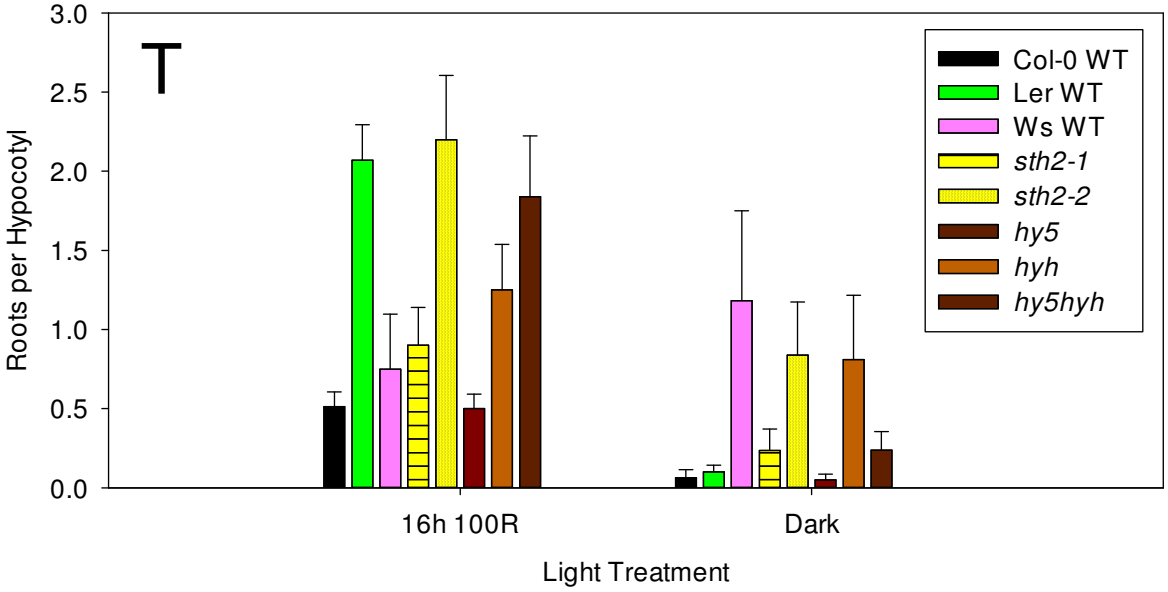
T
Roots per Hypocotyl
3.0
2.5
2.0
1.5
1.0
0.5
0.0
Col-0 WT
Ler WT
Ws WT
sth2-1
sth2-2
hy5
hyh
hy5hyh
16h 100R
Dark
Light Treatment

Figure A-12 (A-T). Adventitious root formation in various *Arabidopsis* genotypes under different light conditions. *Arabidopsis* seeds (see genotype descriptions in Table A-1) were surface sterilized and imbibed in a 100 μM gibberellic acid 4 (GA_4) solution for up to one week at 4°C, and then sown on square Petri plates containing 0.5X strength MS medium with 3% sucrose. Plates were stored vertically in darkness at 20°C for 7 d, then transferred to Conviron PGR15 growth chambers equipped with Heliospectra L4A Series 10 LED lamps where they were exposed to various light conditions or kept in continued darkness by keeping plates wrapped in 4-5 layers of aluminum foil. Light quality settings LED included White (380, 400, 420, 450, 530, 620, 660, 735 nm and 6500K), Red (R; 660 nm), Far Red (FR; 735 nm), and Blue (400, 420, and 450 nm). Light intensity under each condition was 100 μmol m^{-2} s^{-1}, and the number of adventitious roots visibly emerged from hypocotyls was counted after 7 d of light treatment unless otherwise noted. Error bars represent ±SE.

Red, blue, and white (but not far red) light treatments can induce adventitious root formation, and root number is positively correlated with duration of light exposure. This response was not photoreversible. Adventitious root formation is elevated in mutants of phototropin blue light receptors and in the unidentified mutant *hrdl*, as well the light signaling intermediate mutants *sth2* (also called *bbx21*) and *hy5hyh*, suggesting these light response genes negatively regulate root formation.

Appendix B: Collaborative Projects

The following are collaborative research projects to which I have contributed that have been published or will be published in peer-reviewed journals. Each of these studies provided new insight into the role of auxin in plant growth and development. Presented here are brief summaries and conclusions of these studies, followed by more detailed descriptions of my specific contributions and experimental results.

B.1: Loss of GSNOR1 function leads to compromised auxin signaling and polar auxin transport

Ya-Fei Shi, Da-Li Wang, Chao Wang, Angela Hendrickson Culler, Molly A Kreiser, Jayanti Suresh, Jerry D Cohen, Jianwei Pan, Barbara Baker, Jian-Zhong Liu*

*Corresponding author; College of Chemistry and Life Sciences, Zhejiang Normal University, Jinhua, Zhejiang 321004, China

Published in *Molecular Plant* 8.9 (2015): 1350-1365.
https://doi.org/10.1016/j.molp.2015.04.008

Abstract

Cross talk between phytohormones, nitric oxide (NO), and auxin has been implicated in the control of plant growth and development. Two recent reports indicate that NO promoted auxin signaling but inhibited auxin transport probably through S-nitrosylation. However, genetic evidence for the effect of S-nitrosylation on auxin physiology has been lacking. In this study, we used a genetic approach to understand the broader role of S-nitrosylation in auxin physiology in *Arabidopsis*. We compared auxin signaling and transport in Col-0 and *gsnor1-3*, a loss-of-function GSNOR1 mutant defective in protein de-nitrosylation. Our results showed that auxin signaling was impaired in the *gsnor1-3* mutant as revealed by significantly reduced DR5-GUS/DR5-GFP accumulation and compromised degradation of AXR3NT-GUS, a useful reporter in interrogating auxin-mediated degradation of Aux/IAA by auxin receptors. In addition, polar auxin transport was compromised in *gsnor1-3*, which was correlated with universally reduced levels of PIN or GFP-PIN proteins in the roots of the mutant in a manner independent of transcription and 26S proteasome degradation. Our results suggest that S-nitrosylation and GSNOR1-mediated de-nitrosylation contribute to auxin physiology, and impaired

auxin signaling and compromised auxin transport are responsible for the auxin-related morphological phenotypes displayed by the *gsnor1-3* mutant.

Similar Levels of Indole Acetic Acid in *gsnor1-3* and Col-0 Wild-Type

Because the *gsnor1-3* mutant phenotypes are similar to those of auxin mutants (Noh et al., 2001; Dai et al., 2006), we speculated that some of the defects might be caused by aberrant auxin biosynthesis/degradation in different tissues of different development stages. To explore the possibility, we used gas chromatography–mass spectrometry to quantify free indole acetic acid (IAA) levels in the leaves of 30-day-old plants and 12-day-old seedlings of both Col-0 and *gsnor1-3*. As shown in Figure B.1A and B.1B, free IAA levels in the leaves and seedlings of *gsnor1-3* were similar to those of Col-0. Because many assays were performed in the roots of seedlings, we also subdivided whole 12-day-old seedlings below the cotyledonary node and at the root-shoot junction to yield three fractions (leaves and epicotyl [labeled leaves], hypocotyl, and root) and used a sensitive isotope dilution assay based on selective reaction monitoring using gas chromatography–tandem mass spectrometry (GC–MS/MS) to determine the free IAA levels in each tissue fraction. No significant differences in IAA levels were observed between Col-0 and *gsnor1-3* mutants in any of the tissues (Figure B.1C), indicating that the auxin-related developmental phenotypes observed for *gsnor1-3* plants do not result from changes in free IAA levels.

Free IAA Extraction and Measurement

Free IAA extraction and quantification were performed essentially as described previously (Barkawi et al., 2008; Barkawi et al., 2010). Levels of endogenous IAA were calculated by monitoring ions at *m/z* 130 and 189 for endogenous IAA, and *m/z* 136 and 195 for the [$^{13}C_6$]IAA added internal standard as their methyl esters. For studies of smaller tissue sections, selected reaction monitoring GC-MS/MS was used following the *m/z* 189 to *m/z* 130 and *m/z* 195 to *m/z* 136 transitions exactly as described (Liu et al.,

2012). Quantities were calculated by using standard isotope dilution equations (Cohen et al., 1986).

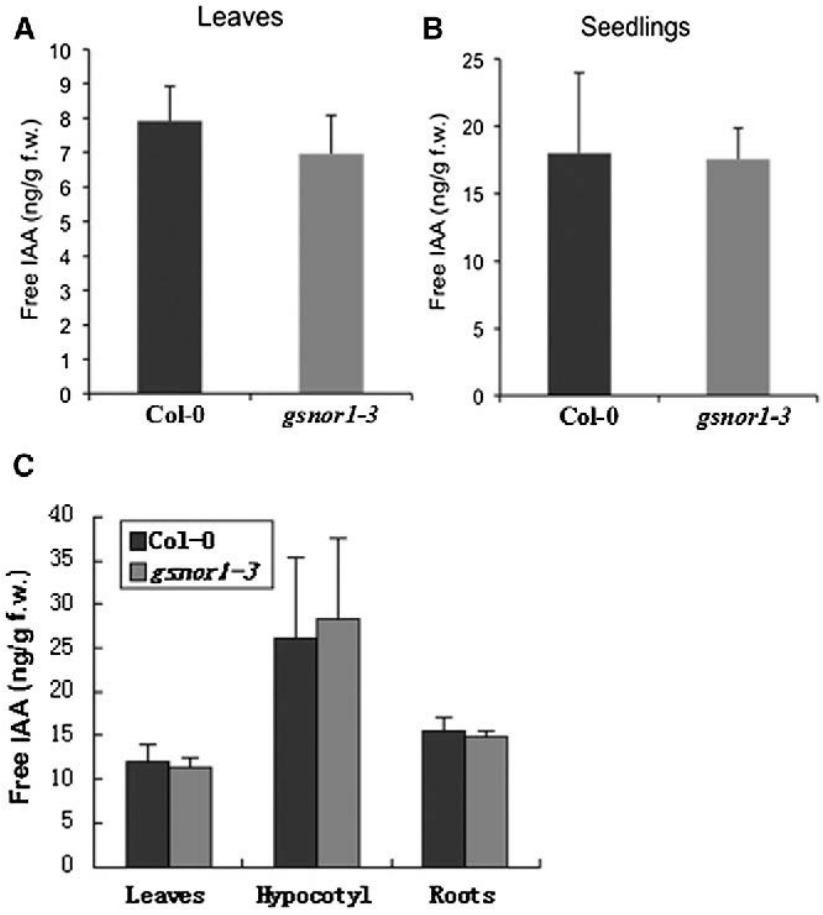

Figure B-1. The *gsnor1-3* mutant contains normal levels of free IAA.

(A) Free IAA levels were measured in 30-day-old Col-0 and *gsnor1-3* plants.

(B) Free IAA levels were measured in 12-day-old Col-0 and *gsnor1-3* seedlings.

(C) Free IAA levels were measured in 12-day-old seedlings subdivided below the cotyledonary node and at the root-shoot junction to yield three fractions (leaves and epicotyl [labeled 'leaves'], hypocotyl, and roots). Errors bars represent the SE for four to six independent samples. The differences in (C) are not significant ($p > 0.1$ for Student 's t-tests).

B.2: Auxin analysis using laser microdissected plant tissues sections

Luz G. Muñoz-Sanhueza, YeonKyeong Lee, Molly Tillmann, Jerry D. Cohen & Anne Kathrine Hvoslef-Eide*

*Corresponding author; Department of Plant Sciences (IPV), Faculty of Biosciences, Norwegian University of Life Sciences, Norway Campus Ås, Universitetstunet 3, 1430 Ås, Norway

Published in *BMC Plant Biology* 18.1 (2018): 133. https://doi.org/10.1186/s12870-018-1352-z

Abstract

Background: Quantitative measurement of actual auxin levels in plant tissue is complimentary to molecular methods measuring the expression of auxin related genes. Current analytical methods to quantify auxin have pushed the limit of detection to where auxin can be routinely quantified at the picogram (pg) level, reducing the amount of tissue needed to perform these kinds of studies to amounts never imagined a few years ago. In parallel, the development of technologies like laser microdissection microscopy (LMD) has allowed specific cells to be harvested from discrete tissues without including adjacent cells. This method has gained popularity in recent years, especially for enabling a higher degree of spatial resolution in transcriptome profiling. As with other quantitative measurements, including hormone quantifications, sampling using traditional LMD is still challenging because sample preparation clearly compromises the preservation of analytes. Thus, we have developed and validated a sample preparation protocol combining cryosectioning, freeze-drying, and capturing with a laser microdissection microscope to provide high-quality and well-preserved plant materials suitable for ultrasensitive, spatially-resolved auxin quantification.

Results: We developed a new method to provide discrete plant tissues for indole-3-acetic acid (IAA) quantification while preserving the plant tissue in the best possible condition to prevent auxin degradation. The method combines the use of cryosectioning, freeze-drying, and LMD. The protocol may also be used for other applications that require small molecule analysis with high tissue-specificity where degradation of biological compounds may be an issue. It was possible to collect the equivalent of 15 mg of very specific tissue in approximately 4 h using LMD.

Conclusions: We have shown, by proof of concept, that freeze dried cryosections of plant tissue were suitable for LMD harvest and quantification of the phytohormone auxin using GC-MS/MS. We expect that the ability to resolve auxin levels with both spatial- and temporal resolution with high accuracy will enable experiments on complex processes, which will increase our knowledge of the many roles of auxins (and, in time, other phytohormones) in plant development.

Auxin quantification

The protocol for auxin extraction (Liu et al., 2012) is optimally performed in 1.5 ml microcentrifuge tubes; thus, the tissue collected with LMD in a 0.6 ml microcentrifuge tube was transferred. Due to the small size of the cryosections and the potential presence of the slide membrane underneath them, electrostatic forces require that extra care must be taken. The protocol used in this study can be used to quantify auxin, as well as auxin biosynthetic precursors like tryptophan, indole, indole-3-pyruvic acid (IPyA), and indole-3-butyric acid (IBA). This protocol employs isotope dilution using [$^{13}C_6$] IAA as the internal standard (Cohen et al., 1986) and requires only 2 to 20 mg of plant material. Approximately 340 pg of internal standard was added to every replicate in this study. The metabolite extract was derivatized with diazomethane (Barkawi et al., 2010) and analyzed by selecting reaction monitoring (SRM) mode on a GC-MS/MS according to Liu et al. (Liu et al., 2012). A small modification to the original protocol was made in the final resuspension step following derivatization, using 10 µL of ethyl acetate instead of 15 µL. Samples were analysed by GC-MS/MS immediately after preparation in this study,

although when necessary, samples can be stored at − 80 °C. A representative figure is displayed in Figure B.2.

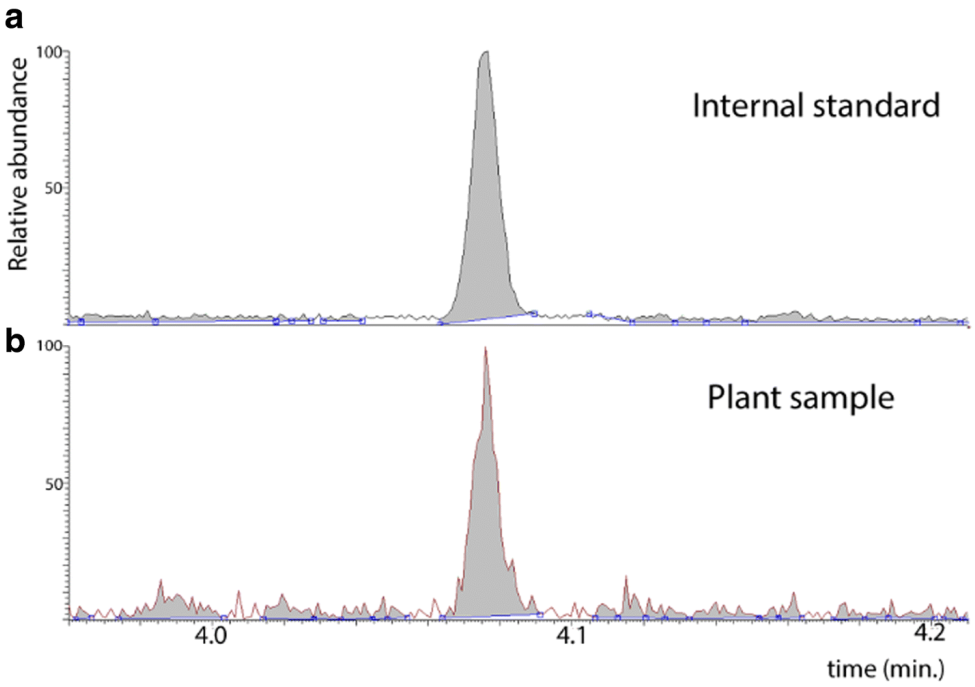

Figure B-2. Chromatograph of auxin quantification in a poinsettia bud from laser microdissection microscope sampling combined with GC-SRM-MS for auxin analysis.

(A) The internal standard [$^{13}C_6$]IAA.

(B) Poinsettias bud sample corresponding to the abscission zone (AZ) from the day of decapitation (D0), i.e. a Control sample.

B.3: Indole-3-acetylaspartate and indole-3-acetylglutamate, the IAA-amide conjugates in the diploid strawberry achene, are hydrolyzed in growing seedlings

Qian Tang, Peng Yu, Molly Tillmann, Jerry D. Cohen[1]* & Janet P. Slovin[2]*

*Corresponding authors; [1]Department of Horticultural Science and Microbial and Plant Genome Institute, University of Minnesota, Saint Paul, MN, USA; [2] USDA/ARS Genetic Improvement of Fruit and Vegetables Laboratory, Beltsville, MD, USA

Published in *Planta* 249.4 (2019): 1073-1085. https://doi.org/10.1007/s00425-018-3061-0

Abstract

Main conclusion: Indole-3-acetylaspartate and indole-3-acetylglutamate are the stored auxin amino acid conjugates in the achene of the diploid strawberry and serve as sources of auxin during seedling growth.

The edible part of the strawberry, a pseudocarp, has long been known to enlarge in response to auxin produced by the developing achenes, the botanical true fruit. Auxin homeostasis involves a complex interaction among biosynthesis, conjugate formation and hydrolysis, catabolism, and transport. Strawberry tissues are capable of synthesizing auxin conjugates, and transcriptome data support the expression of genes involved in IAA conjugate formation and hydrolysis throughout embryo development and subsequent seedling growth. Using a highly sensitive and selective mass spectrometric method, we identified all the low molecular weight indole-auxin amino acid conjugates in achenes of *F. vesca* as consisting of indole-3-acetylaspartate (IAasp) and indole-3-acetylglutamate (IAglu). In contrast to what has been proposed to occur in *Arabidopsis*, we determined that IAasp and IAglu are hydrolyzed by seedlings to provide a source of free IAA for growth.

Free IAA quantitation in strawberry achenes

Free IAA in the H4F7-3 achenes was measured by isotope dilution as previously described (Liu et al., 2012), except the methylation step was omitted and the samples were analyzed by LC–MS/MS at high resolution on the Q Exactive system (see below) used for conjugate analysis. The internal standard, 0.25 ng of [$^{13}C_6$]IAA, was added in 30 µL homogenization buffer (Liu et al., 2012) to each of 12 biological replicates, each weighing 8–12 mg, prior to homogenization with a 3 mm tungsten carbide bead using a Mixer Mill MM 400 (Qiagen, Germantown, MD, USA). After incubating the homogenate approximately 1 h on ice, 275 µL water was added to each sample. Samples were then centrifuged and IAA was extracted from the supernatant using amino and polymethylmethacrylate epoxide (PMME) solid phase extraction resins in Top Tips spin tips (Glygen, Columbia, MD, USA) as described by Liu et al. (Liu et al., 2012). After elution from PMME tips with 2 × 50 µL volumes of methanol into 1.5 mL microcentrifuge tubes, sample volumes were reduced to approximately 20 µL with a SpeedVac vacuum concentrator (Savant/Thermo, Milford, MA, USA). Concentrated samples were transferred to 50 µL inserts in amber autosampler vials for LC–MS/MS analysis with a Dionex Ultimate 3000 RSLC HPLC coupled to a hybrid quadrupole Orbitrap Q Exactive mass spectrometer (Thermo Scientific). 5 µL of strawberry achene extract were injected onto a 50 × 2.1 mm Force C18 column with 1.8 µm particle size (Restek, Bellefonte, PA, USA) and run with a solvent gradient of 0.1% formic acid in water (solvent A) and 0.1% formic acid in acetonitrile (solvent B) at a flow rate of 0.4 mL min−1. Gradient parameters were as follows: − 1 to 0 min, 5% B; 0–3 min, 5–20% B; 3–6 min, 20–80% B; and 6–6.5 min, 80% B. Mass spectrometry data were collected in the parallel reaction monitoring scan mode with the [M + 1] for IAA and [$^{13}C_6$]IAA at *m/z* 176.1 and 182.1, respectively, in the inclusion list and with the following settings: isolation width of 2.0 *m/z*, resolution of 17,500, automatic gain control target of 2 × 105, maximum accumulation time of 50 ms, and normalized collision energy of 20%.

Hydrolysis of IAasp and IAglu in growing strawberry seedlings

To determine if IAasp and IAglu were hydrolyzed and provide a source of free IAA during seedling growth, ~ 175 mg of YW5AF7 achenes were surface sterilized by

shaking in 95% ethanol for 5 min followed by 5 rinses in sterile H_2O. The achenes were left in the final rinse and imbibed by rocking on a shaker overnight at 6 °C. The achenes were further disinfected by shaking for 15 min in 30% commercial bleach (to a final concentration of ~ 2% sodium hypochlorite) followed by five rinses with sterile water. The achenes were left in the final rinse and poured into a deep Petri dish that was then taped with Micropore tape (3M, St. Paul, MN, USA) and kept at 27 °C for 4 days until the radicle just emerged. Square Petri dishes (100 × 100 mm with grid), were prepared containing 15 ml 0.5× Murashige and Skoog medium (Caisson Laboratories, Smithfield, UT, USA), pH 6.0, 0.8% Phytoblend agar (Caisson), and 40 µM of either [$^{13}C_6$]IAasp or [$^{13}C_6$]IAglu. Germinated achenes were placed along the mid-line in a single band spaced at ~ 3 mm intervals and the plates sealed with Micropore tape (3M). These were then incubated in vertical racks in a growth chamber at 24 °C under constant cool white fluorescent lights at ~ 100 µmol m^{-2} s^{-1} for 6 days. Seedlings were collected from the plates, rinsed with sterile water, blotted dry, weighed, and frozen in liquid N_2, stored at − 80 °C, and shipped between labs on dry ice. Samples from each independent Petri dish were homogenized in a bead mill in 65% isopropanol buffer with 0.2 M imidazole, pH 7.0 containing 1, 1.5, or 3 ng of [$^{2}H_4$]IAA internal standard (depending on fresh weight of the sample from each plate, which ranged from 19–57 mg). IAA was extracted from plant tissue by micro solid phase extraction using NH2 and polymethylmethacrylate epoxide (PMME) resins, essentially as described in Liu et al. (2012). Samples were derivatized with diazomethane prior to GC–MS/MS analysis to form the IAA methyl ester, using ethereal diazomethane synthesized as described (Cohen, 1984; Barkawi et al., 2010). Samples were analyzed on a Thermo Trace GC Ultra gas chromatograph with a 5 m Zebron Z-Guard GC guard column connected to a 15 m Zebron ZB5MS analytical column with a 0.25 mm diameter and 0.25 µm film thickness (Phenomenex), coupled with a Thermo TSQ Quantum XLS mass spectrometer. The GC temperature profile was set to 70 °C for 1 min, then increased by 50 °C per minute to 240° and was held at 240° for 1.5 min. Compounds eluted from the GC column were ionized by electron ionization with an emission current of 100 µA. Selected reaction monitoring acquisition mode was used to select the molecular ions of *m/z* 189, 193, and 195 and detect quinolinium product ions of *m/z* 130, 134, and 136 of native IAA, [$^{2}H_4$]IAA, and [$^{13}C_6$]IAA methyl esters,

respectively. Quinolinium product ions were produced by collision with argon gas using a collision energy of 10 V and 1.5 mTorr collision gas pressure and detected using scan times of 0.025 s. Peak areas were calculated using Qual Browser in Xcalibur software and were then used to determine concentration of both native IAA and [$^{13}C_6$]IAA in treated tissue by isotope dilution (Cohen et al., 1986; Barkawi et al., 2010) (Fig. B.3).

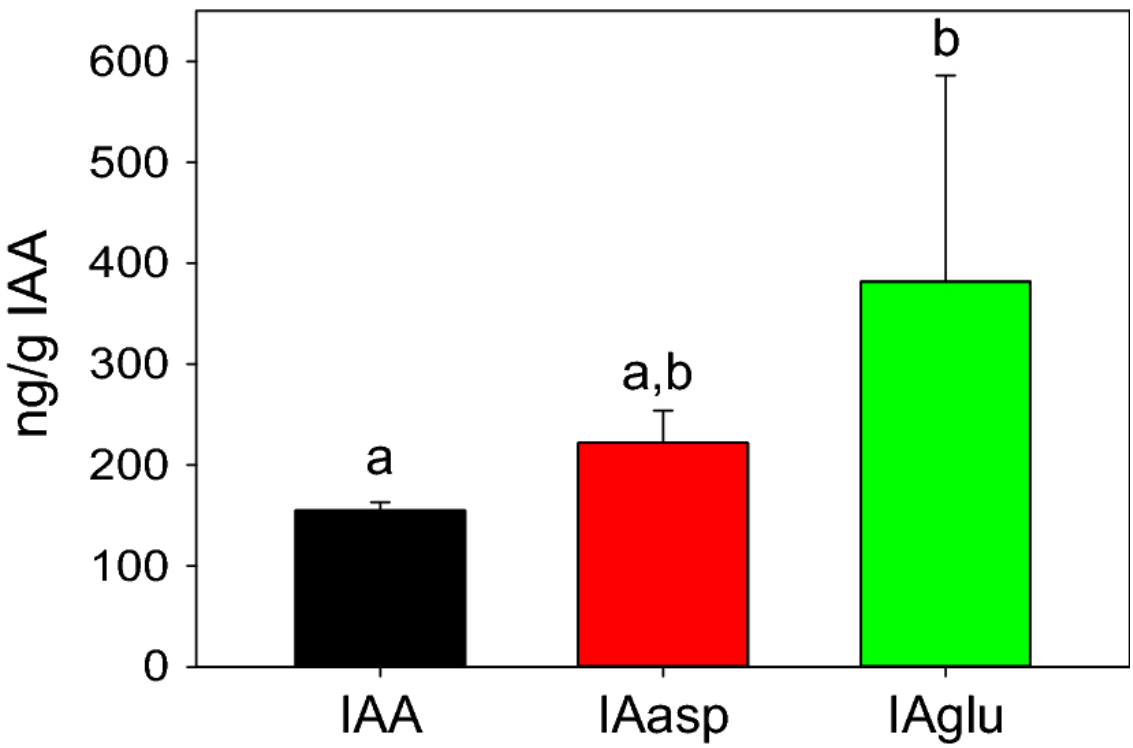

Figure B-3. Levels of free IAA and of IAasp and IAglu measured by isotope dilution analysis LC–MS using [$^{13}C_6$]-labeled internal standards. Values for the conjugates were obtained from nine biological replicates from a single harvest of achenes while the free IAA levels represent three biological replicates from each of four individual harvests. As discussed in the text, the high variation in conjugate levels and the stability of the free IAA levels may suggest an active regulatory role for conjugate metabolism within the achene. Different letters above error bars indicate a significant difference (Tukey HSD, $p < 0.05$).

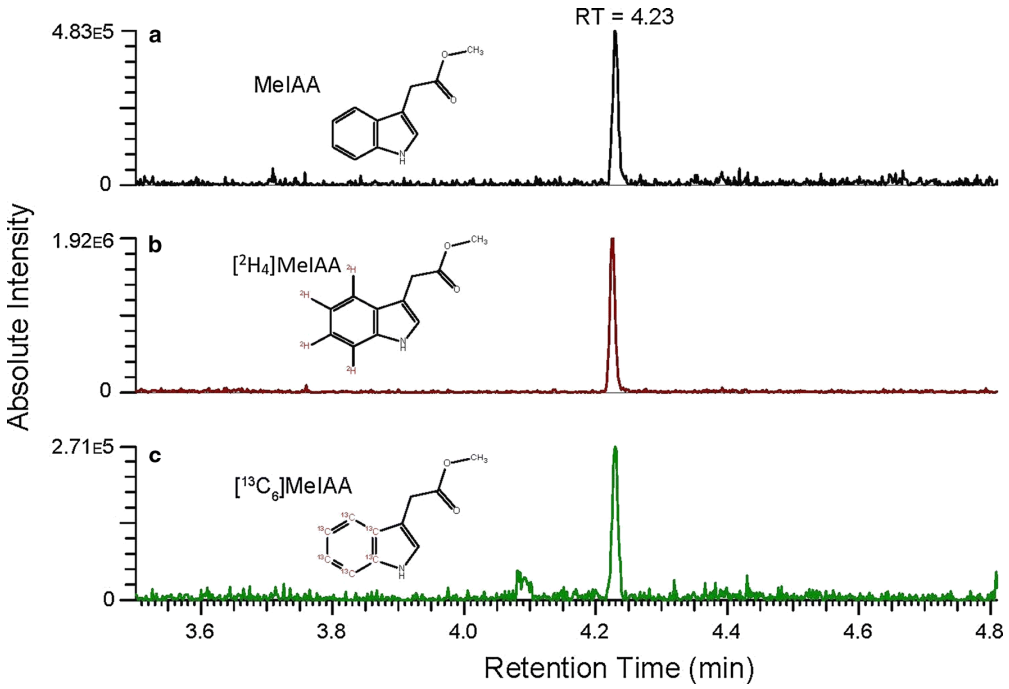

Figure B-4. Selected Reaction Monitoring (SRM) ion chromatograms from IAA analysis showing the quinolinium product ions of *m/z* 130, 134 and 136 of methyl esters of native IAA (a), [$^{2}H_4$]IAA (b), and [$^{13}C_6$]IAA (c). The quinolinium ions were detected after selection of their molecular ions at *m/z* 189, 193, and 195 followed by collision of the molecular ions with argon gas using a collision energy of 10 V and 1.5 mTorr collision gas pressure. This scheme allowed calculation of the quantity of both IAA and [$^{13}C_6$]IAA in the plant material by isotope dilution analysis using [$^{2}H_4$]IAA as the quantitative internal standard

B.4: NECLIN1 is a novel cupin involved in nectar production in *Arabidopsis thaliana*.

Rahul Roy, Mengyuan Jia, Molly Tillmann, Ricci Bender, Elizabeth Johnson, Catherine Holl, Michael Millican, Jerry D. Cohen and Clay Carter*

*Corresponding author; Department of Plant and Microbial Biology, University of Minnesota, St. Paul, MN, USA

Manuscript in preparation

Abstract

Auxin responses are key regulators of nectar production, and PIN6, an auxin transporter, is required for nectar production in *Arabidopsis*. We find that loss of PIN6 upregulates a gene encoding a cupin domain-containing protein in the nectaries of *Arabidopsis* flowers. We have named this NECLIN1, short for Nectary Localized Cupin 1, owing to its strong expression in the nectaries, though other sites of expression such as lateral roots and funiculi are also reported. NECLIN1 is a negative regulator of nectar sugar levels since loss of NECLIN1 causes an increase in nectar glucose levels and whole plant overexpression represses nectar production. Expression of nectary specific genes previously implicated in nectary function are unchanged in *neclin1* mutants as are nectary auxin responses, though PIN6 loss-of-function mutants display a decrease in transcript abundance of SWEET9, a sucrose uniporter, and CRABSCLAW, a transcription factor required for nectary development. NECLIN1 expression is repressed in TIR1 F-box mutants and is induced by exogenous auxin treatment. It is involved in auxin homeostasis, though the mechanism is independent of transcriptional regulation of certain auxin signaling genes such as ARF6, ARF8, IAA8, SAUR66, and DAO1.

Quantitative analysis of free auxin (IAA) levels

Free IAA levels in flower bases of Columbia-0 wild type (WT), *neclin1-1 (mnc1-1), neclin1-2 (mnc1-2),* and *pinoid6-2 (pin6-2) Arabidopsis* plants were determined using isotope dilution and LC-MS/MS (Figure B.5). Microcentrifuge tubes containing frozen samples were placed on ice, and to each was added 0.1 ng of [$^{13}C_6$]IAA internal standard in 20 µL of homogenization buffer (65% isopropanol, 35% 0.1M imidazole) and two 1.6 mm stainless steel beads (Next Advance, Troy, NY). Samples were homogenized with a Geno/Grinder tissue homogenizer (SPEX Sample Prep, Metuchen, NJ) for 4 minutes at 1500 rpm and placed on ice for approximately 1 hour for equilibration. IAA was extracted essentially as described (Liu et al., 2012), except the methylation step was omitted and instead the methanol eluted from PMME tips was reduced to approximately 20 µL using a SpeedVac vacuum concentrator (Savant/Thermo, Milford, MA). Concentrated samples were analyzed by LC-MS/MS with a Dionex Ultimate 3000 RSLC HPLC coupled to a hybrid quadrupole Orbitrap Q Exactive mass spectrometer (Thermo Scientific, Waltham, MA). 5-10 µL of each sample was injected onto a 50 × 2.1 mm Force C18 column with 1.8 µm particle size (Restek, Bellefonte, PA) and run with a solvent gradient of 0.1% formic acid in water (solvent A) and 0.1% formic acid in acetonitrile (solvent B) at a flow rate of 0.4 mL min^{-1}. Gradient parameters were as follows: − 1 to 0 min, 5% B; 0–3 min, 5–20% B; 3–6 min, 20–80% B; and 6–6.5 min, 80% B. Mass spectrometry data were collected in the parallel reaction monitoring (PRM) scan mode with the [M + 1] for IAA and [$^{13}C_6$]IAA at *m/z* 176.1 and 182.1, respectively, in the inclusion list and with the following settings: isolation width of 2.0 *m/z*, resolution of 17500, automatic gain control target of 2 × 105, maximum accumulation time of 50 ms, and normalized collision energy of 20%. Peaks generated from the quinolinium ions produced by fragmentation of the [M + 1] for IAA and [$^{13}C_6$]IAA were viewed as extracted ion chromatograms for *m/z* 130.065 and 136.085, respectively, using a mass range window of ±0.001, and their areas were calculated using the peak selection tool in Xcalibur software (Thermo Scientific).

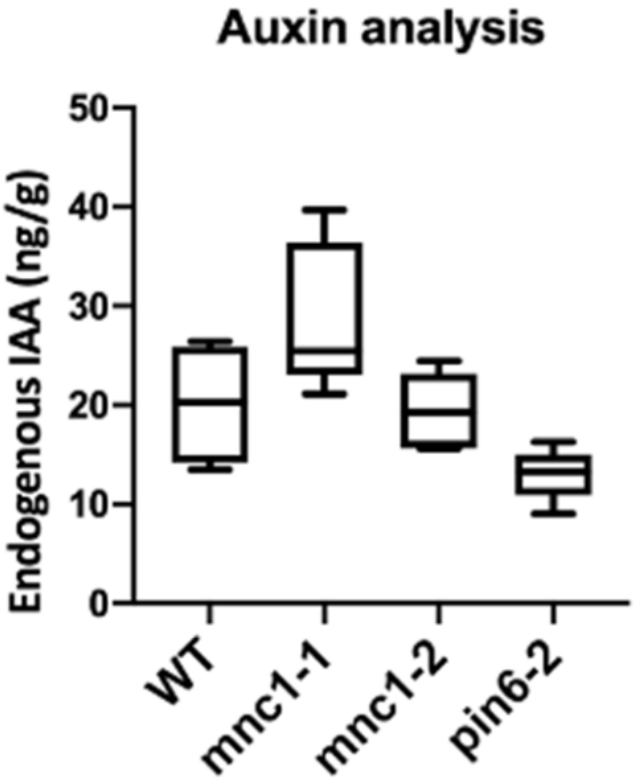

Figure B-5. Free IAA levels in flower bases. Columbia-0 wild type (WT), *neclin1-1 (mnc1-1), neclin1-2 (mnc1-2),* and *pinoid6-2 (pin6-2) Arabidopsis* plants were grown under a 16 h:8 h photoperiod of white light (150 µmol m^{-2} sec^{-1}) at 22 °C. Floral bases were dissected with surgical scissors and frozen in liquid nitrogen. Free IAA was extracted essentially as described by Liu et al. (Liu et al., 2012) and analyzed LC-MS/MS using [$^{13}C_6$]IAA as the internal standard for absolute quantitation (Cohen et al., 1986).

References

Atkinson JA, Rasmussen A, Traini R, Voß U, Sturrock C, Mooney SJ, Wells DM, Bennett MJ (2014) Branching out in roots: uncovering form, function, and regulation. Plant Physiology **166:** 538-550

Awika JM (2011) Major cereal grains production and use around the world. *In* Advances in cereal science: implications to food processing and health promotion. ACS Publications, pp 1-13

Barkawi LS, Tam Y-Y, Tillman JA, Normanly J, Cohen JD (2010) A high-throughput method for the quantitative analysis of auxins. Nature Protocols **5:** 1609-1618

Barkawi LS, Tam Y-Y, Tillman JA, Pederson B, Calio J, Al-Amier H, Emerick M, Normanly J, Cohen JD (2008) A high-throughput method for the quantitative analysis of indole-3-acetic acid and other auxins from plant tissue. Analytical Biochemistry **372:** 177-188

Bellini C, Pacurar DI, Perrone I (2014) Adventitious roots and lateral roots: similarities and differences. Annual Review of Plant Biology **65:** 639-666

Christiaens A, Gobin B, Van Labeke M (2016) Light quality and adventitious rooting: a mini-review. *In* VIII International Symposium on Light in Horticulture 1134, pp 385-394

Cohen JD (1984) Convenient apparatus for the generation of small amounts of diazomethane. Journal of Chromatography A **303:** 193-196

Cohen JD, Baldi BG, Slovin JP (1986) $^{13}C_6$-[Benzene Ring]-indole-3-acetic acid a new internal standard for quantitative mass spectral analysis of indole-3-acetic acid in plants. Plant Physiology **80:** 14-19

Dai Y, Wang H, Li B, Huang J, Liu X, Zhou Y, Mou Z, Li J (2006) Increased expression of MAP KINASE KINASE7 causes deficiency in polar auxin transport and leads to plant architectural abnormality in Arabidopsis. The Plant Cell **18:** 308-320

Dirr M, Heuser CW (1987) The reference manual of woody plant propagation: from seed to tissue culture. Varsity Press

Klopotek Y, Haensch K-T, Hause B, Hajirezaei M-R, Druege U (2010) Dark exposure of petunia cuttings strongly improves adventitious root formation and enhances carbohydrate availability during rooting in the light. Journal of Plant Physiology **167:** 547-554

Liu X, Hegeman AD, Gardner G, Cohen JD (2012) Protocol: high-throughput and quantitative assays of auxin and auxin precursors from minute tissue samples. Plant Methods **8:** 1-17

Noh B, Murphy AS, Spalding EP (2001) Multidrug resistance–like genes of Arabidopsis required for auxin transport and auxin-mediated development. The Plant Cell **13:** 2441-2454

Sorin C, Bussell JD, Camus I, Ljung K, Kowalczyk M, Geiss G, McKhann H, Garcion C, Vaucheret H, Sandberg G (2005) Auxin and light control of adventitious rooting in Arabidopsis require ARGONAUTE1. The Plant Cell **17:** 1343-1359

Steffens B, Rasmussen A (2016) The physiology of adventitious roots. Plant Physiology **170:** 603-617

Takahashi F, Sato-Nara K, Kobayashi K, Suzuki M, Suzuki H (2003) Sugar-induced adventitious roots in Arabidopsis seedlings. Journal of Plant Research **116:** 83-91

Zerche S, Haensch K-T, Druege U, Hajirezaei M-R (2016) Nitrogen remobilisation facilitates adventitious root formation on reversible dark-induced carbohydrate depletion in Petunia hybrida. BMC Plant Biology **16:** 219